Phenomenology of Models with New Scalar Particles

Matthew Sullivan

B.S. Physics, University of Kansas 2013

B.S. Mathematics, University of Kansas 2013

Submitted to the graduate degree program in Department of Physics and Astronomy and the Graduate Faculty of the University of Kansas in partial fulfillment of the requirements for the degree of Doctor of Philosophy.

Committee members

Ian M. Lewis, Chairperson

David Besson

Kyoungchul Kong

Doug McKay

Agnieszka Miedlar

Date defended: June 24, 2020

The Dissertation Committee for Matthew Sullivan certifies
that this is the approved version of the following dissertation :

Phenomenology of Models with New Scalar Particles

Ian M. Lewis, Chairperson

Date approved: June 24, 2020

Abstract

The discovery of a 125 GeV Higgs boson is one of the greatest successes of the Standard Model of particle physics, but it is also one of the paths to finding its failings. The scalar sector of the Standard Model is only a minimal implementation of electroweak symmetry breaking. In spite of a rich sector of fermions and gauge bosons, the Standard Model predicts the existence of only one scalar particle, and the properties of this scalar particle are fully determined. Precisely measuring the properties of this Higgs boson is thus one of the main paths avenues to looking for new physics. A detailed analysis of the Higgs boson inevitably leads to studying the phenomenology of extended scalar sectors. The vast landscape of models with extended scalar sectors is also relevent many of the unanswered questions in particle physics. This dissertation aims to demonstrate the many possible phenomenological consequences of new scalars. We will explore some scalar models with important phenomenological consequences relevant to the frontiers of fundamental physics. We first cover benchmarks of the simplest scalar extensions. These extensions can greatly change the picture of electroweak symmetry breaking. Such models also can lead to large cross sections for the production of pairs of scalars, an important signal to search for at colliders. Then we move on to a more complicated scalar sector with three Higgs doublets. This extension can accomodate a mechanism that explains the asymmetry between matter and anti-matter in the universe while also predicting observable consequences for Higgs boson properties and production of new scalars. We then move on to dark sectors that connect the Standard Model to dark matter. The properties of dark matter are largely unknown, but scalar portals are one potential avenue of study. In one model, we examine the possibility of connecting dark matter and neutrino masses with a scalar portal. This provides a novel explanation of neutrino masses with potentially observable consequences for cosmic neutrino detection. In the final model, we discuss the

combination of a dark sector, with a dark force and dark Higgs mechanism, and a popular vector like quark model. The inclusion of dark sector particles turns out to vastly change the phenomenology of this popular model, with entirely different decay patterns for the vector like quark. We conclude that Standard Model extensions containing new scalars have immense potential for new physics and answers to open questions in the field.

Acknowledgements

I would like to begin by extending my deepest gratitude to my advisor, Ian Lewis. Since I began working with him more than four years ago, Ian has given me endless guidance and support. He has provided me with many opportunities over the last several years, and I am grateful for all the conferences and summer schools that I was able to attend thanks to Ian. I would not have been able to reach this point without him. Even when I came to doubt whether I would succeed in physics, Ian believed in me and supported me. For that, I will always be grateful.

I would also like to extend my deepest gratitude to Dave Besson. I first began physics research with Dave as an undergraduate at KU. At the time, I was plagued with doubt and unsure of what I wanted to do in the future. It is only due to Dave's support and encouragement that I decided to pursue a PhD. When I decided to switch research groups, Dave continued to encourage me. I would not have even begun on this path if not for Dave, and I will always be grateful.

I would like to thank the rest of my committee members for dedicating their time and being a part of my committee. I would also like to thank all the people in the department who have been both friends and valuable colleagues to me. In particular, sharing ideas back and forth with the other students was always a valuable experience. John Ralston was also a great mentor to me, and discussing physics of any sort with him was a joy.

Furthermore, I would like to thank Brookhaven National Laboratory for hosting me for a semester. Being at Brookhaven was a fantastic learning experience as well as a big life event for me. I would like to thank Sally Dawson for being my sponsor and for being incredibly helpful and supportive in our research together. I would like to thank Hooman Davoudiasl for providing me with multiple interesting research opportunities that expanded my horizons.

I would also like to thank the many other people at Brookhaven that I interacted with regularly, in particular the postdocs who made me feel at home.

Parts of this research were supported by the University of Kansas General Research Fund allocation 2302091; the U.S. Department of Energy, Office of Science, Office of Workforce Development for Teachers and Scientists, Office of Science Graduate Student Research (SCGSR) program; the United States Department of Energy grant number DE-SC0017988; the State of Kansas EPSCoR grant program; the United States Department of Energy grant number DE-SC0019474; and a Summer Research Scholarship from the University of Kansas. The SCGSR program is administered by the Oak Ridge Institute for Science and Education (ORISE) for the DOE. ORISE is managed by ORAU under contract number DE-SC0014664.

I wish to dedicate this dissertation to my mother, Elizabeth Sullivan.

Contents

List of Figures

List of Tables

Chapter 1

Introduction

The Standard Model (SM) of particle physics is one of the most well-tested scientific theories. It is a quantum field theory that describes all the known elementary particles with great accuracy. The gauge group $SU(3)_c \times SU(2)_L \times U(1)_Y$ describes the interactions between particles[1, 2, 3]. One of the predictions of the SM was the existence of a scalar particle known as a Higgs boson[4, 5, 6]. The Higgs boson plays a crucial role in electroweak symmetry breaking, an essential part of our understanding of the gauge sector of the SM. CERN announced in 2012 that the Large Hadron Collider (LHC) discovered a scalar CERN announced in 2012 that the Large Hadron Collider (LHC) discovered a scalar particle with a mass of around 125 GeV[1] that is a candidate for the Higgs boson of the SM.

The formulation of the SM was a process of providing theoretical explanations for unexplained phenomena and finding the experimental confirmation. At one time, only three quarks were known: the up, down, and strange quarks. The lack of flavor changing neutral currents led to a prediction of a fourth quark partnering the the strange quark[7]; this partner, the charm quark, was discovered in 1974[8, 9]. The observed violation of CP symmetry[10] did not fit with only two generations of quarks, and so a third generation of quarks was predicted[11]; these quarks, the bottom and the top, were discovered in 1977[12] and 1995[13, 14], respectively. Electroweak interactions, like those mediating muon decays, were formulated as a gauge theory which predicted new gauge bosons[1, 2, 3]; these bosons, the W and the Z, were then discovered in 1983[15, 16, 17, 18]. The Higgs boson was the final predicted particle. Now, one of the main goals of the LHC and proposed future colliders is

[1]Throughout this dissertation, natural units are used: $\hbar = 1$, $c = 1$

to more thoroughly measure the interactions and properties of this new particle.

The mass of the Higgs boson was the last free parameter to be measured in the SM. With its measurement, the SM now predicts all the properties of every particle, including the Higgs boson. However, in spite of the success of the SM's many predictions, the SM lacks an explanation for such things as dark matter, non-zero neutrino masses, and the asymmetry between matter and antimatter in the universe. This is a good reason to believe that the SM is not a complete description of high energy physics but instead a low energy effective field theory. Measuring the properties of this new SM-like Higgs particle to check whether it matches the predictions of the SM Higgs boson is vital to the search for new physics beyond the SM (BSM). In addition, searches for BSM physics can directly look for signs of completely new particles. Investigating BSM models with more scalars is a natural step in furthering our understanding of high energy physics.

1.1 Standard Model Fields and Gauge Symmetries

The gauge sector of the SM contains the spin 1 vector bosons. There are eight types of gluons G corresponding to the eight generators of $SU(3)_c$. The subgroup $SU(2)_L \times U(1)_Y$ is known as the electroweak (EW) gauge group, and its corresponding particles are a massless photon and the massive Z, W^+, and W^- bosons. The process of electroweak symmetry breaking (EWSB) reduces the EW gauge group to the single unbroken $U(1)_{EM} \subset SU(2)_L \times U(1)_Y$. The massless photon corresponds to the unbroken subgroup, while the massive Ws and Z correspond to the other three generators of the broken symmetry; this correspondence will be covered in Section 1.2.

The SM has three generations of spin $\frac{1}{2}$ fermions, with each generation containing an up-type quark in three colors, a down-type quark also in three colors, a charged lepton, and a neutrino. For spin 0 particles, or scalars, there is only the one Higgs boson in the SM. Figure 1.1 shows a graphical depiction of the SM particles and their interactions.

Gauge symmetry is an invariance under gauge transformations. Before symmetry break-

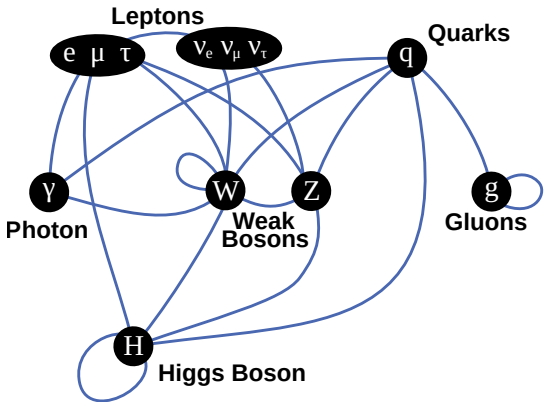

Figure 1.1: A pictorial representation of the particles in the SM and their interactions. Particles that can interact are connected by lines. The quarks (q), charged leptons (e, μ, τ , and neutrinos (ν_e, ν_μ, ν_τ) are all fermions, the Higgs (H) is a scalar boson, and the photon (γ), gluon (g), W, and Z are vector bosons. The image, from wikimedia, is in the public domain.

ing, the gauge fields in the SM are G^A_μ with A = 1,2,...,8 corresponding to $SU(3)_c$, W^a_μ with a = 1,2,3 corresponding to $SU(2)_L$, and B_μ corresponding to $U(1)_Y$. The infinitessimal gauge transformations of the SM gauge fields take the form

$$\begin{aligned} B_\mu(x) &\rightarrow B'_\mu(x) = B_\mu(x) + \frac{1}{g'}\partial_\mu\phi(x) \\ W^a_\mu(x) &\rightarrow W'^a_\mu(x) = W^a_\mu(x) + \frac{1}{g}\partial_\mu\theta^a(x) + \varepsilon^{abc}\theta^b(x)W^c_\mu(x) \\ G^I_\mu(x) &\rightarrow G'^I_\mu(x) = G^I_\mu(x) + \frac{1}{g_S}\partial_\mu\tilde{\theta}^I(x) + f^{IJK}\tilde{\theta}^J(x)G^K_\mu(x) \ , \end{aligned} \tag{1.1}$$

where g', g, and g_S are the coupling constants of $U(1)_Y$, $SU(2)_L$, and $SU(3)_c$, respectively, ε^{abc} and f^{IJK} are the structure constants of $SU(2)$ and $SU(3)$, respectively, and $\phi(x)$, $\theta^a(x)$, and $\tilde{\theta}^I(x)$ are arbitrary functions of space and time. Under global transformations, i.e. transformations where the arbitrary functions of spacetime are constants, the gauge fields transform in the adjoint representation of the gauge group.

Each field has a fixed representation under the gauge group, but different fields can belong

	$SU(3)_c$	$SU(2)_L$	Y
G	**8**	**1**	0
W	**1**	**3**	0
B	**1**	**1**	0
u_R	**3**	**1**	2/3
d_R	**3**	**1**	-1/3
$Q_L = \begin{pmatrix} u_L \\ d_L \end{pmatrix}$	**3**	**2**	1/6
e_R	**1**	**1**	-1
$L_L = \begin{pmatrix} \nu_L \\ e_L \end{pmatrix}$	**1**	**2**	-1/2
H	**1**	**2**	1/2

Table 1.1: The field content of the SM and their charges, before electroweak symmetry breaking. G, W, and B are the gauge fields of $SU(3)_c$, $SU(2)_L$, and $U(1)_Y$, respectively. u_R, d_R, and Q_L are SM quarks coming in three generations, e_R and L_L are SM leptons coming in three generations. H is the SM Higgs doublet. Y is the weak hypercharge.

to different representations. A (complex) field $f(x)$, with indices suppressed, transforms as

$$f(x) \to f'(x) = \exp(i\theta^a(x)T^a)\exp(i\tilde{\theta}^I(x)\tilde{T}^I)\exp(iY\phi(x))f(x) \ , \tag{1.2}$$

where θ^a, $\tilde{\theta}^I$, and ϕ are the same functions of space and time as from Eq. (1.1), T^a and $\tilde{T}^I$ are the generators of a unitary representation of $SU(2)$ and $SU(3)$, respectively, and Y is the weak hypercharge of the field f corresponding to its representation under $U(1)_Y$.

The SM can be described in two phases: the unbroken phase and the broken phase, that is, before and after EWSB. The field content and gauge group representations are described in Tables 1.1 and 1.2 for the unbroken and broken phases, respectively.

1.2 Review of Electroweak Symmetry Breaking

This section will give a brief overview of electroweak symmetry breaking, a form of spontaneous symmetry breaking in the SM. For a more detailed review, see e.g. Refs [19, 20]. As a terminology note, though "spontaneous symmetry breaking" sounds as if the gauge

	$SU(3)_c$	Q
G	**8**	0
A	**1**	0
Z	**1**	0
W^+	**1**	1
W^-	**1**	-1
u	**3**	2/3
d	**3**	-1/3
e	**1**	-1
ν_L	**1**	0
h	**1**	0

Table 1.2: The field content of the SM and their charges, after electroweak symmetry breaking. G and A are the gauge fields of $SU(3)_c$ and $U(1)_{EM}$, respectively. Z, W^+, and W^- are the massive vector bosons coming from EWSB. u and d, and Q_L are SM quarks coming in three generations, e and ν_L are SM charged leptons and neutrinos, respectively, coming in three generations. h is the SM Higgs boson. Q is the electric charge.

symmetry is gone, in reality, the ground state of the quantum field theory merely transforms non-trivially under the gauge symmetry.

Focusing only on the EW sector for simplicity, we want a theory that is invariant under gauge transformations, or gauge invariant. For this purpose, it is useful to define field strength tensors,

$$\begin{aligned} B_{\mu\nu} &= \partial_\mu B_\nu - \partial_\nu B_\mu \\ W^a_{\mu\nu} &= \partial_\mu W^a_\nu - \partial_\nu W^a_\mu + g\varepsilon^{abc} W^b_\mu W^c_\nu \ , \end{aligned} \tag{1.3}$$

where we have suppressed the coordinate dependence of the fields. The Lagrangian describing only the gauge sector of EW theory is then

$$\mathcal{L}_{EW,\text{gauge}} = -\frac{1}{4} B_{\mu\nu} B^{\mu\nu} - \frac{1}{4} W^a_{\mu\nu} W^{a,\mu\nu} \ , \tag{1.4}$$

which is invariant under the gauge transformations of Eq. (1.1). Experimentally, three of the four vector bosons in the electroweak sector, the W^+, W^-, and Z bosons, have non-zero

masses. A mass term for a vector boson, e.g. B_μ with mass m would look like $-\frac{1}{2}m^2 B_\mu B^\mu$. Under transformations like Eq. (1.1), a mass term would transform as

$$\begin{aligned} B_\mu(x)B^\mu(x) \to B'_\mu(x)B'^\mu(x) &= B_\mu(x)B^\mu(x) + 2\frac{1}{g'}\partial_\mu\phi(x)B^\mu(x) + \frac{1}{(g')^2}\partial_\mu\phi(x)\partial^\mu\phi(x) \\ &\neq B_\mu(x)B^\mu(x) \ , \end{aligned} \tag{1.5}$$

which is crucially not gauge invariant. Massive vector bosons have a longitudinal polarization, and scattering amplitudes involving these longitudinal polarizations tend to grow rapidly with energy, leading to violations of unitarity. Gauge invariance is important for taming this high energy behavior and preserving unitarity. Thus, a quantum field theory of vector bosons without gauge invariance does not have sensible behavior at high energies. So the task is to find a way to accomodate massive gauge bosons in a gauge invariant manner.

Scalar fields are special in that they can have a non-zero vacuum expectation value (vev). The vacuum expectation value of a field is the average value of that field in the ground state of the quantum field theory. The ground state of a quantum field theory should be Lorentz invariant, and this means that any field that transforms non-trivially under Lorentz transformations must have a vev of zero. Scalar fields are the only fields that transform trivially, and so only scalars can get non-zero vevs. The Higgs mechanism uses scalars with non-zero vevs in order to get a theory with massive gauge bosons[4, 5, 6, 21, 22, 23]. For the Higgs mechanism in the SM, we give a vev to a scalar field that is an $SU(2)_L$ doublet with weak hypercharge $Y = \frac{1}{2}$, and then perform an expansion around that vev. We will now go over the specifics of this in more detail.

We need to know more about forming gauge invariant Lagrangians using fields other than gauge fields. Because the gauge transformations depend on space and time, partial derivatives of fields will not have the same transformation properties as the fields themselves.

The gauge covariant derivative,

$$D_\mu f = (\partial_\mu - ig'YB_\mu - igT^aW_\mu^a)f \ , \tag{1.6}$$

does have the same gauge transformation properties as the field f, namely the transformation in Eq. (1.2). At this point, we note that the typical form of kinetic terms in Lagrangians, for fermions and scalars respectively, are

$$\mathcal{L}_{\rm F,kin} = \bar{\Psi} D_\mu \gamma^\mu \Psi \quad \text{and} \quad \mathcal{L}_{\rm S,kin} = (D_\mu S)^\dagger (D^\mu S) \ , \tag{1.7}$$

which are invariant under gauge transformations of Eqs. (1.1,1.2).

For the Higgs mechanism[4, 5, 6, 21, 22, 23], we begin with a two component complex doublet scalar H, referred to as a Higgs doublet, and the electroweak gauge bosons. The Lagrangian is

$$\mathcal{L}_{EW} = \mathcal{L}_{EW,\rm gauge} + (D_\mu H)^\dagger (D^\mu H) - V(H) \ , \tag{1.8}$$

where $\mathcal{L}_{EW,\rm gauge}$ is from Eq. (1.4) and $V(H)$, referred to as the potential, is given by

$$V(H) = -\mu^2 H^\dagger H + \lambda (H^\dagger H)^2 \ . \tag{1.9}$$

The vev of H, denoted as $\langle H \rangle$, should be at a minimum of the potential, such that $V'(\langle H \rangle) = 0$. The condition $\lambda > 0$ is necessary for the potential to be bounded from below, a necessary condition for a lowest energy ground state to exist. With that condition, the sign of μ^2 determines whether H gets a non-zero vev. If $\mu^2 < 0$, the minimum of the potential $V(H)$ is just at $H = 0$. However, if $\mu^2 > 0$, the two terms in Eq. (1.9) have opposite sign and the minimum of the potential is at some $H \neq 0$. Thus, $\mu^2 > 0$ leads to $\langle H \rangle \neq 0$.

We will now expand H around this minimum as

$$H = \exp\left(\frac{i\chi}{v}\right)\begin{pmatrix} 0 \\ (h+v)/\sqrt{2} \end{pmatrix} , \tag{1.10}$$

where h is a real scalar field, $v \equiv \sqrt{\frac{\lambda}{\mu^2}} = \sqrt{2}\,|\langle H\rangle|$ is the Higgs vev with a conventional normalization factor, and $\chi = \omega^a T^a$ with T^a being the generators of the doublet representation of $SU(2)_L$ and ω^a being three real scalar fields called Nambu-Goldstone bosons[24, 25]. Note that the degree of freedom counting is the same: two complex components versus three (ω^a) plus one (h) real components.

We now wish to write the covariant derivative of H explicitly in matrix form. The generators of $SU(2)_L$ in the doublet representation are $T^a = \frac{\sigma^a}{2}$ where σ^a are the three Pauli matrices. So the covariant derivative for a doublet with weak hypercharge $Y = \frac{1}{2}$ is

$$D_\mu H = \partial_\mu H - i\frac{1}{2}\begin{pmatrix} g'B_\mu + gW^3_\mu & gW^1_\mu - igW^2_\mu \\ W^1_\mu + igW^2_\mu & g'B_\mu - gW^3_\mu \end{pmatrix} H \ . \tag{1.11}$$

If we substitute the expansion from Eq. (1.10) into Eq. (1.11), we will see that the Lagrangian from Eq. (1.8) contains terms quadratic in the gauge fields with no derivatives:

$$\mathcal{L}_{EW} \supset \frac{v^2}{8}\left(g^2(W^1 - iW^2)_\mu(W^1 + iW^2)^\mu + (gW^3 - g'B)_\mu(gW^3 - g'B)^\mu\right) \ . \tag{1.12}$$

The terms in Eq. (1.12) are exactly mass terms for the gauge bosons. Switching to a different basis, $W^\pm_\mu = (W^1_\mu \mp iW^2_\mu)/\sqrt{2}$, $Z_\mu = \cos\theta_W W^3_\mu - \sin\theta_W B_\mu$, and $A_\mu = \cos\theta_W B_\mu + \sin\theta_W W^3_\mu$, where $\tan\theta_W = \frac{g'}{g}$, we can rewrite this as

$$\mathcal{L}_{EW} \supset \frac{1}{2}M_Z^2 Z_\mu Z^\mu + M_W^2 W^+_\mu W^{-,\mu} + 0 \times A_\mu A^\mu, \tag{1.13}$$

where $M_W^2 = \frac{g^2v^2}{4}$ and $M_Z^2 = \frac{(g^2+g'^2)v^2}{4}$. The field corresponding to the photon, A_μ, remains

massless, which reflects the remaining unbroken $U(1)_{EM}$ of electromagnetism. Through this Higgs mechanism, we have seen that gauge bosons can obtain mass. We now have a specific mechanism that produces the observed massive W^+, W^-, and Z and massless photon.

Having finished the main demonstration of gauge boson masses, we now quickly turn back to the Higgs doublet. We had split the degrees of freedom of H using a unitary transformation defined by χ and a real scalar field h in Eq. (1.10). The potential in Eq. (1.9) depends only on $H^\dagger H$ and is independent of the unitary transformation piece. However, χ will still show up in the kinetic part of the Lagrangian in Eq. (1.8), so one may worry that this theory predicts extra massless scalars, in conflict with observational data. However, the unitary transformation where χ appeared is equivalent to a gauge transformation on H as in Eq. (1.2). This means there is a gauge choice where the χ fields are removed from the theory, and since the theory is gauge invariant, this means the χ are unphysical. So in the end, starting from a complex Higgs doublet H, the only scalar in the final theory after EWSB is the real scalar h.

There is one other purpose of the Higgs mechanism in the SM: giving masses to fermions. A fermionic mass term requires both a left chiral field Ψ_L and a right chiral field Ψ_R and takes the form

$$\mathcal{L}_m = -m\bar{\Psi}_L\Psi_R \ . \tag{1.14}$$

In order for such a mass term to be gauge invariant, Ψ_L and Ψ_R must belong to the same representation of the gauge group. Because the left and right chiral fields transform differently under the EW gauge group, as seen in Table 1.1, such mass terms are forbidden in the SM. However, terms coupling the fermions to the Higgs doublet,

$$\mathcal{L}_{\text{Yukawa}} = -y^u\bar{Q}_L\tilde{H}u_R - y^d\bar{Q}_L H d_R - y^e\bar{L}_L H e_R + \text{h.c.} \ , \tag{1.15}$$

are gauge invariant, where generation indices are suppressed, $\tilde{H} = i\sigma^2 H^*$ is the conjugate doublet of H with opposite hypercharge, h.c. means the Hermitian conjugate terms, and

y^u, y^d, and y^e are the Yukawa coupling matrices for up-type quarks, down-type quarks, and charged leptons respectively. After EWSB, Eq. (1.15) contains terms like

$$\mathcal{L}_{\text{Yukawa}} \supset -\frac{y^u v}{\sqrt{2}}\bar{u}_L u_R - \frac{y^d v}{\sqrt{2}}(v+h)\bar{d}_L d_R - \frac{y^e v}{\sqrt{2}}(v+h)\bar{e}_L e_R + \text{h.c.}\ , \tag{1.16}$$

which are mass terms for the fermions e, u, and d with masses $m_a = \frac{v y^a}{\sqrt{2}}$. Note that since there were no ν_R fields in Table 1.1, there can be no mass terms for neutrinos, and so neutrinos are still massless left chiral fermions in the SM.

1.3 Motivation for New Scalars

The scenario of EWSB laid out in Section 1.2 is only the minimal implementation of EWSB. A BSM model with more Higgs fields can also implement EWSB, and the new fields could potentially be in representations of $SU(2)_L \times U(1)_Y$ other than the doublet with hypercharge $\frac{1}{2}$. Any additional scalars will appear in the Higgs potential, changing it from the SM potential of Eq. (1.9). Since the minimization of the Higgs potential is the source of the Higgs vev, the shape of the Higgs potential is vital to understanding the mechanism of EWSB and the source of fundamental particle masses. The specifics of EWSB have important cosmological consequences. In the early universe there was a phase transition from the unbroken phase to the broken phase of EW symmetry; depending on the Higgs potential, this phase transition might be a first order phase transition. A first order EW phase transition is a part of many models that hope to explain the asymmetry between matter and anti-matter in our universe. Thus, it is crucial to measure the shape of the Higgs potential, which means measuring the interactions of any Higgs particles.

In the SM, a final state with two Higgs bosons is an extremely rare process, but measuring the cross section for this process tells us about the self-interactions of the SM-like Higgs as well as the potential presence of new scalar particles in the Higgs sector. Figure 1.2 shows the sorts of diagrams that lead to the production of two SM-like Higgs bosons, here called h_1.

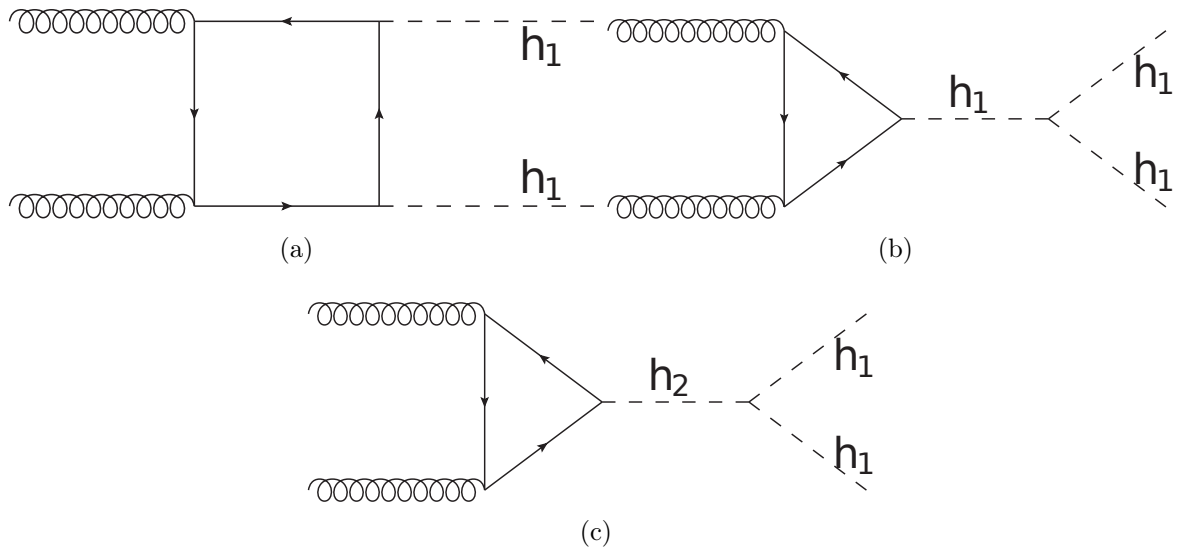

Figure 1.2: Representative diagrams for the production of two SM-like Higgs bosons h_1 corresponding to (a) box diagram, (b) triangle diagram with the SM-like Higgs boson h_1 that depends on the h_1 self-coupling, and (c) triangle diagram with a potential BSM scalar h_2 as an intermediate state.

In the SM, Fig. 1.2a and Fig. 1.2b, contribute to the process, though the relevant couplings might be different in a BSM model. On the other hand, Fig. 1.2c represents a process only available in BSM models due to the presence of a new scalar particle, here called h_2. Measuring two Higgs production process is crucial to understanding the Higgs potential and EWSB because it can tell us about the couplings that show up in Fig. 1.2. Thus, looking at BSM models with new scalars and working through the phenomenology provides important benchmarks for how well we can measure the Higgs potential in experiments. The simplest models for benchmarks are models that add gauge singlet scalars, meaning scalars that are invariant under gauge transformations.

Scalars can also serve as a connection to dark matter. Though we know of dark matter's existence from gravitational and cosmological data, we do not know much about it except that it interacts very weakly, if at all, electromagnetically. One attractive possibility is that dark matter may be part of a whole "dark sector" with its own interactions and forces. A dark sector with scalars has the interesting possibility of a so-called scalar portal, where

scalars in the dark sector mix with the SM Higgs boson. The SM-like Higgs boson then inherits some interactions with dark matter particles, and the dark sector scalars similarly inherit some interactions with SM particles. The possibility of such a scalar portal is a very good reason to not only very closely examine the properties of the SM-like Higgs, but also to look for new scalars.

Dark sectors could also have new gauge groups. New massless gauge bosons would lead to new long range forces, however, and long range forces are generally very highly constrained. This motivates another use of scalars: spontaneously breaking any dark sector gauge groups and making new forces short ranged. Such a dark Higgs sector could be looked for by directly looking for dark Higgses or indirectly by looking for massive dark sector gauge bosons.

1.4 Outline

In experimental searches for BSM physics, it is crucial to know what to look for. The range of possible signals is vast, and models are needed in order to motivate experimental searches. There are also many possible models to choose from, so some motivation is needed to decide which models to examine phenomenologically. Models that are simple, well-motivated, or have stark new signals often make good candidates.

In this dissertation, we study BSM models with extended scalar sectors and lay out their phenomenological predictions. Different models have unique physics aspects and propose answers to various questions.

Chapters 2 and 3 discuss simple extensions of the SM that add additional gauge singlet scalars. This leads to additional scalar particles that are motivated to be around the weak scale. Heavy scalars can decay to pairs of lighter scalars, and this is one of the main signals of interest in these models. In Chapter 2, based on Ref. [26], the singlet is a real field, and there is one additional heavy scalar that can decay predominantly to two 125 GeV SM-like Higgses. This can result in a resonant cross section much larger than the corresponding SM cross section. In Chapter 3, based on Ref. [27], the singlet is a complex field. This model

is slightly more complicated, and has two additional scalar particles. In this model, the heaviest scalar can decay to a pair of the SM-like Higgs and the other new scalar. This sort of two scalar final state with different mass scalars is not present in the SM, which only has one scalar particle, and makes for an interesting signal.

Chapter 4, based on Ref. [28], is a more complicated extension of the SM with a total of three Higgs doublets instead of one. This allows for a mechanism that can explain the asymmetry between matter and anti-matter in the universe using the two new Higgs doublets. This asymmetry, referred to as the baryon asymmetry of the universe, is something that the SM has no way to dynamically generate. The model discussed has three Higgs doublets, which matches the number of generations of fermions in the SM, and has a mechanism for explaining the non-zero masses of neutrinos. This model also makes predictions of Higgs measurements and new Higgs bosons that could be experimentally measured at future colliders.

Chapters 5 and 6 deal with dark sector forces. In Chapter 5, based on Ref. [29], there is a scalar portal between neutrinos and dark matter. On scales $\lesssim 1$ kpc, dark matter might have self-interactions through new forces. This BSM model uses this possibility to offer a new explanation for how neutrinos have their small but non-zero masses. Chapter 6, based on Ref. [30], involves a new dark sector containing a dark Higgs which spontaneously breaks a new gauge symmetry. There is a corresponding dark Higgs boson as well as a massive gauge boson, often called a dark photon. In this model, the dark Higg and dark photon couple to a new vector like quark, which is common in many well-motivated BSM models. However, due to the presence of the rest of this dark sector, the phenomenology of this vector like quark ends up being far different from the simplest models, with very different signals.

This dissertation finishes with the conclusions of these different models and a discussion of some of the phenomenology of new scalars.

Chapter 2

Double Higgs Production with a Real Scalar Singlet[2]

One of the main objectives of the LHC is to further our understanding of EW physics at the EW scale. Of particular interest are the interactions of the observed Higgs boson [31, 32]. Although current measurements of the Higgs production and decay rates help us determine if the observed Higgs boson is related to the source of fundamental masses within the SM, there are still many unanswered questions. One of the most pressing is the mechanism of EWSB. In the SM the source of EWSB is the scalar potential. Hence, it is interesting to study extensions of the SM that change the potential and their signatures at the LHC. In particular, simple extensions allow us to investigate phenomenology that is generic to more complete models.

The simplest extension of the SM is the addition of a real gauge singlet real scalar, S: the singlet extended SM. At the renormalizable level, the only allowed interactions between S and the SM are with the Higgs field. Hence, this model is a useful laboratory to investigate deviations from the SM Higgs potential. Although this is the simplest possible extension, it is well-motivated. This scenario arises in Higgs portal models [33, 34, 35, 36, 37, 38, 39, 40, 41, 42]. In these models, the scalar singlet couples to a dark matter sector. Through its interactions with the Higgs field, the new scalar provides couplings between the dark sector and the SM. Additionally, scalar singlets can help provide the strong first order EW phase transition necessary for EW baryogenesis [43, 44, 45, 46, 47, 48, 42, 49, 50, 51, 52, 53, 54, 55, 56, 57, 58, 59].

If there is no $\mathbb{Z}_2$ symmetry, $S \to -S$, after EWSB the new scalar will mix with the SM

[2]This chapter is based on Ref. [26], which is

Higgs boson. This mixing induces couplings between the new scalar and the rest of the SM particles. Hence, the new scalar can be produced and searched for at the LHC, as well as affecting precision Higgs measurements. The simplicity of the singlet extended SM allows for easy interpretation of precision Higgs measurements [60, 61] and resonant searches for heavy scalars [62, 63, 64, 65, 66, 67, 68, 69, 70, 71, 72, 73, 74, 75, 76, 77, 78, 79].

There have been many phenomenological studies of the singlet extended SM at the LHC [35, 80, 37, 44, 81, 82, 41, 83, 84, 85, 49, 86, 50, 87, 88, 89, 90, 91, 92, 93]. Of particular interest to us is if the new scalar is sufficiently heavy, it can decay on-shell into two SM-like Higgs bosons, mediating resonant double Higgs production at the LHC [94, 95, 48, 96, 97, 98, 99, 100, 101, 102, 103, 104, 105]. This can greatly enhance the double Higgs rate over the SM prediction. We will provide benchmark points that maximize double Higgs production in the singlet extended SM. These benchmark points are needed to help determine when the experimental searches for resonant double Higgs production [70, 71, 69, 68, 66, 67, 65] are probing interesting regions of parameter space.[3]

In Section 2.1 we provide an overview of the model, including the theoretical constraints on the model. Experimental constraints are discussed in Section 2.2. Resonant double Higgs production is discussed in Section 2.3. In Section 2.4 we discuss the maximization of the double Higgs rate and provide the benchmark points.

2.1 The Real Singlet Model

In this section we give an overview of the singlet extended SM, following the notation of Ref. [96]. The results of Ref. [96] are important for establishing our benchmark points. Hence, we summarize the results of this chapter regarding global minimization of the potential, vacuum stability, and perturbative unitarity. In the remaining part of the chapter we will extend upon this work, thoroughly investigating the relationship of these theoretical

[3]A similar study has been done in the case of a broken $\mathbb{Z}_2$ symmetry $S \to -S$ [100]. Here we work in the singlet extended SM with no $\mathbb{Z}_2$. This model has more free parameters allowing for different benchmark rates.

constraints and maximization of double Higgs production.

The model contains the SM Higgs doublet, H, and a new real gauge singlet scalar, S. The new singlet does not directly couple to SM particles except for the Higgs doublet. Allowing for all renormalizable terms, the most general scalar potential is

$$V(H,S) = -\mu^2 H^\dagger H + \lambda (H^\dagger H)^2 + \frac{a_1}{2} H^\dagger H S + \frac{a_2}{2} H^\dagger H S^2 + b_1 S + \frac{b_2}{2} S^2 + \frac{b_3}{3} S^3 + \frac{b_4}{4} S^4. \quad (2.1)$$

The neutral scalar component of H is denoted as $\phi_0 = (h+v)/\sqrt{2}$ with the vev being $\langle \phi_0 \rangle = \frac{v}{\sqrt{2}}$. We similarly write $S = s + x$, where the vev of S is denoted as x.

We require that EWSB occurs at an extremum of the potential, so that $v = v_{EW} = 246$ GeV. Shifting the field $S \to S + \delta S$ does not introduce any new terms to the potential, and is only a meaningless change in parameters. Using this freedom, we can additionally choose that the EWSB minimum satisfies $x = 0$. Requiring that $(v, x) = (v_{EW}, 0)$ be an extremum of the potential gives

$$\begin{aligned} \mu^2 &= \lambda v_{EW}^2, \\ b_1 &= -\frac{v_{EW}^2}{4} a_1. \end{aligned} \quad (2.2)$$

After symmetry breaking, there are two mass eigenstates denoted as h_1 and h_2 with masses m_1 and m_2, respectively. The new fields are related to the gauge eigenstate fields by

$$\begin{pmatrix} h_1 \\ h_2 \end{pmatrix} = \begin{pmatrix} \cos\theta & \sin\theta \\ -\sin\theta & \cos\theta \end{pmatrix} \begin{pmatrix} h \\ s \end{pmatrix}. \quad (2.3)$$

where θ is the mixing angle. The masses, m_1 and m_2, and the mixing angle, θ, are related

to the scalar potential parameters

$$\begin{aligned} a_1 &= \frac{m_1^2 - m_2^2}{v_{EW}} \sin 2\theta, \\ b_2 + \frac{a_2}{2} v_{EW}^2 &= m_1^2 \sin^2\theta + m_2^2 \cos^2\theta, \\ \lambda &= \frac{m_1^2 \cos^2\theta + m_2^2 \sin^2\theta}{2 v_{EW}^2}. \end{aligned} \tag{2.4}$$

We set the mass $m_1 = 125$ GeV to reproduce the discovered Higgs. The free parameter space is then

$$m_2,\ \theta,\ a_2,\ b_3, \text{ and } b_4. \tag{2.5}$$

We are interested in the scenario with $m_2 \geq 2m_1$, where h_2 can decay on-shell to two SM-like Higgs bosons, h_1. After symmetry breaking, the trilinear scalar terms in the potential which are relevant to double Higgs production are

$$V(h_1, h_2) \supset \frac{\lambda_{111}}{3!} h_1^3 + \frac{\lambda_{211}}{2!} h_2 h_1^2. \tag{2.6}$$

The trilinear coupling λ_{211} allows for the tree level decay of $h_2 \to h_1 h_1$. At the EWSB minimum $(v, x) = (v_{EW}, 0)$, the trilinear couplings are given by [96]

$$\lambda_{111} = 2\sin^3\theta\, b_3 + \frac{3a_1}{2} \sin\theta \cos^2\theta + 3\, a_2 \sin^2\theta \cos\theta\, v_{EW} + 6\,\lambda\, \cos^3\theta\, v_{EW}, \tag{2.7}$$

$$\begin{aligned} \lambda_{211} &= 2\sin^2\theta\cos\theta\, b_3 + \frac{a_1}{2}\cos\theta(\cos^2\theta - 2\sin^2\theta) + (2\cos^2\theta - \sin^2\theta)\sin\theta\, v_{EW}\, a_2 \\ &\quad -6\lambda \sin\theta\cos^2\theta\, v_{EW}. \end{aligned}$$

2.1.1 Global Minimization of the Potential

The scalar potential, Eq (2.1), allows for many extrema (v, x). There are two classes that need to be considered: $v \neq 0$ and $v = 0$. The $v \neq 0$ extrema are given by $(v, x) = (v_{EW}, 0)$

and $(v, x) = (v_\pm, x_\pm)$ where [96]

$$\begin{aligned} x_\pm &\equiv \frac{v_{EW}(3a_1a_2 - 8b_3\lambda) \pm 8\sqrt{\Delta}}{4v_{EW}(4b_4\lambda - a_2^2)}, \\ v_\pm^2 &\equiv v_{EW}^2 - \frac{1}{2\lambda}\left(a_1 x_\pm + a_2 x_\pm^2\right), \\ \Delta &= \frac{v_{EW}^2}{64}\left(8b_3\lambda - 3a_1a_2\right)^2 - \frac{m_1^2 m_2^2}{2}\left(4b_4\lambda - a_2^2\right). \end{aligned} \tag{2.8}$$

For all of these three solutions to be real, there are constraints $\Delta > 0$ and $v_\pm^2 > 0$.

The $v = 0$ extrema are given by solutions of the following cubic equation:

$$b_1 + b_2 x + b_3 x^2 + b_4 x^3 = 0. \tag{2.9}$$

Only real solutions for x are of interest.

As can be seen, there is only one extremum with $v = v_{EW}$. Since the scalar S is a gauge singlet, it does not contribute to the gauge boson or SM fermion masses. Hence, to reproduce the correct EWSB pattern, we require that $(v_{EW}, 0)$ is the global minimum.

2.1.2 Vacuum Stability

To avoid instability of the vacuum from runaway negative energy solutions, the scalar potential should be bounded from below at large field values. Vacuum stability of the potential then requires that

$$4\lambda\phi_0^4 + 2a_2\phi_0^2 s^2 + b_4 s^2 > 0. \tag{2.10}$$

It is clear that bounding the potential from below along the axes $s = 0$ and ϕ_0=0 requires

$$\lambda > 0 \qquad \text{and} \qquad b_4 > 0. \tag{2.11}$$

If $a_2 > 0$ as well, then the potential is always positive definite for large field values. However, $a_2 < 0$ is also allowed. Eq. (2.10) can be rewritten as

$$\lambda(2\phi_0^2 + \frac{a_2}{2\lambda}s^2)^2 + (b_4 - \frac{a_2^2}{4\lambda})s^4 > 0. \tag{2.12}$$

The first term in Eq. (2.12) is always positive definite. Requiring the second term to be nonnegative for $a_2 < 0$ gives the bound [96]

$$-2\sqrt{\lambda b_4} \leq a_2. \tag{2.13}$$

2.1.3 Perturbative Unitarity

Perturbative unitarity of the partial wave expansion for the scattering also constrains quartic scalar couplings,

$$\mathcal{M} = 16\pi \sum_{j=0}^{\infty} (2j+1) a_j P_j(\cos\theta), \tag{2.14}$$

where $P_j(\cos\theta)$ are Legendre polynomials. Looking at the process $h_2h_2 \to h_2h_2$ for large energies, the first term in the partial wave expansion at leading order, accounting for the normalization of states with identical particles, is

$$a_0(h_2h_2 \to h_2h_2) = \frac{3b_4}{16\pi}. \tag{2.15}$$

The perturbative unitarity requirement $|a_0| \leq 0.5$ gives the constraint $b_4 \lesssim 8.4$. When this bound is saturated, a minimum higher order correction of 41% is needed to restore the unitarity of the amplitude [106].

There are also perturbative unitarity constraints on the other quartic couplings: $\lambda \lesssim 8.4$ and $a_2 \lesssim 25$. However, for all parameter points we consider, these constraints on λ and a_2 are automatically satisfied when all other constraints are applied.

2.2 Experimental Constraints

The singlet model predicts that the couplings of h_1 to other SM fermions and gauge bosons are suppressed from the SM predictions by $\cos\theta$. Hence, the single Higgs production cross section is suppressed by $\cos^2\theta$,

$$\sigma(pp \to h_1) = \cos^2\theta \sigma_{SM}(pp \to h_1) \tag{2.16}$$

where $\sigma_{SM}(pp \to h_1)$ is the SM cross section for Higgs production at $m_1 = 125$ GeV. Since all couplings between h_1 and SM fermions and gauge bosons are universally suppressed, the branching ratios for h_1 decay agree with SM branching ratios,

$$\mathrm{BR}(h_1 \to X_{SM}) = \mathrm{BR}_{SM}(h_1 \to X_{SM}) \tag{2.17}$$

where X_{SM} is any allowed SM final state. Using these properties, the most stringent constraint from observed Higgs signal strengths at the time of this analysis was from ATLAS: $\sin^2\theta \leq 0.12$ at 95% C. L. [60]. More recent analyses with more data [107, 108] lead to stronger constraints. We included benchmarks for future projected limits which are still allowed.

As mentioned earlier, there are also direct constraints from searches for heavy scalar particles [63, 64, 62, 65, 67, 66, 68, 69, 70, 71, 72, 73, 74, 75, 76, 77, 78, 79]. For the mass range 250 GeV $\leq m_2 \leq$ 1000 GeV considered here, the direct constraints on $\sin\theta$ are weaker than those from the Higgs signal strengths [100]. Nevertheless, independently and using `HiggsBounds` [109, 110, 111, 112, 113], we verified that our benchmark points satisfy all experimental constraints.

2.3 Production and Decay Rates

The contributions to double Higgs production in the singlet model are as shown in Fig. 1.2. Figures 1.2a and 1.2b are present in the SM double Higgs production, while the s-channel h_2 contribution in Fig. 1.2c is responsible for the resonant h_1h_1 production. The s-channel h_1 (h_2) contribution in Fig. 1.2b (Fig. 1.2c) depends on the scalar trilinear couplings λ_{111} (λ_{211}) in Eq. 2.7. Hence, this process is clearly sensitive to the shape of the scalar potential.

It is expected that the resonant h_2 contribution dominates the double Higgs production cross section. We then use the narrow width approximation as follows:

$$\sigma(pp \to h_2 \to h_1h_1) \approx \sigma(pp \to h_2)\mathrm{BR}(h_2 \to h_1h_1). \tag{2.18}$$

Although interference effects between the different contributions in Fig. 1.2 can be significant [98], our purpose here is to maximize the double Higgs rate in this model. Hence, for simplicity we focus on maximizing the cross section in Eq. (2.18). This is sufficient to attain our goal.

Due to mixing with the Higgs boson, h_2 has couplings to SM fermions and gauge bosons proportional to $\sin\theta$. The cross section for production of h_2 is then

$$\sigma(pp \to h_2) = \sin^2\theta\, \sigma_{SM}(pp \to h_2) \tag{2.19}$$

with $\sigma_{SM}(pp \to h_2)$ being the SM Higgs production cross section evaluated at a Higgs mass of m_2. Since the couplings to fermions and gauge bosons are proportional to the SM values, the intuition about the dominant SM Higgs production channels is valid for the production of h_2. Hence, gluon fusion $gg \to h_2$ is the dominant channel, as illustrated in Fig. 1.2c.

The heavy scalar h_2 can decay to SM gauge bosons and fermions with partial widths of

$$\Gamma(h_2 \to X_{SM}) = \sin^2\theta\, \Gamma_{SM}(h_2 \to X_{SM}) \tag{2.20}$$

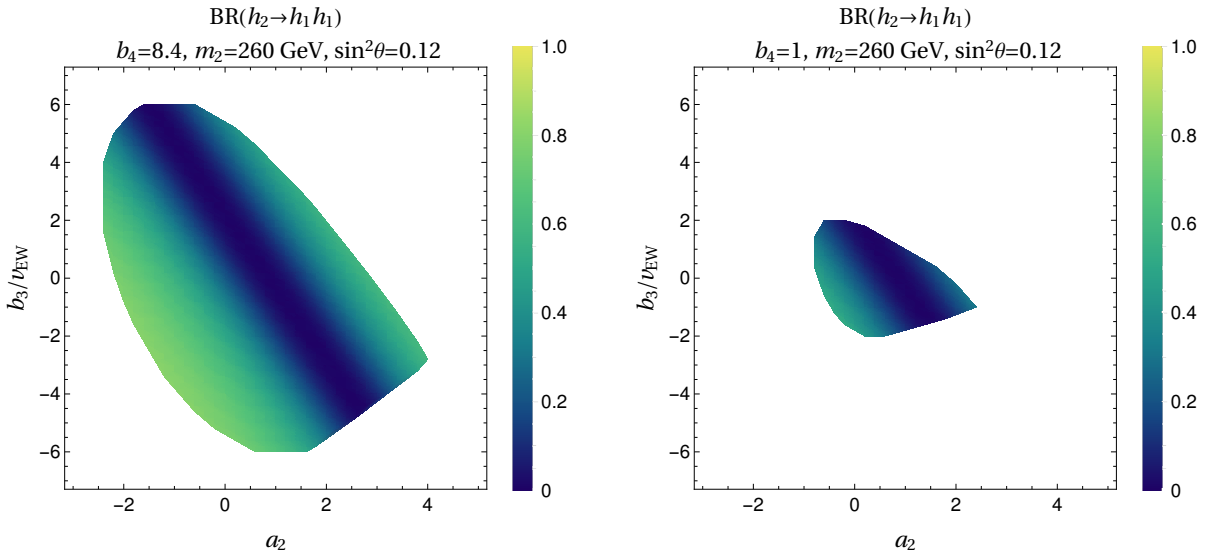

(a) (b)

Figure 2.1: BR($h_2 \to h_1 h_1$) as a function of b_3 and a_2 for $m_2 = 260$ GeV and $\sin^2\theta = 0.12$. In (a) $b_4 = 8.4$ and (b) $b_4 = 1$. The shaded regions are allowed by the global minimum and vacuum stability constraints. The color indicates BR($h_2 \to h_1 h_1$).

where $\Gamma_{SM}(h_2 \to X_{SM})$ is the SM decay width for a Higgs boson into SM final states $X_{SM} \neq h_1 h_1$ evaluated at a mass of m_2. The tree level decay for $h_2 \to h_1 h_1$ has a partial width given by

$$\Gamma(h_2 \to h_1 h_1) = \frac{\lambda_{211}^2}{32\pi m_2}\sqrt{1 - \frac{4m_1^2}{m_2^2}} \tag{2.21}$$

The branching ratio for $h_2 \to h_1 h_1$ is

$$\mathrm{BR}(h_2 \to h_1 h_1) = \frac{\Gamma(h_2 \to h_1 h_1)}{\Gamma(h_2)}, \tag{2.22}$$

where

$$\Gamma(h_2) = \Gamma(h_2 \to h_1 h_1) + \sin^2\theta\,\Gamma_{SM}(h_2 \to X_{SM}) \tag{2.23}$$

is the total width of h_2.

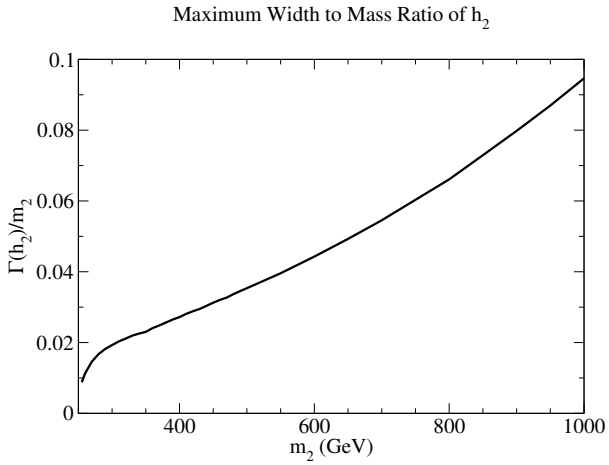

Figure 2.2: The ranges of $\Gamma(h_2)/m_2$ allowed by the theoretical constraints in Secs. 2.1.1 and 2.1.2 as a function of m_2 for $b_4 = 8.4$ and $\sin^2\theta = 0.12$.

The parameter b_4 does not explicitly affect $\mathrm{BR}(h_2 \to h_1 h_1)$. However, through the constraints of vacuum stability and $(v, x) = (v_{EW}, 0)$ being the global minimum of the scalar potential [Sec. 2.1.1], b_4 affects the allowed ranges for the other parameters a_2 and b_3. These parameters appear in the trilinear coupling λ_{211} in Eq. (2.7), which is relevant for $\Gamma(h_2 \to h_1 h_1)$. Figure 2.1 shows the allowed parameter region satisfying these constraints for (a) $b_4 = 8.4$ and (b) $b_4 = 1$ with $m_2 = 260$ GeV and $\sin^2\theta = 0.12$. It is clear from the figures that a lower value of b_4 shrinks the allowed region. The coloring in the figures indicates the value of $\mathrm{BR}(h_2 \to h_1 h_1)$, where the values of $\Gamma_{SM}(h_2 \to X_{SM})$ were obtained from Ref. [114]. It was found that the maximum $\mathrm{BR}(h_2 \to h_1 h_1)$ always occurs with $b_4 = 8.4$ at the unitarity bound.

In Fig. 2.2 we show allowed ranges of $\Gamma(h_2)/m_2$ as a function of the mass of m_2 for $b_4 = 8.4$ and $\sin^2\theta = 0.12$. The total width is always bounded by $\Gamma(h_2)/m_2 \lesssim 0.09$. For $m_2 \lesssim 700$ GeV, we also have $\Gamma(h_2)/m_2 \lesssim 0.05$. As $\sin\theta$ decreases below its upper bound, the total width of h_2 will decrease as well. The value of b_4 has no effect on the partial widths of h_2 into SM fermions or gauge bosons. However, as b_4 decreases, the partial width of $\Gamma(h_2 \to h_1 h_1)$ decreases as shown in Fig. 2.1. Hence, the upper bound on $\Gamma(h_2)$ in Fig. 2.2 is the upper bound throughout the allowed parameter regions, and h_2 is sufficiently narrow

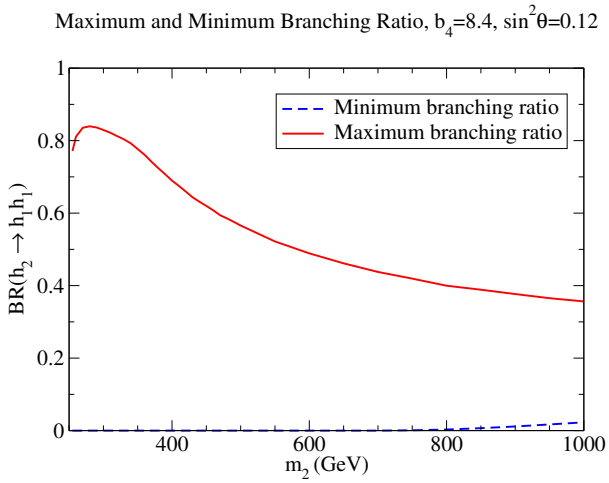

Figure 2.3: Maximum and minimum allowed BR($h_2 \to h_1 h_1$) as a function of m_2 for $b_4 = 8.4$ and $\sin^2\theta = 0.12$.

to justify the narrow width approximation in Eq. (2.18).

2.4 Results

We maximize the production rate in Eq. (2.18) by fixing m_2 and θ, then scanning over the remaining parameters

$$a_2,\ b_3, \text{ and } b_4. \tag{2.24}$$

For all numerical results, the SM production cross sections and widths for a Higgs boson in Eqs. (2.16), (2.17), (2.19), and (2.20) were obtained from Ref. [114].

The maximum and minimum BR($h_2 \to h_1 h_1$) for different values of m_2 are shown in Fig. 2.3. We set $b_4 = 8.4$ at the perturbative unitarity bound and $\sin^2\theta = 0.12$ at the experimental bound [60]. The largest possible branching ratio occurs at around 280 GeV with BR($h_2 \to h_1 h_1$) = 0.76. Even up to masses of 1000 GeV the branching ratio to double Higgs can be larger than 0.3. Additionally, for $m_2 \gtrsim 600$ GeV there is a minimum on BR($h_2 \to h_1 h_1$).

Figure 2.4a shows the dependence of the maximum branching ratio BR($h_2 \to h_1 h_1$) on the parameter b_4. As can be seen, if the parameter b_4 is less than the unitarity bound of 8.4

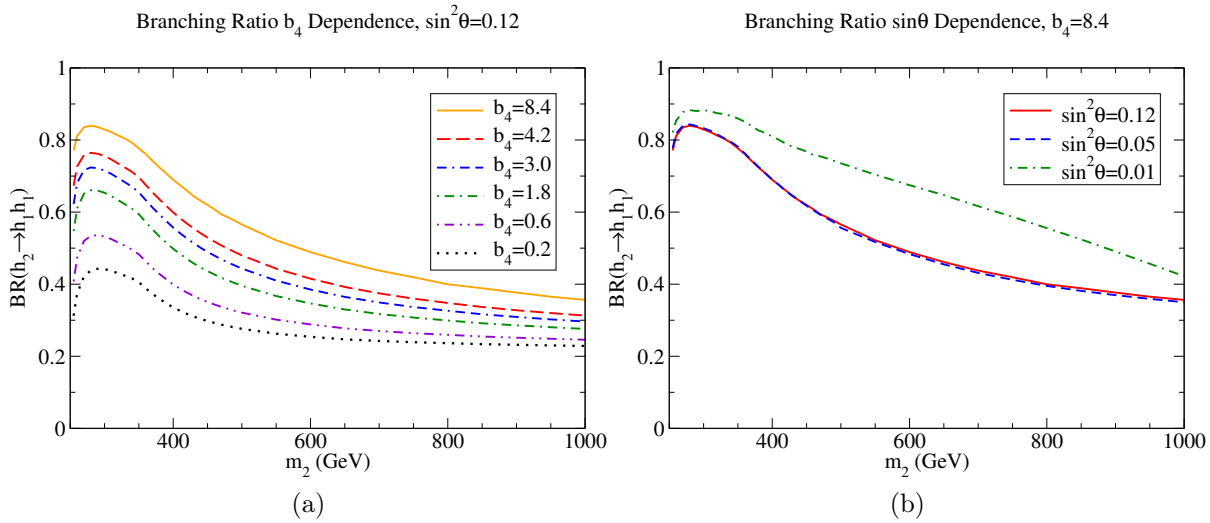

Figure 2.4: Maximum allowed BR($h_2 \to h_1 h_1$) as a function of m_2 for different values of (a) b_4 and (b) $\sin\theta$.

then the largest possible branching ratio becomes smaller. This is due to the shrinking of the allowed range for the parameters a_2 and b_3, as shown in Fig. 2.1. Even for small values of b_4, the branching ratio can still be quite substantial.

The maximum possible value of $\sin^2\theta$ is expected to decrease as more data is taken at the LHC and the measurements of the observed Higgs couplings become more precise. Figure 2.4b shows the maximum possible BR($h_2 \to h_1 h_1$) for several values of $\sin^2\theta$. As can be seen, the branching ratio can be larger for smaller $\sin\theta$. Hence, maximization of BR($h_2 \to h_1 h_1$) occurs at small $\sin\theta$. However, double Higgs production is not maximized with this condition.

Now we turn our attention to maximizing the double Higgs production rate. Figure 2.5 shows the maximum $\sigma(pp \to h_2)$BR($h_2 \to h_1 h_1$) at an LHC energy of $\sqrt{S_H} = 13$ TeV for various (a) b_4 and (b) $\sin\theta$ values as a function of mass m_2. The values are scaled by the SM double Higgs production cross section at 13 TeV of $33.53^{+5.3\%}_{-6.8\%}$ fb [114], calculated at NNLL matched to NNLO in QCD with NLO top quark mass dependence [115]. As mentioned earlier, the maximum rates occur when b_4 is at the unitarity bound $b_4 = 8.4$. For $\sin\theta$, although the maximum BR($h_2 \to h_1 h_1$) increases as $\sin\theta$ decreases, this increase is not

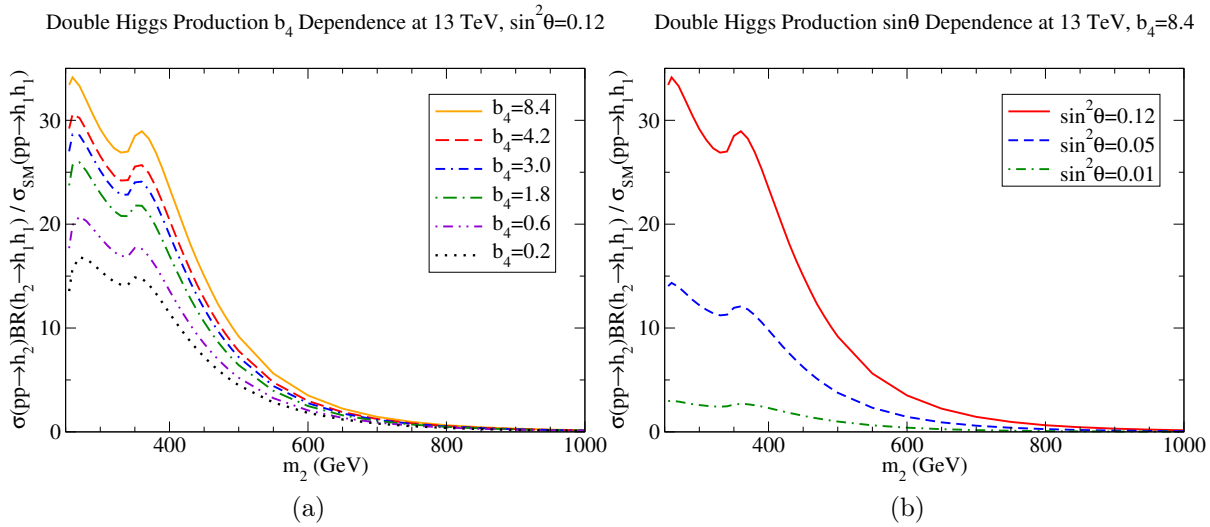

Figure 2.5: Maximum $\sigma(pp \to h_2)\text{BR}(h_2 \to h_1 h_1)$, scaled by the calculated SM double Higgs production, as a function of m_2 for different values of (a) b_4 and (b) $\sin\theta$.

m_2	a_2	b_3/v_{EW}	$\text{BR}(h_2 \to h_1 h_1)$	$\sigma(pp \to h_2)\text{BR}(h_2 \to h_1 h_1)$
300 GeV	-1.1	-3.7	0.83	0.98 pb
400 GeV	-0.85	-4.8	0.69	0.79 pb
500 GeV	0.18	-7.9	0.57	0.31 pb
600 GeV	0.76	-9.9	0.49	0.12 pb
700 GeV	1.7	-13	0.44	0.049 pb
800 GeV	2.1	-15	0.40	0.022 pb

Table 2.1: Benchmark points that maximize $\text{BR}(h_2 \to h_1 h_1)$ with $b_4 = 8.4$ and $\sin^2\theta = 0.12$. The cross sections are evaluated at a lab frame energy of $\sqrt{S_H} = 13$ TeV.

enough to compensate for the $\sin^2\theta$ suppression of the production cross section $\sigma(pp \to h_2)$ in Eq. (2.19). Hence, the maximum double Higgs production cross section occurs at the experimental bound $\sin^2\theta = 0.12$. In the best case, the resonant double Higgs production is roughly 30 times the SM double Higgs cross section.

Finally, we provide our benchmark points in Tables 2.1 and 2.2. We provide the parameter points that maximize the $h_1 h_1$ production in the singlet extended SM, as well as the corresponding $\text{BR}(h_2 \to h_1 h_1)$ and $h_1 h_1$ production cross section at a lab frame energy of $\sqrt{S_H} = 13$ TeV. As discussed before, the maximum $\text{BR}(h_2 \to h_1 h_1)$ occurs for $b_4 = 8.4$ at

m_2	a_2	b_3/v_{EW}	$\mathrm{BR}(h_2 \to h_1 h_1)$	$\sigma(pp \to h_2)\mathrm{BR}(h_2 \to h_1 h_1)$
300 GeV	-1.6	-2.8	0.83	0.41 pb
400 GeV	-1.2	-4.7	0.69	0.32 pb
500 GeV	-1.3	-4.8	0.56	0.13 pb
600 GeV	-0.58	-8.2	0.48	0.048 pb
700 GeV	-0.46	-9.1	0.43	0.020 pb
800 GeV	0.32	-13	0.40	0.0089 pb

Table 2.2: Benchmark points that maximize $\mathrm{BR}(h_2 \to h_1 h_1)$ with $b_4 = 8.4$ and $\sin^2\theta = 0.05$. The cross sections are evaluated at a lab frame energy of $\sqrt{S_H} = 13$ TeV.

the unitarity bound. Hence, we fix $b_4 = 8.4$ for all benchmark points. Also, the maximum $h_1 h_1$ production cross section occurs for $\sin^2\theta = 0.12$ at the current limit [60]. Table 2.1 contains the benchmark points for $\sin^2\theta = 0.12$. However, as mentioned earlier, as the LHC continues to gather data it is expected that the precision Higgs measurements will further limit $\sin\theta$. The uncertainties in Higgs coupling measurements are projected to be $\sim 5\%$ with 3000 fb^{-1} of integrated luminosity at the LHC [116]. This corresponds to a bound of $\sin^2\theta \lesssim 0.05$ due to the overall $\cos^2\theta$ suppression of the h_1 rate of production. Hence, we also provide benchmark points for $\sin^2\theta = 0.05$ in Table 2.2.

Chapter 3

Double Higgs Production with a Complex Scalar Singlet[4]

As discussed in the previous chapter, the exploration of the Higgs sector is a primary focus of the LHC physics program, with measurements of the Higgs couplings to fermions and gauge bosons, the Higgs mass, and Higgs CP properties becoming ever more precise. Measuring the Higgs potential is crucial to understanding the full picture of EWSB. In continuing the previous chapter's discussion of simple scalar extensions, we now proceed from the real scalar singlet extension to the complex scalar singlet extension.

The complex scalar singlet extension has new features beyond the real singlet case. It has several phases, 2 of which can accommodate a dark matter candidate[117, 118]. In the broken phase of this model (which is the subject of this chapter) there are 3 neutral scalar particles which mix to form the mass eigenstates, one of which is the 125 GeV scalar. While the real singlet had the scalar decay $h_2 \to h_1 h_1$, this model also allows for decays like $h_2 \to h_1 h_3$ and $h_2 \to h_3 h_3$. Because of this, final states with 2 different mass scalar particles can be resonantly produced in this scenario and there are large regions of parameter space where the couplings of the new scalars to SM particles are highly suppressed, making the dominant production mechanism of the new scalars the Higgs decays to other Higgs-like particles. The resonant production of two different mass Higgs particles is a smoking gun for this class of theories.

We study the most general case of a complex scalar singlet extension of the SM, without the introduction of any new symmetries for the potential. The complex singlet model has been previously studied imposing a softly broken $U(1)$ symmetry and benchmark points

[4]This chapter is based on Ref. [27], which is

described for the study of the decay of the heavy scalar to the SM Higgs boson and the lighter scalar of the model[91, 119]. The parameter space of the model we study is larger, allowing for new phenomenology. The basic features of the model are discussed in Section II and the limits on the model from perturbativity, unitarity and the oblique parameters are presented in Sec. 3.2. Our most interesting results are the implications for double Higgs studies and the description of scenarios where one of the new Higgs bosons is predominantly produced in association with the 125 GeV boson. This is discussed in Sec. 3.3.

3.1 The Complex Singlet Model

We consider a model containing the SM $SU(2)$ doublet, H, and a complex scalar singlet, S_c. Since S_c has hypercharge -0 it does not couple directly to SM fermion or gauge fields, and its tree level interactions with SM fermions and gauge bosons result entirely from mixing with H. The most general renormalizable scalar potential is[81],

$$\begin{aligned}\mathcal{V}(H,S_c) &= \frac{\mu^2}{2}H^\dagger H+\frac{\lambda}{4}(H^\dagger H)^2+\left(\frac{1}{4}\delta_1 H^\dagger H S_c+\frac{1}{4}\delta_3 H^\dagger H S_c^2+a_1 S_c\right.\\ &\left.+\frac{1}{4}b_1 S_c^2+\frac{1}{6}e_1 S_c^3+\frac{1}{6}e_2 S_c\mid S_c\mid^2+\frac{1}{8}d_1 S_c^4+\frac{1}{8}d_3 S_c^2\mid S_c\mid^2+h.c.\right)\\ &+\frac{1}{4}d_2(\mid S_c\mid^2)^2+\frac{\delta_2}{2}H^\dagger H\mid S_c\mid^2+\frac{1}{2}b_2\mid S_c\mid^2, \end{aligned} \tag{3.1}$$

where $a_1, b_1, e_1, e_2, d_1, d_3, \delta_1$ and δ_3 are complex. After spontaneous symmetry breaking, in unitary gauge,

$$H=\begin{pmatrix}0\\ \frac{h+v}{\sqrt{2}}\end{pmatrix},\quad S_c=\frac{1}{\sqrt{2}}\Big(S+v_S+i(A+v_A)\Big). \tag{3.2}$$

Since we have included all allowed terms in Eq. (3.1), the coefficients can always be redefined such that $v_S = v_A = 0$. This makes the potential of Eq. (3.1) identical to that obtained by adding 2 real singlets to the SM and there is no CP violation. Previous work[91, 81] imposed a global $U(1)$ symmetry or a $\mathbb{Z}_2$ symmetry to eliminate some of the terms in the potential,

making the shift to $v_S = v_A = 0$ in general not possible.

The mass eigenstate fields are h_1, h_2, h_3 (masses m_1, m_2, m_3) are found from the rotation,

$$\begin{pmatrix} h_1 \\ h_2 \\ h_3 \end{pmatrix} = V \begin{pmatrix} h \\ S \\ A \end{pmatrix} , \tag{3.3}$$

where V is a 3×3 unitary matrix with,

$$V \equiv \begin{pmatrix} c_1 & -s_1 c_3 & -s_1 s_3 \\ s_1 c_2 & c_1 c_2 c_3 - s_2 s_3 & c_1 c_2 s_3 + s_2 c_3 \\ s_1 s_2 & c_1 s_2 c_3 + c_2 s_3 & c_1 s_2 s_3 - c_2 c_3 \end{pmatrix} \tag{3.4}$$

and we abbreviate $c_i = \cos\theta_i$, etc. Note that the phase usually associated with the CKM-like mixing matrix does not appear since the mass matrix in terms of the real fields h, S, and A is strictly real by hermiticity. Since all allowed terms are included in Eq. (3.1), we are free to perform a field redefinition $S_c \to S_c e^{i\phi}$ while leaving the form of the potential unchanged. We choose to take $S_c \to S_c e^{i\theta_3}$. This results in the field redefinitions,

$$\begin{pmatrix} h \\ S \\ A \end{pmatrix} \to \begin{pmatrix} 1 & 0 & 0 \\ 0 & c_3 & -s_3 \\ 0 & s_3 & c_3 \end{pmatrix} \begin{pmatrix} h \\ S \\ A \end{pmatrix} , \tag{3.5}$$

which, when combined with Eqs. (3.3,3.4) with matrix multiplication, leads to a simplified mixing matrix,

$$V \to \begin{pmatrix} c_1 & -s_1 & 0 \\ s_1 c_2 & c_1 c_2 & s_2 \\ s_1 s_2 & c_1 s_2 & -c_2 \end{pmatrix} . \tag{3.6}$$

So we see that performing a suitable phase rotation is equivalent to setting $\theta_3 = 0$. For the rest of the chapter, we use this convention to eliminate θ_3.

We take as inputs to our scans,

$$v = 246\ GeV, m_1 = 125\ GeV, m_2, m_3, \theta_1, \theta_2, \delta_2, \delta_3, d_1, d_2, d_3, e_1, e_2 \tag{3.7}$$

where δ_3, d_1, d_3, e_1 and e_2 can be complex and are defined in Eq. (3.1).

The SM-like Higgs boson is identified with h_1 with $m_1 = 125\ GeV$. The couplings of h_1 to SM particles are suppressed by a factor c_1 relative to the SM rate. The states are ordered according to their couplings to SM particles. h_1 has the strongest couplings to SM particles, h_2 couplings are suppressed by $s_1 c_2$ relative to the SM couplings, and h_3 couplings are the smallest, and are suppressed by $s_1 s_2$ relative to SM couplings. The mass ordering of h_2 and h_3 is arbitrary. At the time of the original analysis, the ATLAS experiment restricted the value of c_1 to be,

$$c_1 = \mid V_{11} \mid > \ 0.94\,, \tag{3.8}$$

at 95% confidence level using Run-1 Higgs coupling fits[60]. Similarly, a global fit to Higgs coupling strengths by CMS and ATLAS[61],

$$\mu = 1.09 \pm .11\,, \tag{3.9}$$

yielded an identical limit on c_1. A similar analysis was performed in Ref. [120] with more recent experimental limits with similar results.

3.2 Limits from Perturbativity, Oblique Parameters and Unitarity

The parameters of the model must satisfy constraints from electroweak precision measurements, searches for heavy Higgs bosons, and limits from perturbative unitarity, along with the restrictions from single Higgs production discussed in the previous section. The oblique parameters quantify the deviation of EW precision measurements from SM predictions, and are a way to constrain BSM models. Fits to the oblique parameters place strong limits on

the allowed scalar masses and mixings. Analytic results for a model with 2 additional scalar singlets are given in Ref. [82]. For $m_i >> M_W, M_Z$, the approximate contributions are ,

$$\begin{aligned}
\Delta\mathcal{S} &\sim (1- \mid V_{11} \mid^2)\mathcal{S}_{SM} + \frac{1}{12\pi}\Sigma_{i=1,2,3} \mid V_{i1} \mid^2 \log\left(\frac{m_i^2}{m_1^2}\right) \\
\Delta\mathcal{T} &\sim (1- \mid V_{11} \mid^2)\mathcal{T}_{SM} - \frac{3}{16\pi c_W^2}\Sigma_{i=1,2,3} \mid V_{i1} \mid^2 \log\left(\frac{m_i^2}{m_1^2}\right) \\
\Delta\mathcal{U} &\sim (1- \mid V_{11} \mid^2)\mathcal{U}_{SM} \, . \qquad (3.10)
\end{aligned}$$

The restrictions from the oblique parameters[121] on $V_{21} = s_1 c_2$ for the minimum value of $c_1 = .94$ allowed by single Higgs production are shown on the LHS and for $c_1 = .96$ on the RHS of Fig. 3.1. TeV scale masses require quite small values of V_{21}, which is the parameter that determines the coupling of h_2 to SM particles. The flat portions of the curves for small m_2 in Fig. 3.1 represent the imposed limit on θ_1 from single Higgs production. As this limit becomes stronger, the limits from oblique parameters becomes less and less relevant. As the h_1 couplings become more and more SM-like ($\theta_1 \to 0$), the allowed coupling of h_2 to SM particles becomes highly suppressed. The constraints from the oblique parameters shown in Fig. 3.1 are consistent with those obtained in the real singlet model in Ref. [84]. For the values of θ_2 allowed by Fig. 3.1, the direct searches, $pp \to h_2(h_3) \to W^+W^-$ do not provide additional restrictions on V_{21}[122, 63].

In the real singlet model, much stronger constraints are placed on the parameters from the W boson mass than from the oblique parameters[123, 86]. For example, in the real singlet model for $m_2 = 1\ TeV$, the W mass measurement requires $\mid V_{21} \mid < .19$. For $\theta_2 = 0$, h_3 does not couple to SM particles and the results of Refs. [123, 86] can be applied directly to the complex singlet case. The results of Ref. [86] are shown in Fig. 3.2. The calculation of the limit from the W mass in the complex singlet model for non-zero θ_2 is beyond the scope of this chapter and involves contributions from all 3 Higgs bosons and could potentially yield interesting limits. The limits from the oblique parameters in the complex singlet case, (Fig. 3.1), demonstrates that the dependence of the limits on m_3 is non-trivial.

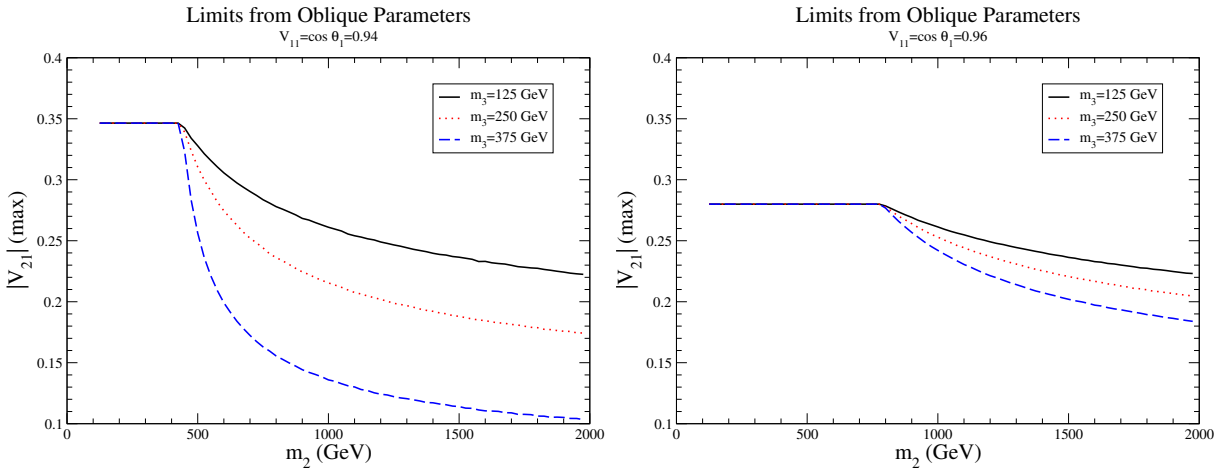

Figure 3.1: Limits on m_2 for allowed couplings of h_1 to SM particles[$\cos\theta_1 = .94$ (LHS) and $\cos\theta_1 = .96$ (RHS)] for various values of m_3 using the oblique parameter $(\mathcal{S},\mathcal{T},\mathcal{U})$ limits of Ref. [121].

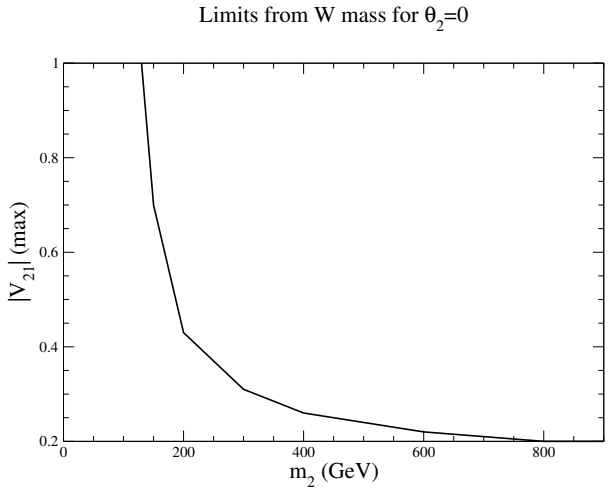

Figure 3.2: Maximum allowed value of V_{21} from the W mass measurement as a function of m_2 in the real singlet model and in the complex singlet model with $\theta_2 = 0$ from Ref. [86].

The quartic couplings in the potential are strongly limited by the requirement of perturbative unitarity of the $2 \to 2$ scattering processes[124]. We compute the $J = 0$ partial waves, a_0, in the high energy limit where only the quartic couplings contribute and require $\mid a_0 \mid < \frac{1}{2}$. The contributions from the trilinear couplings are suppressed at high energy and do not contribute in this limit. For example, we find the restriction from the process, $(SS)/\sqrt{2} \to (SS)/\sqrt{2}$,

$$Re(d_1 + d_2 + d_3) \lesssim 32\frac{\pi}{3}\,. \tag{3.11}$$

Similarly, from $hS \to hS$, we find,

$$Re(\delta_2 + \delta_3) \lesssim 16\pi\,. \tag{3.12}$$

Looking at the eigenvectors for neutral CP even scattering processes,

$$\left\{\omega^+\omega^-\,, \frac{zz}{\sqrt{2}}\,, \frac{hh}{\sqrt{2}}\,, hS\,, hA\,, \frac{SS}{\sqrt{2}}\,, \frac{AA}{\sqrt{2}}\,, AS\right\}, \tag{3.13}$$

($\omega^\pm, z$ are the Goldstone bosons), we find the generic upper limits on the real and imaginary quartic couplings,

$$\begin{aligned} Re(d_i), Im(d_i) \;&\lesssim\; \frac{32\pi}{3}\,, i = 1,2,3 \\ \delta_2, Re(\delta_3), Im(\delta_3) &\lesssim 16\pi\,. \end{aligned} \tag{3.14}$$

These upper limits are conservative bounds, and more stringent bounds are obtained from looking at the eigenvalues of the 8 by 8 scattering matrix. These upper bounds on the parameters involve finding solutions to higher order polynomials and do not have simple analytic solutions. Thus, the bounds from perturbative unitarity are determined numerically and imposed in the scans of the next section.

The trilinear Higgs couplings depend on the scalar masses and could potentially become

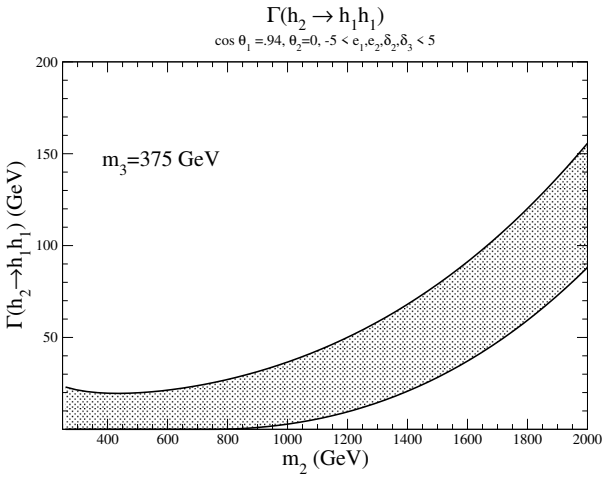

Figure 3.3: Decay width for $h_2 \to h_1 h_1$ when all parameters are taken real and δ_2 and δ_3 are scanned over.

large. In the limit of small mixing, $\theta_1 << 1$ and $\theta_2 = 0$, the $h_2 h_1 h_1$ coupling is,

$$\lambda_{211} \to \sin\theta_1 \left\{ \frac{2m_1^2}{v}\left(1 + \frac{m_2^2}{2m_1^2}\right) - v\left(\delta_2 + Re(\delta_3)\right)\right\}, \text{ small angle limit} \tag{3.15}$$

and we see that the growth of λ_{211} with large m_2 is mitigated by the $\sin(\theta_1)$ suppression. The decay width for $h_2 \to h_1 h_1$ is[96],

$$\Gamma(h_2 \to h_1 h_1) = \frac{\lambda_{211}^2}{32\pi m_2}\sqrt{1 - \frac{4m_1^2}{m_2^2}}\,. \tag{3.16}$$

In Fig. 3.3, we have taken all parameters real and scanned over $-5 < \delta_2, \delta_3 < 5$ for fixed m_3, θ_1 and θ_2. The dependence on e_1 and e_2 is minimal in the small angle limit, as demonstrated in Eq. (3.15). In all cases, we have $\Gamma(h_2 \to h_1 h_1) << m_2$, showing that there is no problem with the trilinear couplings becoming non-perturbative in the small angle limit. Increasing the range we scan over changes the numerical results, but $\Gamma(h_2 \to h_1 h_1)/m_2$ is always $<< 1$.

Finally, we require that the parameters correspond to an absolute minimum of the potential. This has been extensively studied for the real singlet model in Refs. [26, 47, 117] and analytic results derived. For the case of the complex singlet, we scan over parameter space for numerically allowed values of the parameters[118] and do not obtain an analytic

solution.

3.3 Results

In the limit of $\theta_2 \to 0$, (as suggested by the single Higgs rates), the scalar h_3 does not couple directly to SM particles and it can only be observed through double Higgs production. We will consider h_3 to be in the $100 - 400\ GeV$ mass range. The largest production rate at the LHC is through the resonant process $gg \to h_2 \to h_1 h_3$. The complex singlet model is thus an example of new physics that will first be seen in the study of double Higgs resonances[119, 37]. We perform a scan over the parameters of Eq. (3.7), subject to the restrictions discussed in the previous section[5]. We always fix $c_1 = 0.94$ and consider the 2 cases, $\theta_2 = 0$ and $\theta_2 = \frac{\pi}{12}$.

For the allowed parameter space, we compute the amplitude for $gg \to h_1 h_3$ shown in Fig. 3.4. Analytic results in the context of the MSSM are given in Ref. [125]. We use the central NLO LHAPDF set[126, 127], with $\mu_R = \mu_F = M_{hh}$[6]. In Fig. 3.5, we show the invariant M_{hh} spectrum for resonant $h_1 h_3$ production compared to the SM $h_1 h_1$ spectrum at 13 TeV. The complex singlet model curves are more sharply peaked than those of the SM and demonstrate a significant enhancement of the rate relative to the SM double Higgs rate for the parameters we have chosen. The spectrum has only a small dependence on θ_2, visible at high M_{hh}. We have included a finite width for m_2 in the calculation: For $m_2 = 400\ GeV$ and $m_3 = 130\ GeV$, the width is quite large, $\Gamma_2 = 263\ GeV(\theta = 0)$ and $\Gamma_2 = 295\ GeV(\theta = \pi/12)$. We have included the width using the Breit-Wigner approximation, although typically $\Gamma_2/m_2 \sim \mathcal{O}(\frac{1}{2})$. The shoulder due to the width is clear on the LHS of Fig. 3.4. There is a smaller width for h_2 when m_3 is increased to 250 GeV: $\Gamma_2 = 129\ GeV(\theta = 0)$ and $\Gamma_2 = 137\ GeV(\theta = \pi/12)$ on the RHS of Fig. 3.4. The widths are calculated by scaling the SM results from Ref. [128] with the appropriate mixing angles and adding the relevant widths $h_i \to h_j h_k$.

In Figs. 3.6 and 3.7, we show mass regions where the rate for $h_1 h_3$ production is signif-

[5]For the complex singlet model with a $U(1)$ symmetry, a comparable scan can be performed using the program ScannerS[117].

[6]$M_{hh} \equiv (p_{h_1} + p_{h_3})^2$.

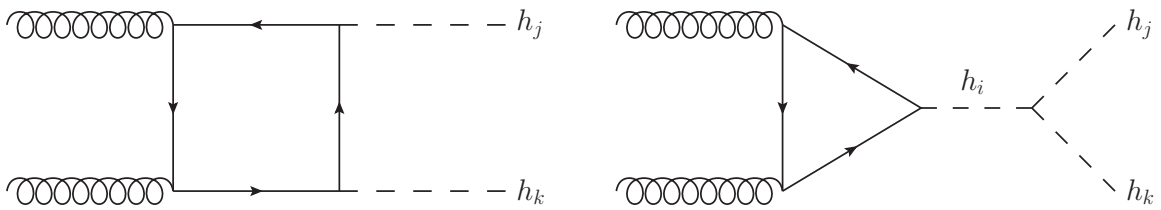

Figure 3.4: Feynman diagrams for the production of $h_j h_k$, $i, j, k = 1, 2, 3$.

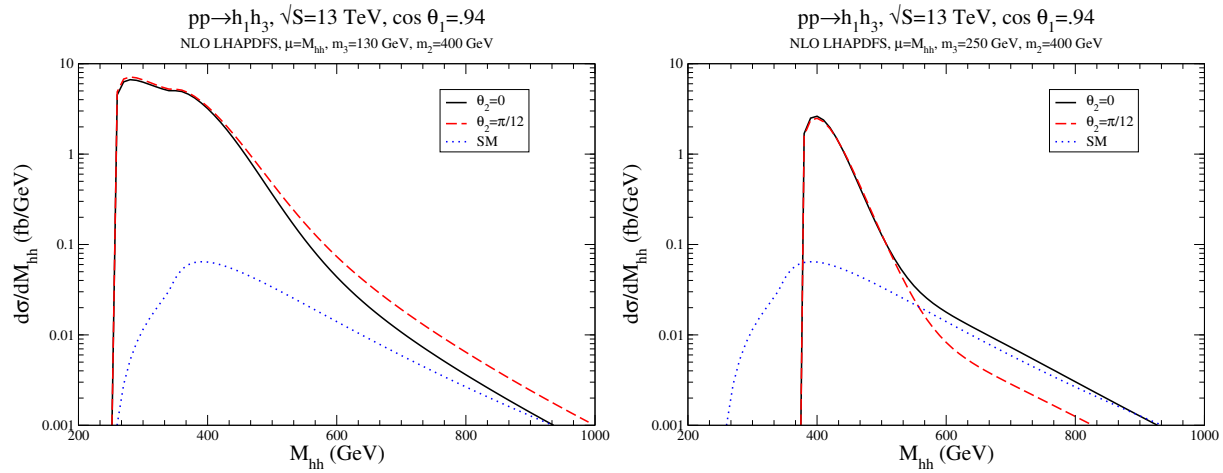

Figure 3.5: M_{hh} spectrum of the complex singlet model production of $h_1 h_3$ from the resonant exchange of h_2. The dominant contribution in the loops is from the top quark.

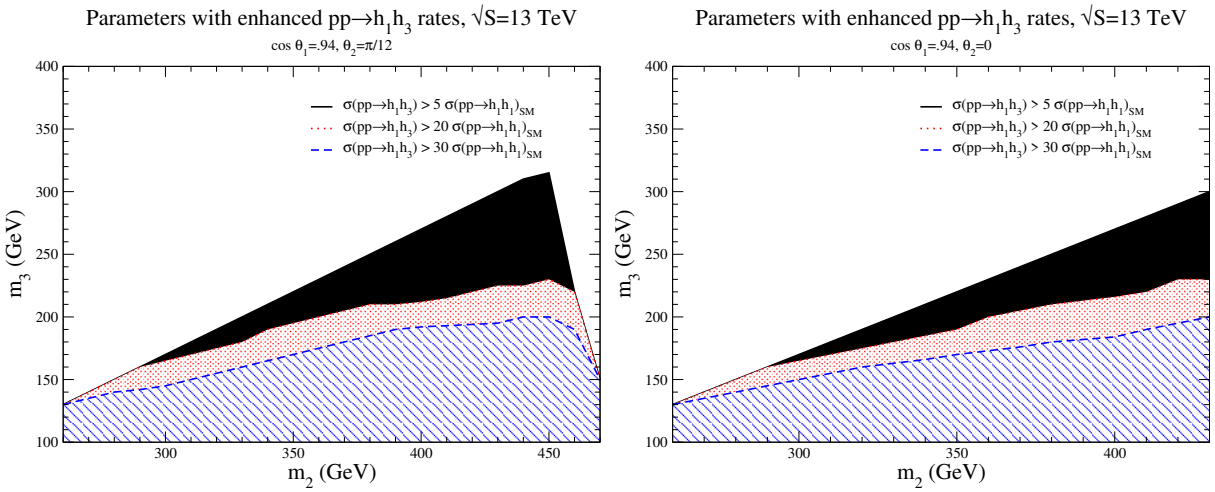

Figure 3.6: Regions of parameter space allowed by limits on oblique parameters, perturbative unitarity, and the minimization of the potential where the rate for h_1h_3 production is significantly larger than the SM h_1h_1 rate at $\sqrt{S} = 13\ TeV$.

icantly enhanced relative to the SM h_1h_1 production. This enhancement can be traced to the relatively large values of the trilinear Higgs couplings defined from Eq. (3.1),

$$\mathcal{V} \to \frac{1}{2}\lambda_{211}h_1^2h_2 + \frac{1}{2}\lambda_{311}h_1^2h_3 + \frac{1}{2}\lambda_{331}h_1h_3^2 + \lambda_{321}h_1h_2h_3 + \cdots , \tag{3.17}$$

that are allowed by the imposed restrictions. In the SM, the hhh coupling is fixed by m_h, whereas here, the trilinear couplings of the potential are relatively unconstrained.

In Fig. 3.8, we show the region of parameter space allowed by limits on the oblique parameters, perturbative unitarity, and the minimization of the potential where the $h_1h_1h_1$ trilinear coupling is greater than 5 times the SM value. This enhancement of the trilinear scalar coupling requires rather light values of m_2 and m_3 as shown in Fig. 3.8. In roughly the same region as shaded in Fig. 3.8, the $h_2h_1h_1$ and $h_3h_2h_1$ couplings are 8 times the SM $h_1h_1h_1$ coupling. This enhancement is consistent with the results of Ref. [91] in the complex singlet model with a global $U(1)$ symmetry imposed on the potential. The cut-offs on the high m_2 ends of the plots on the LHS in Figs. 3.6 and 3.7 are due to the oblique parameter restrictions in the non-zero θ_2 mixing scenario. The same results for $\sqrt{S} = 27$ and 100 TeV are shown in Fig. 3.7. At all energies there is a significant region of phase space where the

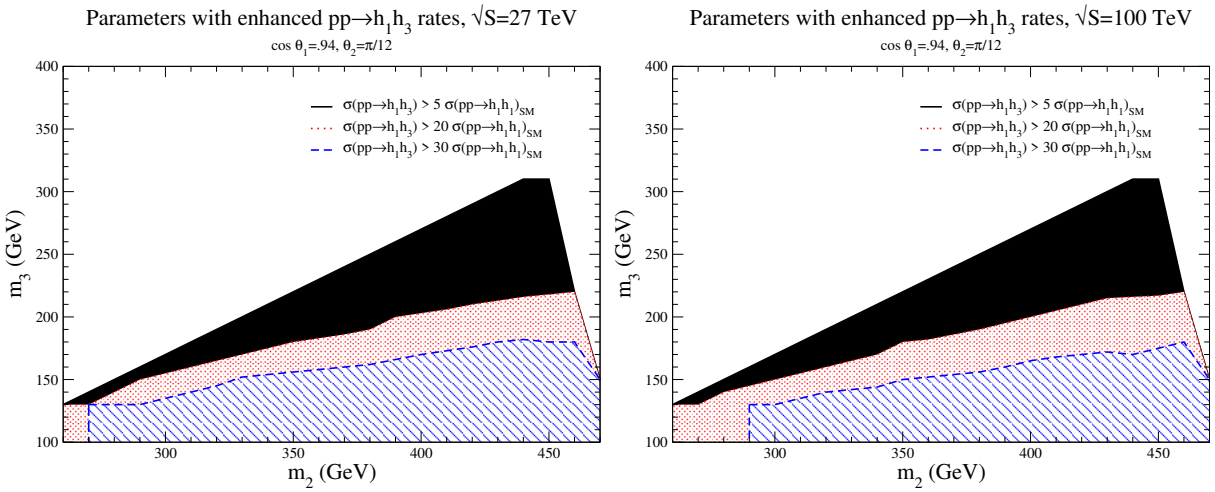

Figure 3.7: Regions of parameter space allowed by limits on oblique parameters, perturbative unitarity, and the minimization of the potential where the rate for h_1h_3 production is significantly larger than the SM h_1h_1 rate at $\sqrt{S} = 27\ TeV$ and $100\ TeV$.

h_1h_3 rate is large, relative to SM double Higgs production.

For $m_3 > 250\ GeV$, the dominant decay chain from h_1h_3 production will be $h_1h_3 \to h_1h_1h_1 \to (b\bar{b})(b\bar{b})(b\bar{b})$. For $m_3 < 2m_1$, h_3 will decay through the extremely small couplings to SM particles and through the off-shell decay $h_3 \to h_1h_1^* \to h_1f\overline{f}$ and will be extremely long lived. In the limiting case where $\theta_2 = 0$, the only allowed decay for h_3 is the off-shell decay chain through the couplings to h_1.

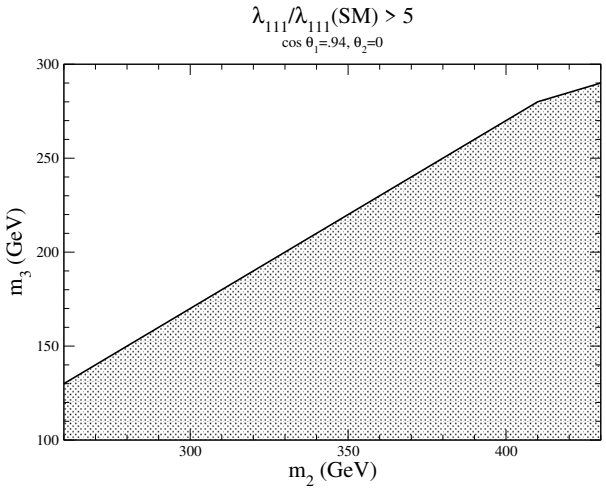

Figure 3.8: Region of parameter space allowed by limits on oblique parameters, perturbative unitarity, and the minimization of the potential where the $h_1h_1h_1$ trilinear coupling is greater than 5 times the SM value.

Chapter 4

Baryon Asymmetry from Three Higgs Doublets[7]

We now propose a more complicated extension of the SM scalar sector. We supplement the SM field content with two additional Higgs doublets with small vevs. While these fields will have a marginal role in EWSB, they could have significant complex-valued couplings to the SM fermions and provide new sources of CP violation.

Despite the success of the SM, the source of the baryon asymmetry of the universe (BAU) - of great importance to our understanding of cosmology and matter - remain open problems. It is reasonable to expect that the physics underlying the BAU must have direct and perhaps significant interactions with the SM. We will show that this model with three Higgs doublets is capable of accommodating a baryogenesis mechanism, as long as the new Higgs masses are at or above the TeV scale.

Our basic mechanism is in spirit similar to leptogenesis [129], however we do not require heavy right-handed neutrinos ν_R far above the weak scale, whose role will be assigned to the new Higgs scalars here. We will choose right-handed neutrino masses in the $\sim$ 0.1-10 TeV range to implement our scenario. Our proposal is a minimal realization of "neutrinogenesis" [130, 131]. The SM extended to include a total of three Higgs doublets can then explain the origin of visible matter and the masses of fundamental particles. This setup can be potentially testable at colliders in the future, perhaps even at the High-Luminosity LHC (HL-LHC) with $\mathcal{O}(\text{ab}^{-1})$ levels of data, expected to be available in the coming years.

Next we will briefly outline our mechanism and describe the main ingredients and assumptions underlying our proposal. We will then illustrate the mechanism in a benchmark

[7]This chapter is based on Ref. [28], which is ©2020 American Physical Society

realization of the model and provide some quantitative estimates. A brief discussion of the benchmark collider phenomenology will also be given, in order to highlight some of the key features of the possible signals. For some related ideas in a different context, see Refs. [132, 133].

4.1 The Baryogenesis Mechanism

Here, we briefly describe the general features of the baryogenesis mechanism. Let us denote the Higgs fields by H_a with masses m_a, $a = 1, 2, 3$. We will identify H_1 as the observed ("SM") Higgs with $m_1 \approx 125$ GeV: $H_1 \leftrightarrow H_{\rm SM}$. This implies that H_1 has the same Yukawa interactions as the SM Higgs and generates the known masses of fermions. Also, it is implicitly assumed that new interactions of H_1 with other scalars are sufficiently small to avoid significant deviations from the SM predictions for the main Higgs production and decay modes. To make contact with potential experimental searches, we will generally assume that $m_{2,3} \sim 1$ TeV (this mass scale may also originate from the physics underlying the SM Higgs sector, though we will not dwell on this point further).

In order to generate a baryon asymmetry, we need an asymmetry in the decays of H_i and H_i^* into SM fermions which will lead to an asymmetry in the number density of the SM fermions. The total decay rates of H_i and H_i^* are equal by CPT. However, the partial decay rates of H_i and H_i^* do not have to be equal. Hence, to generate an asymmetry ε, we need at least two different decay channels for the new scalars. We will specify those interactions later, however, here we will only mention that one of the channels is $\bar{L}\nu_R$ (which we will refer to as "neutrinos"), with L a lepton doublet in the SM.

Nonperturbative EW processes, called sphalerons, violate baryon number and lepton number by 3 units each. Although ν_R is a lepton, it is a gauge singlet. Hence, sphalerons will not operate on ν_R. The relevant non-zero $\Delta(B - L)$ is then for quark and lepton doublets; where B is baryon number and L is lepton number. That is, sphalerons will not act on an asymmetry in ν_R nor alter the baryon asymmetry generated via the lepton

doublets [130, 131]. The other channel is provided by coupling to SM charged fermions. The asymmetry requires a non-zero CP violating phase to remain in the interference of tree and 1-loop diagrams; this in turn requires at least two Higgs scalars that couple to leptons and quarks, implying that we at least need H_2. Below, we will illustrate why we also need H_3, on general grounds. However, briefly put, since the H_1 mass is at the EW scale and not larger than the reheat temperature, it could efficiently mediate processes that washout the baryon asymmetry. Hence, we need three Higgs doublets.

Let us denote a typical Higgs coupling to $\bar{L}\,\nu_R$ by λ_a^ν and to charged fermions by λ_a^f. For concreteness and simplicity, we will assume that the asymmetry is dominated by the f intermediate fermion, but the width of H_2 is set by decays into the fermion f'. This assumption implies $\lambda_2^{f'}$ is the dominant Yukawa coupling of H_2; we consider this a fairly generic assumption. The asymmetry, as will be discussed later in more detail, is typically then given by

$$\varepsilon \sim \frac{\lambda_1^\nu \lambda_1^f \lambda_2^\nu \lambda_2^f}{8\pi\,(\lambda_2^{f'})^2}. \tag{4.1}$$

On general grounds, an asymmetry parameter of order $\varepsilon \gtrsim 10^{-9}$ is needed to generate the BAU [134]

$$\frac{n_B}{s} \approx 9 \times 10^{-11}\,, \tag{4.2}$$

where n_B is the baryon number density and s is the entropy density.

Here, we note that the success of our baryogenesis scenario requires that $2 \to 2$ processes $Ff \to L\nu_R$, where F is an $SU(2)_L$ doublet and f an $SU(2)_L$ singlet, through the interactions of H_1 should not washout the generated $\Delta(B-L)$. This requirement should be maintained down to a temperature of $T_* \sim 100$ GeV, below which EWSB takes place. Above that temperature all SM fields, except the Higgs, can be assumed to be massless. Hence, the rate for washout at $T = T_*$ is roughly given by $\Gamma_* \sim (\lambda_1^\nu \lambda_1^f)^2 T_*$. Requiring that $\Gamma_* \lesssim H(T_*)$,

where $H(T) \approx g_*^{1/2} T^2/M_P$ is the Hubble scale, one finds

$$\lambda_1^\nu \lambda_1^f \lesssim \left(\frac{g_*^{1/2} T_*}{M_P} \right)^{1/2} , \tag{4.3}$$

where $g_* \sim 100$ denotes relativistic degrees of freedom and $M_P \approx 1.2 \times 10^{19}$ GeV is the Planck mass. The above yields $\lambda_1^\nu \lambda_1^f \lesssim 10^{-8}$.

To generate the asymmetry parameter in Eq. (4.1), there are three interesting cases for the relative strengths of the different H_2 couplings:

1. First consider $\lambda_2^\nu \lambda_2^f \ll (\lambda_2^{f'})^2$. The washout bound then implies $\varepsilon \ll 4 \times 10^{-10}$, which suggests that baryogenesis is not feasible.

2. Next, $\lambda_2^\nu \ll \lambda_2^f \sim \lambda_2^{f'}$. The washout bound together with $\varepsilon \gtrsim 10^{-9}$ then implies that

$$\lambda_2^\nu \gtrsim 2.8\, \lambda_2^f. \tag{4.4}$$

   This bound is inconsistent with our starting assumption implying that a baryon asymmetry cannot be generated with this hierarchy of couplings. The results are similar for $\lambda_2^f \ll \lambda_2^\nu \sim \lambda_2^{f'}$.

3. Finally, assume all couplings are similar $\lambda_2^f \sim \lambda_2^\nu \sim \lambda_2^{f'}$. The washout bound implies that $\varepsilon \lesssim 4 \times 10^{-10}$. That is, baryogenesis is still not feasible.

This conclusion leads us to require a third Higgs doublet field H_3, to avoid reliance on a light H_1, whose interactions are constrained[8].

Successful baryogenesis requires that the reheat temperature T_{rh}, here assumed to be set by the decay of a modulus Φ, is low enough that $2 \to 2$ washout processes mediated by H_a, $a = 2, 3$, are also inefficient. Note however that we need $T_{rh} > 100$ GeV to have effective electroweak sphaleron processes that are required to provide a source of baryon number

[8]See Refs. [135, 136] for another minimal realization of BAU generation via Higgs decays that relies on highly degenerate Majorana neutrino masses.

violation. Since $T_{rh} < m_a$, for out of equilibrium decay of H_a, the rate for this process is of order $(\lambda_a^f \lambda_a^\nu)^2 T_{rh}^5/m_a^4$. This production rate must be less than the Hubble scale $H(T_{rh})$. We thus obtain

$$(\lambda_a^f \lambda_a^\nu)^2 \lesssim \frac{g_*^{1/2} m_a^4}{M_P T_{rh}^3} \quad ; \quad \text{(no washout)}. \tag{4.5}$$

For $T_{rh} \gtrsim 100$ GeV and $m_a \sim 1$ TeV, we roughly obtain $\lambda_a^f \lambda_a^\nu \lesssim 10^{-6}$. Note that this constraint is much less stringent than the one obtained for H_1 before, which could in principle allow a large enough value of ε, using H_2 and H_3.

As a proof of concept that such a low reheat is possible, consider the decay of a modulus Φ. At an early time, the universe was in a matter dominated era due to the oscillation of Φ. These oscillations are damped via the Φ decays and the universe enters a radiation dominated era. The reheat temperature T_{rh} of the radiation dominated era is estimated as $H(T_{rh}) \sim \Gamma_\Phi$, where Γ_Φ is the total width of the modulus and $H(T_{rh})$ is the Hubble parameter at the reheat temperature. Assuming that Φ couples to a Higgs doublet via the interaction $(\Phi/\Lambda) D_\mu H_i^\dagger D^\mu H_i$, the decay width of Φ is then

$$\Gamma(\Phi) \sim \frac{1}{32\pi} \frac{m_\Phi^3}{\Lambda^2} \tag{4.6}$$

Then the reheat temperature is estimated as

$$T_{rh} \sim \left(\frac{1}{32\,\pi\, g_*^{1/2}} \frac{m_\Phi^3\, M_P}{\Lambda^2} \right)^{1/2}. \tag{4.7}$$

For a modulus mass $m_\Phi \sim 100$ TeV and cut off scale 3×10^{10} TeV, we find a reheat temperature of $T_{rh} \sim 100$ GeV.

Before going further, we will point out an issue that will inform our benchmark model parameter choices later in this chapter. The light neutrino masses m_ν are generated via

integrating out the heavy Majorana neutrinos to create the Weinberg operator:

$$(\lambda_1^\nu)^2 \frac{(LH_1)^2}{m_R}. \tag{4.8}$$

The expression for m_ν is given by

$$m_\nu \sim \frac{(\lambda_1^\nu)^2}{2} \frac{v_{EW}^2}{m_R}\,, \tag{4.9}$$

where $v_{EW} = 246$ GeV. Eq. (4.3) for $f = t$ (the top quark, with $\lambda_t \approx 1$), leads to $\lambda_1^\nu \lesssim 10^{-8}$. Assuming $m_\nu \sim 0.1$ eV, we then find

$$m_R \lesssim 10 \text{ MeV}. \tag{4.10}$$

The above bound on m_R is in conflict with our assumption that the new physics, including ν_R, is at or somewhat above the weak scale. We will address this question later, showing that certain choices of parameters in the minimal model can avoid this conflict. Briefly put, the resolution will amount to the minimal assumption that there are only two massive SM neutrinos around ~ 0.1 eV and that the third eigenstate could be much lighter and nearly massless, given the current state of knowledge of neutrino parameters.

Let us now briefly outline how the above set of three Higgs fields can lead to a viable baryogenesis mechanism. We will assume that a population of (H_3, H_3^*) is produced non-thermally, such as through the modulus Φ decay in the early universe, but no significant population of (H_2, H_2^*) is present; this could be a result of preferential Φ decay (see for example, Ref. [137], for such a possibility in a different model). The CP violating decays of H_3 then generate a non-zero $B - L$ number from $H_3 \to \bar{L}\nu_R$. The asymmetry $\Delta(B - L)$ can get processed into a ΔB and ΔL through electroweak sphaleron processes that are active at temperatures $T \gtrsim 100$ GeV.

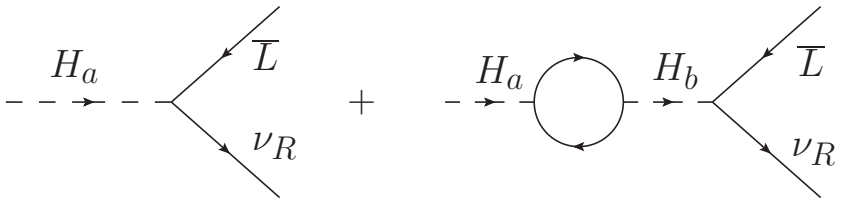

Figure 4.1: Representative tree level and one-loop diagrams that can give rise to a lepton asymmetry.

4.2 The general model

Here we will introduce the general structure of the model that could realize the above baryogenesis mechanism. We will not write down all the possible interactions that the model could contain and only specify those that are key for our discussions. To generate the BAU in the manner described above, let us consider the following Yukawa interactions for the three Higgs doublets

$$\lambda_a^u \tilde{H}_a^* \bar{Q}\, u + \lambda_a^d H_a^* \bar{Q}\, d + \lambda_a^\nu \tilde{H}_a^* \bar{L}\, \nu_R + \lambda_a^\ell H_a^* \bar{L}\, \ell\,, \tag{4.11}$$

where a labels the Higgs scalars, but the implicit fermion generation indices have been suppressed. In the above, λ_a^u and λ_a^d denote couplings associated with the up-type and down-type quarks; the corresponding couplings to neutrinos and charged leptons are denoted by λ_a^ν and λ_a^ℓ.

Let us focus on $a = 2, 3$. The $\Delta(B-L)$ asymmetry ε produced in the out-of-equilibrium decay of H_a is then given by

$$\varepsilon \equiv \frac{\Gamma(H_a \to \bar{L}\nu_R) - \Gamma(H_a^* \to \bar{\nu}_R L)}{2\Gamma(H_a)}, \tag{4.12}$$

where $\Gamma(H_a)$ is the total width of H_a. The above is obtained from the interference of the tree and loop-level diagrams in Fig.4.1. A second "triangle" loop diagram is in general present in our model, but the "bubble" loop diagram gets enhanced if the heavy Higgs states H_2

and H_3 are degenerate in mass (similar arguments apply to heavy right-handed neutrinos in leptogenesis; see for example Refs. [138, 139, 140]).

We will consider the case where the heavy Higgs bosons H_2 and H_3 are mildly degenerate and hence we can mostly ignore the "triangle" contribution to the asymmetry in Fig.4.1. Additionally, since our calculation of the baryon asymmetry is an order of magnitude estimation, this approximation is sufficient to show the viability of our mechanism. For complete expressions see Ref. [130]. This assumption simplifies the treatment and also leads to potentially richer collider phenomenology, as both H_2 and H_3 can, in principle, be experimentally accessed. In this case, the model will yield more easily to direct experimental verification.

From Eq. (4.11), we find

$$\varepsilon = \frac{1}{8\pi} \sum_{b \neq a} \frac{m_a^2}{m_b^2 - m_a^2} \frac{\sum_{f=\ell,u,d} N_{c,f} \, \mathrm{Im} \left(\mathrm{Tr}_{ba}^{\nu} \mathrm{Tr}_{ba}^{f*} \right)}{\sum_{f=\ell,u,d,\nu} N_{c,f} \mathrm{Tr}_{aa}^{f}} \tag{4.13}$$

where

$$\mathrm{Tr}_{ba}^{f} = \mathrm{Tr} \left[\lambda_b^{f\dagger} \lambda_a^{f} \right], \tag{4.14}$$

$$\mathrm{Tr}_{ba}^{\nu} = \mathrm{Tr} \left[\lambda_b^{\nu\dagger} \lambda_a^{\nu} (1 - m_R^2/m_a^2)^2 \right], \tag{4.15}$$

m_R are the masses of the right-handed neutrinos, and $N_{c,f} = 1, 3$ for $f =$ lepton, quark, respectively. The trace in Eqs. (4.14,4.15) is over the fermion generations and we are working in the basis in which m_R are diagonal mass matrices. Note that $m_f = 0$ during the epoch where ε is set, since electroweak symmetry is not broken at that point. As these are traces, the asymmetry parameter in Eq. (4.13) can be evaluated in any fermion basis.

In order to find the baryon asymmetry ΔB, we need to find the relationship between $\Delta(B-L)$ and ΔB in our model, at $T \gtrsim 100$ GeV. We note that our setup is that of the SM augmented by two new doublets, however the new doublets are assumed heavy compared to T_{rh} and the relevant field content is that of the SM only. Also, the processes involving ν_R

are decoupled at these temperatures, as a requirement in our scenario. Using the results of Ref. [141] we then have

$$\Delta B = \frac{28}{79}\,\Delta(B-L). \tag{4.16}$$

We will focus on H_3 decays, and only consider an intermediate H_2. That is, $a = 3$ and $b = 2$ in Eq. (4.13). Given that $\Delta(B-L)$ is generated through the decay of H_3, to calculate the BAU we need to consider the initial energy density ρ_3 of H_3 compared to the radiation energy density ρ_R. In our setup, the radiation is made up of all the SM states, including H_1. The decays of H_3 contribute to reheating the universe. Since $E_3 n_3 \leq \rho_R$, with n_3 the number density of H_3 and E_3 the energy of H_3 from decays of the modulus Φ in Eq. (4.6), the ratio

$$r \equiv \frac{E_3 n_3}{\rho_R}, \tag{4.17}$$

satisfies $r \leq 1$.

We have $\rho_R = (\pi^2/30) g_* T^4$, where g_* is the number of relativistic degrees of freedom, which is $g_* = 106.75$ in the SM. The $B-L$ abundance is then given by

$$\frac{n_{B-L}}{s} = \frac{3\,r\,T_{rh}\,\varepsilon}{4\,E_3}, \tag{4.18}$$

where the entropy density $s = (2\pi^2/45) g_* T^3$. Using Eq. (4.16) we then obtain for the BAU

$$\frac{n_B}{s} = \frac{21}{79}\left(\frac{r\,T_{rh}\,\varepsilon}{E_3}\right). \tag{4.19}$$

As shown in Eq. (4.7), for a modulus $m_\Phi \sim 100$ TeV, we can accommodate a reheat temperature of $T_{rh} \sim 100$ GeV. Then the energy of H_3 is $E_3 \sim 50$ TeV and $T_{rh}/E_3 \sim 2 \times 10^{-3}$. Hence, for $r \lesssim 1$, one then requires $\varepsilon \gtrsim 2 \times 10^{-7}$ to generate the BAU.

To show that all the conditions on washout and BAU can be met, we choose a parameter point for proof of concept:

$$
\begin{aligned}
&m_\Phi = 100 \text{ TeV} && m_3 = 1.5 \text{ TeV} \\
&\lambda_2^\ell \sim 1 && \lambda_2^\nu \sim 2 \times 10^{-6} \\
&\lambda_3^\ell \sim 1.4 \times 10^{-3} && \lambda_3^\nu \sim 1.4 \times 10^{-3}
\end{aligned}
\tag{4.20}
$$

where m_Φ is the mass of the modulus that generates the H_3 population and reheats the universe, see Eqs. (4.6,4.7). Additionally, we will assume H_2 and H_3 only couple to charged leptons and neutrinos. This assumption and these values for the Yukawas will be motivated in the flavor model presented in the next section. First, the values of $\lambda^\ell_{2,3}$ and $\lambda^\nu_{2,3}$ satisfy the wash-out condition of Eq. (4.5): $|\lambda^\ell_a \lambda^\nu_a| \lesssim 2.1 \times 10^{-6}$. Second, we must check that we can produce the correct BAU, i.e. $\varepsilon \gtrsim 2 \times 10^{-7}$. From Eq. (4.13) we have

$$
\varepsilon = \frac{1}{8\pi} \frac{m_3^2}{m_2^2 - m_3^2} \frac{|\lambda^\ell_2 \lambda^\nu_2 \lambda^\ell_3 \lambda^\nu_3| \sin\phi}{|\lambda^\ell_3|^2 + |\lambda^\nu_3|^2} \sim \frac{4 \times 10^{-8}}{(m_2/m_3)^2 - 1}, \tag{4.21}
$$

where ϕ is a generic CP phase. For 10% level degeneracy between the masses $m_2 \sim 1.1 m_3$ and order one phases, the asymmetry parameter is $\varepsilon \sim 2 \times 10^{-7}$ and the BAU can be generated. This level of degeneracy is consistent with our assumption that the diagram in Fig. 4.1 is the dominant contribution to the calculation of ε.

Finally, since H_3 decays are populating the baryon asymmetry, we must check that they decay much quicker than they annihilate away. The annihilation rate of H_3 is calculated by weighting the annihilation cross section, $\sigma_{ann}(H_3)$, by the number density, n_3, of H_3 in the early universe:

$$
\Gamma_{ann}(H_3) \;=\; \sigma_{ann}(H_3) n_3. \tag{4.22}
$$

We assume H_3 couples to one lepton generation with strength 1.4×10^{-3} and the quartic couplings with the other Higgses are of order 0.1. We implement our model into `FeynRules` [142] and output model files for `MadGraph5_aMC@NLO` [143]. The H_3 are produced via the decay

of a modulus with mass of 100 TeV. Hence, they have energies of 50 TeV. The annihilation cross sections for 50 TeV H_3 into fermions, gauge bosons, and scalars are found to be

$$\begin{aligned} \sigma_{ann}(\text{fermions}) &= 0.43 \text{ fb}, \\ \sigma_{ann}(\text{gauge bosons}) &= 0.24 \text{ fb}, \\ \sigma_{ann}(\text{scalars}) &= 0.17 \text{ fb} \end{aligned} \tag{4.23}$$

and the total annihilation rate of H_3 is

$$\Gamma_{ann} \lesssim 1.5 \times 10^{-7} \text{ GeV}, \tag{4.24}$$

assuming $r \leq 1$ and using Eq. (4.17). The boosted decay rate into one lepton generation with H_3 mass 1.5 TeV is

$$\Gamma(H_3 \to SM) = \frac{(\lambda_3^\ell)^2}{16\pi}\frac{m_3}{\gamma} = 1.8 \times 10^{-6} \text{ GeV}, \tag{4.25}$$

where $\gamma = E_3/m_3$ is the boost factor. Hence, the annihilation rate is an order of magnitude smaller than the decay rate, showing the viability of our scenario.

The couplings of H_3 are highly constrained by the combination of washout condition and the creation of a large ε in Eq. (4.21). To maximize Eq. (4.21), we need to $\lambda_3^\ell \sim \lambda_3^\nu$. Together with the washout condition this creates the bound $\lambda_3^{\ell,\nu} \lesssim 1.4 \times 10^{-3}$. The couplings of H_2 are not so tightly constrained and can be generically larger than those of H_3. Hence, the above model could easily lend itself to collider searches. In particular, if the couplings to quarks are not too small, one of the heavy Higgs states could be produced at the LHC or a future hadron collider. Also, depending on the size of the parameters, the rate for decay into charged leptons, a final state with missing energy, or displaced vertices may be large enough to enable clean searches. While there are too many possibilities to consider, we will examine a sample benchmark flavor structure choice and describe the main aspects of its

phenomenology, below.

4.3 A benchmark model of flavor

Now we give a more complete model of flavor to show our leptogenesis mechanism can work in realistic scenarios. We introduce three Higgs doublets Φ_1, Φ_2, Φ_3. All three scalar doublets obtain vacuum expectation values $\langle \Phi_i \rangle = v_i/\sqrt{2}$. The Higgs doublets $\Phi_{2,3}$ and lepton doublets L are odd under a $\mathbb{Z}_2$ symmetry while all other fields are even. The Yukawa interactions are then

$$y_1^u \tilde{\Phi}_1^* \bar{Q} u + y_1^d \Phi_1^* \bar{Q} d + \sum_{b=2,3} y_b^\nu \tilde{\Phi}_b^* \bar{L} \nu_R + y_b^\ell \Phi_b^* \bar{L} \ell. \tag{4.26}$$

The organizing principle for the charged fermion flavor is that the largest Yukawa coupling for quarks and charged leptons should be order one. To get the top mass correctly, we need $v_1 \approx v_{EW} = 246$ GeV. If there are no fine cancellations there must also be a hierarchy between the vevs $v_{1,2}$ in order to have order one Yukawa for τ. We would then need $v_2 \sim 2.5$ GeV for $\lambda_a^\tau \sim 1$, while the top quark mass is obtained from the coupling to H_1 with a Yukawa coupling near unity. Since neutrino masses and mixing are rather special and do not follow the patterns of quarks or charged leptons, we do not impose any requirement on their Yukawa couplings. In principle all neutrinos can get their masses from H_2 and one could assume $v_3 \to 0$, though this is not strictly necessary.

Next, we will illustrate how the necessary vev hierarchy can be easily obtained. Allowing for soft-breaking of the $\mathbb{Z}_2$, the relevant terms in the scalar potential are

$$\begin{aligned} &-\mu^2 \Phi_1^\dagger \Phi_1 + m_2^2 \Phi_2^\dagger \Phi_2 + m_3^2 \Phi_3^\dagger \Phi_3 \\ &- \left(\mu_{12}^2 \Phi_1^\dagger \Phi_2 + \mu_{13}^2 \Phi_1^\dagger \Phi_3 + \text{h.c.} \right) + \lambda (\Phi_1^\dagger \Phi_1)^2 + \cdots , \end{aligned} \tag{4.27}$$

where $\cdots$ are additional quartics that are not important to this story[9]. In principle, there is also a $\mu_{23}^2 \Phi_2^\dagger \Phi_3$ term, but it can be removed via a rotation of $\Phi_{2,3}$. This rotation leaves the picture unchanged since $\Phi_{2,3}$ have the same quantum numbers.

For the baryogenesis mechanism to work, we assume the fields $\Phi_{2,3}$ are heavy with $m_2, m_3 \sim 1$ TeV. In order for the $\mathbb{Z}_2$ breaking to be soft and below the highest scales in our theory, we will additionally assume $\mu_{12}, \mu_{13} \ll m_{2,3}$. Once Φ_1 obtains a vev, it induces tadpole terms for $\Phi_{2,3}$. These tadpoles in turn induce vevs in Φ_2 and Φ_3:

$$v_2 \approx v_1 \frac{\mu_{12}^2}{m_2^2} \ll v_1 \text{ and } v_3 \approx v_1 \frac{\mu_{13}^2}{m_3^2} \ll v_1. \tag{4.28}$$

Hence, the tadpole terms give a seesaw where the smallness of $v_{2,3}$ comes from the larger values of the masses $m_{2,3}$. For $m_2 \sim 1$ TeV, $v_2 \sim 2.5$ GeV can be generated with $\mu_{12} \sim 100$ GeV.

In order to relate this model to the baryogenesis mechanism, we need to rotate the gauge eigenbasis $\Phi_{1,2,3}$ into the doublet mass eigenbasis $H_{1,2,3}$. To order $\mu^2/m_{2,3}^2$, this can be accomplished via the rotation

$$\begin{pmatrix} H_1 \\ H_2 \\ H_3 \end{pmatrix} \approx \begin{pmatrix} 1 & \mu_{12}^2/m_2^2 & \mu_{13}^2/m_3^2 \\ -\mu_{12}^2/m_2^2 & 1 & 0 \\ -\mu_{13}^3/m_3^2 & 0 & 1 \end{pmatrix} \begin{pmatrix} \Phi_1 \\ \Phi_2 \\ \Phi_3 \end{pmatrix}. \tag{4.29}$$

From Eq. (4.28), this is precisely the rotation into the Higgs basis such that $\langle H_1 \rangle = v_{EW}/\sqrt{2}$ and $\langle H_2 \rangle = \langle H_3 \rangle = 0$, where $v_{EW}^2 = v_1^2 + v_2^2 + v_3^2 \approx v_1^2$. The Higgs potential is then

$$-\mu^2 H_1^\dagger H_1 + m_2^2 H_2^\dagger H_2 + m_3^2 H_3^\dagger H_3 + \lambda (H_1^\dagger H_1)^2 + \cdots \tag{4.30}$$

That is, $H_{2,3}$ are the doublet mass eigenstates appearing in Eqs. (4.11-4.13), as we desired.

[9] Assuming our hierarchy of scales, we have explicitly checked that the additional quartics make only non-leading contributions to our mechanism.

The Yukawas in Eq. (4.11) are related to those in Eq. (4.26) via

$$\begin{aligned}
&\lambda_1^{u,d} \approx y_1^{u,d}, && \lambda_{2,3}^{u,d} \approx y_1^{u,d} v_{2,3}/v_{EW}, \\
&\lambda_1^{\ell} \approx y_2^{\ell} v_2/v_{EW}, && \lambda_{2,3}^{\ell} \approx y_{2,3}^{\ell}, \\
&\lambda_1^{\nu} \approx (y_2^{\nu} v_2 + y_3^{\nu} v_3)/v_{EW}, && \lambda_{2,3}^{\nu} \approx y_{2,3}^{\nu},
\end{aligned} \tag{4.31}$$

where we have used $v_2 \gg v_3$.

As discussed previously, there is some tension between washout conditions, having heavy right-handed neutrinos, and generating the light neutrino masses $m_\nu \sim 0.1$ eV. We now discuss the neutrino parameters needed to alleviate this tension, supplementing the parameter choices in Eq. (4.20). Other choices of parameters may be possible, yet it suffices for our purposes to provide a particular, but not very special, realization of our model. Let m_{Ri}, with $i = 1, 2, 3$ denote the masses of the three right-handed neutrinos ν_{Ri}. We will assume that $m_{R1,2} \gg m_{2,3}$ and hence the $H_{2,3}$ would not decay into them, while ν_{R3} is light compared to $H_{2,3}$. We will choose $m_{R3} \sim 100$ GeV and $m_{R1,2} \sim 10$ TeV. This means that the generation of asymmetry will result from the decay of $H_3 \to \nu_{R3}\, \bar{L}$, with the other channel provided by decay into charged leptons.

Let us take the simplified limit of $v_3 \to 0$, corresponding to $\mu_{13} \to 0$, for illustrative purposes. We will also take the minimal approach of providing two neutrino masses of $\mathcal{O}(0.1\text{eV})$, with the third state very light or massless, as allowed by all available data. For $m_{R1,2} \sim 10$ TeV and $m_\nu \sim 0.1$ eV, Eq. (4.9) requires $\lambda_1^\nu \sim 10^{-5}$ which from Eq. (4.31) yields $y_2^\nu \sim 10^{-3}$. From the discussion leading to Eq. (4.5), one could easily determine that washout mediated by $H_{2,3}$ could be avoided if we have

$$|\lambda_{2,3}^{\ell}\, \lambda_{2,3}^{\nu}| \lesssim 2.1 \times 10^{-6}, \tag{4.32}$$

where $\ell = e, \mu, \tau$. The lepton number violating processes that we would like to avoid correspond to the final states $\bar{L}\, \nu_R$ and its Hermitian conjugate. Note that for $T_{rh} \gtrsim 100$ GeV,

production of $\nu_{R1,2}$ would be severely Boltzmann suppressed, since $m_{R1,2}/T_{rh} \sim 100$. For final states including ν_{R3}, processes mediated by H_1 can be decoupled, since ν_{R3} is not required to have substantial coupling to H_1 if we only need two mass eigenstates with $m_\nu \sim 0.1$ eV. Hence, we only need to make sure that processes mediated via $H_{2,3}$ that lead to a ν_{R3} in the final state are sufficiently suppressed, corresponding to condition Eq. (4.32).

Note that since we require $\lambda_2^\tau \sim 1$, suppression of washout mediated by H_2 requires $\lambda_2^{\nu_{R3}} \lesssim 10^{-6}$, where the superscript is specified for clarity. This, according to Eq. (4.31), would lead to $\lambda_1^{\nu_{R3}} \lesssim 10^{-8}$, which is too small to generate $m_\nu \sim 0.1$ eV. However, as mentioned before, this is consistent with the phenomenologically viable possibility of having one very light neutrino. Also, as shown in the discussion around Eq. (4.21), these parameter choices are consistent with our baryogenesis mechanism.

We also note that the above sample parameter space leads to $\nu_{R3} \to L\, H_1$ being a typical decay mode of ν_{R3}, as will be shown later when we discuss collider signatures of our model. The rate for this decay is estimated to be $\Gamma(\nu_{R3} \to L\, H_1) \sim (32\pi)^{-1}\, |\lambda_1^{\nu_{R3}}|^2 m_{R3} \lesssim 10^{-16}$ GeV which leads to decays *after* EWSB when sphalerons are decoupled. Hence, ν_{R3} decays would not interfere with our baryogenesis mechanism. We then conclude that baryogenesis can be successful in our scenario with the above choice of parameters, as a concrete example.

4.4 Low Energy Searches

We must ensure that the values of Yukawas and CP phases deduced from our benchmark flavor model are consistent with low energy observables such as electric dipole moments. Additionally, to have a non-zero asymmetry parameter ε, the Yukawas of $H_{2,3}$ must be misaligned. This misalignment necessarily gives rise to flavor changes that can be searched for. Up until now we have discussed the couplings of the Higgs doublets. However, after EWSB we should consider the mass eigenstates in the broken phase, i.e. neutral scalars, neutral pseudoscalars, and charged scalars. Since the mass eigenstates can mix, their couplings are different than the doublets. For simplicity of notation, in this section and the next we keep

the notation λ_a^f for the Yukawas after EWSB.

- Electric Dipole Moments (EDMs): The nucleon EDM gets contributions from complex Yukawa couplings of the Higgs fields as well as a θ term in the QCD Lagrangian. Assuming a sufficiently small θ (the usual "strong CP problem"), we will consider the contribution of H_2, since the Yukawa coupling of H_3 to light quarks is relatively suppressed by a factor of $v_3/v_2 \ll 1$ in our flavor model. See for example Ref. [144] for bounds on a neutrinophilic Higgs doublet.

  As we are mostly interested in illustrating that typical values of parameters in our scenario lead to successful baryogenesis and acceptable phenomenology, we will only present order-of-magnitude estimates here. Since the coupling of quarks to H_2 is suppressed by v_2/v_{EW} in our flavor model, we find that the 2-loop "Barr-Zee" diagrams [145, 146] are more important that the 1-loop process. Here, the coupling of H_2 to photons is dominated by the τ loop, which couples to H_2 with strength $\lambda_2^\tau \sim 1$, whereas the coupling of the top quark to H_2 is $\lambda_2^t \sim 0.01$. However, the top mass is about two orders of magnitude larger, which compensates for the suppressed coupling. Given that these two contributions are roughly similar, we will only use the τ contribution for our estimate of the effect.

  The 2-loop contribution of H_2 (for $v_3 \to 0$ we can ignore H_3) to the EDM of a light quark q can then be estimated by

$$d_q \sim \frac{e^3\,\lambda_2^\tau\,\lambda_2^q\,m_\tau\,\sin\omega}{(16\pi^2)^2\,m_a^2}\,, \tag{4.33}$$

  where we have $\lambda_2^q \sim 10^{-7}$; we have denoted a typical phase by ω. For $m_2 \sim 1$ TeV, we then find $d_q \sim 10^{-32}\sin\omega\ e$ cm. The current 90% C.L. bound on neutron EDM is $d_n < 3.0 \times 10^{-26}\ e$ cm [134], which indicates our model is not constrained much by the neutron EDM experiments.

  In order to go further and study electron EDM bound constraints, we need to have a

measure of how large lepton flavor violating couplings can be in our model. We will parametrize flavor violation by $\lambda_a^{e\mu}$, $\lambda_a^{\mu\tau}$, and $\lambda_a^{e\tau}$, for tree-level transitions mediated by H_a for $a = 2, 3$, in an obvious notation. Since H_1 couplings to leptons are severely suppressed, we will only consider the dominant contributions from H_a for $a = 2, 3$.

With the above assumptions, we have

$$\Gamma(\ell \to 3\, f) \approx \frac{\lambda_a^{f\,2} \lambda_a^{f\ell\,2}}{1536\pi^3} \frac{m_\ell^5}{m_a^4}\,, \tag{4.34}$$

where $\ell = \mu, \tau$ and f is a light final state charged lepton; we have ignored the effect of final state masses on the phase space.

We have $\lambda_a^e \sim 3 \times 10^{-4}$, $\lambda_a^\mu \sim 6 \times 10^{-2}$, and as before $m_a \sim$ TeV. We then find

$$\Gamma(\mu \to 3\, e) \sim 10^{-28} |\lambda_a^{e\mu}|^2\, m_\mu \tag{4.35}$$

and

$$\Gamma(\tau \to 3\, \mu) \sim 10^{-18} |\lambda_a^{\mu\tau}|^2\, m_\tau \tag{4.36}$$

where m_μ and m_τ are the masses of the μ and τ leptons, respectively. The width $\Gamma(\tau \to e\mu\mu)$ is given by the above formula, with $\lambda_a^{\mu\tau} \to \lambda_a^{e\tau}$. The total widths are given by $\Gamma_\mu \approx 2.8 \times 10^{-18}\, m_\mu$ and $\Gamma_\tau \approx 1.3 \times 10^{-12}\, m_\tau$, in an obvious notation. The current 90% C.L. bounds on the above decays are $\mathrm{BR}(\mu \to 3\, e) < 1.0 \times 10^{-12}$, $\mathrm{BR}(\tau \to 3\, \mu) < 2.1 \times 10^{-8}$, and $\mathrm{BR}(\tau \to e\mu\mu) < 2.7 \times 10^{-8}$ [134]. Hence, we find

$$|\lambda_a^{e\mu}| \lesssim 0.2,\ |\lambda_a^{\mu\tau}| \lesssim 0.2,\ \text{and}\ |\lambda_a^{e\tau}| \lesssim 0.2. \tag{4.37}$$

The dominant contribution to the electron EDM d_e, based on our model assumptions will then be mediated by a 1-loop H_a diagram through the flavor-changing $e\mu$ or $e\tau$

coupling of H_a. We then estimate a typical value by

$$d_e \sim \frac{e\,\lambda_a^{e\ell\,2}\,m_\ell\,\sin\omega}{16\pi^2\,m_a^2} \tag{4.38}$$

$$\sim \begin{cases} 10^{-23}\,|\lambda_a^{e\mu}|^2 \sin\omega\, e\ \text{cm} & \text{for}\ \ell=\mu \\ 10^{-22}\,|\lambda_a^{e\tau}|^2 \sin\omega\, e\ \text{cm} & \text{for}\ \ell=\tau \end{cases} \tag{4.39}$$

Note that the while we are using the same notation for the phase ω as before, it only is meant to denote a typical phase and is not assumed to have the same numerical value. The 90% C.L. bound $d_e < 1.1\times 10^{-28}\ e$ cm [147] then implies bounds of

$$|\lambda_a^{e\mu}|\sqrt{\sin\omega} \lesssim 3\times 10^{-3} \tag{4.40}$$

$$|\lambda_a^{e\tau}|\sqrt{\sin\omega} \lesssim 1\times 10^{-3}. \tag{4.41}$$

- $\mu\to e\gamma$: This process provides a potentially severe constraint on models of new physics. Here, with our preceding assumptions, we expect the main contribution to $\mu\to e\gamma$ to arise from the λ_a^μ and $\lambda_a^{e\mu}$, or $\lambda_a^{\mu\tau}$ and $\lambda_a^{e\tau}$ couplings at 1-loop order, depending on if the internal fermion is a muon or tau. The resulting effective operator can be estimated by

$$O \sim \frac{e\,m_\ell \lambda_a^{\mu\ell}\,\lambda_a^{e\ell}}{16\pi^2\,m_a^2}\,\bar\mu\,\sigma_{\mu\nu}eF^{\mu\nu}\,, \tag{4.42}$$

where $\sigma_{\mu\nu} = (i/2)[\gamma_\mu,\gamma_\nu]$ and $\ell=\mu,\tau$. This dipole operator yields the branching fraction

$$\text{Br}(\mu\to e\gamma) \sim 3\times 10^{-4}|\lambda_a^{e\ell}\,\lambda_a^{\mu\ell}|^2\left(\frac{m_\ell}{\text{GeV}}\right)^2\,, \tag{4.43}$$

which should be compared with the 90% C.L. constraint $\text{Br}(\mu\to e\gamma) < 4.2\times 10^{-13}$ [148].

The bounds on the flavor off-diagonal couplings are then

$$|\lambda_a^{e\mu}| \lesssim 8 \times 10^{-3} \tag{4.44}$$

$$|\lambda_a^{e\tau}\lambda_a^{\mu\tau}| \lesssim 2 \times 10^{-5}\,. \tag{4.45}$$

If the bound in Eq. (4.41) is saturated and $\sin\omega \sim 0.1$, we obtain $|\lambda_a^{\mu\tau}| \lesssim 2 \times 10^{-2}$.

- $(g-2)$: From the above discussion we can conclude that the dominant contribution to the muon anomalous magnetic moment $g_\mu - 2$ will come from the flavor-changing H_a-μ-τ coupling $\lambda_a^{\mu\tau}$ which is the least constrained. We can then estimate the contribution to $(g_\mu - 2)/2$ by

$$\Delta a_\mu \sim \frac{\lambda_a^{\mu\tau\,2}\, m_\tau^2}{16\pi^2\, m_a^2}\,, \tag{4.46}$$

which yields $|\Delta a_\mu| \lesssim 2 \times 10^{-12}$ (for $\sin\omega \sim 0.1$), which is too small to account for the current $\sim 3.5\sigma$ anomaly [134].

Ref. [149] suggests that a Yukawa flavor structure of $\lambda^{ij} \sim \min(m_i, m_j)/v_{EW}$ is in good agreement with data[10]. Here, we will determine the compatibility of our Yukawa couplings with this ansatz. Note that since the leptons only obtain their mass from one Higgs doublet (Φ_2) in the $v_3 \to 0$ limit, their couplings to Φ_2 will be diagonal after diagonalizing the lepton mass matrix. Since H_2 is mostly Φ_2, its couplings are also mostly diagonal while H_3 couplings can be flavor off-diagonal. However, as mentioned above, the scalar mass eigenstates after EWSB are superpositions of the components of $H_{2,3}$ with a small component from H_1, and can have flavor off-diagonal couplings to leptons. We maintain the generic notation λ_a^{ij}.

In order to keep $\lambda_a^\tau \sim 1$, for the charged leptons we modify the ansatz of Ref. [149] to $\lambda_a^{ij} \sim \min(m_i, m_j)/m_\tau$. Hence, we have $\lambda_a^{e\mu} \sim \lambda_a^{e\tau} \sim 3 \times 10^{-4}$, and $\lambda_a^{\mu\tau} \sim 0.06$. The constraint from $\ell \to 3f$ in Eq. (4.37) is clearly satisfied. For $\sin\omega \sim 0.1$, the bounds in Eqs. (4.40,4.41,4.44,4.45) are also satisfied, although we are within order one of many of

[10] Another well-known flavor structure is the Cheng-Sher [150] ansatz $\lambda^{ij} = \sqrt{m_i m_j}/v_{EW}$. However, Ref. [149] suggests that $\lambda^{ij} \sim \min(m_i, m_j)/v_{EW}$ is in better agreement with observations

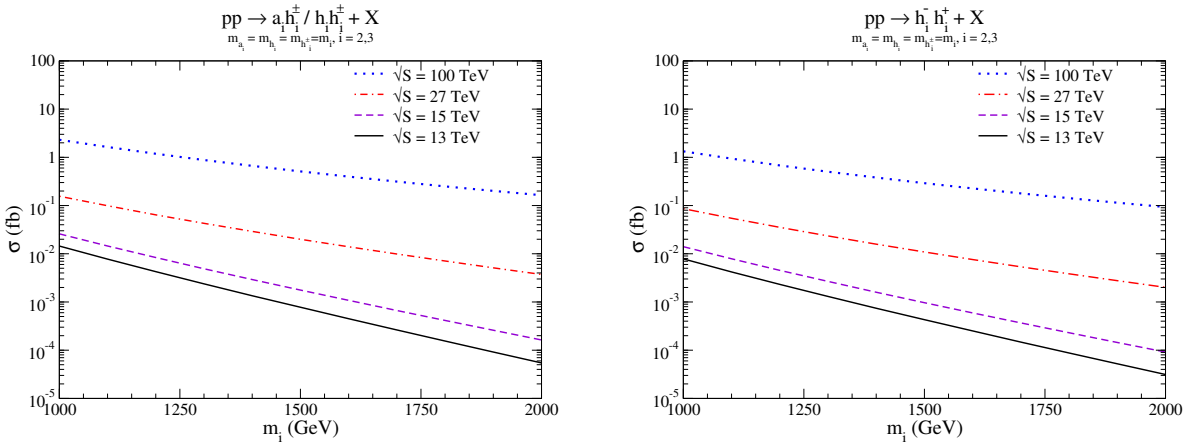

(a) (b)

Figure 4.2: Production cross sections for heavy scalars (a) $h_i h_i^\pm$ and $h_i h_i^\pm$, and (b) $h_i^+ h_i^-$. Both Drell-Yan and VBF production mechanisms are included for all processes. We show the cross sections for lab frame energies of (blue dotted) $\sqrt{S} = 100$ TeV, (red dash-dot) $\sqrt{S} = 27$ TeV, (violet dashed) $\sqrt{S} = 15$ TeV, and (black solid) $\sqrt{S} = 13$ TeV.

these bounds. Hence we conclude that our mechanism is viable, in agreement with low energy observables, and if this ansatz for the charged lepton Yukawas holds we may expect to see a signal in the electron EDM or $\mu \to e\gamma$ [151].

4.5 Collider Searches

Now we discuss some of the aspects of the signals of our model at proton-proton colliders. First, we concentrate on the pair production rates of the new heavy scalars. After electroweak symmetry breaking, the two heavy Higgs doublets in the Higgs basis can be decomposed as

$$H_i = \frac{1}{\sqrt{2}} \begin{pmatrix} \sqrt{2} h_i^\pm \\ h_i + i\, a_i \end{pmatrix}, \quad \text{for } i = 2, 3. \tag{4.47}$$

Hence, we have 4 charged states, 2 pseudoscalar bosons, and 3 scalar bosons (including the scalar h_1 from H_1). The Goldstone bosons completely reside within H_1. Electroweak

precision constraints generally require at least one of the neutral scalars a_i, h_i to be mass degenerate with the charged scalars $h_i^\pm$ [152]. Hence, for simplicity we will assume that $h_i^\pm, h_i$, and a_i have a common mass m_i for each $i = 2, 3$. Production cross sections are computed in `MadGraph5_aMC@NLO` [143] using a model generated via `FeynRules` [142].

In Fig. 4.2 we show the pair production rates for various double scalar final states: (a) $h_i h_i^\pm$ and $a_i h_i^\pm$, and (b) $h_i^+ h_i^-$ for $i = 2, 3$. We provide cross sections for (black solid) the $\sqrt{S} =$ 13 TeV LHC, (violet dashed) the proposed $\sqrt{S} = 15$ TeV upgrade of the LHC [153], (red dot-dash) the proposed $\sqrt{S} = 27$ TeV upgrade of the LHC (HE-LHC) [154], and the proposed $\sqrt{S} = 100$ TeV colliders (FCC-hh/SppC) [155, 156]. The production cross sections for $h_i a_i$, although not shown, are within $\sim 5 - 20\%$ of $h_i^+ h_i^-$. The production modes considered here depend almost exclusively on the gauge couplings of the heavy scalars, and hence have minimal dependence on the model parameters. The double scalar final states $h_i h_i$ and $a_i a_i$ will depend on trilinear scalar couplings and not gauge couplings, so we do not discuss them. Finally, we have included both Drell-Yan and production in association with two jets (similar to vector boson fusion). However, we find the production with two jets to be always subdominant. This is in contrast to the SM case, where the vector boson fusion production rate of the Higgs boson competes with gluon fusion for Higgs mass $\gtrsim 1$ TeV [114].

The benchmark luminosity for the 13 and 15 TeV LHC is 3 ab^{-1}, for the HE-LHC 15 ab^{-1}, and for FCC-hh/SppC 30 ab^{-1}. Hence, for $m_i \sim 1 - 2$ TeV, we can expect between zero and 40 events at the 13 TeV High-Luminosity LHC. At 15 TeV, the situation is slightly improved to an expected number of events between 1 and 80. With between 30 and 2,300 events, the High-Energy LHC would be likely to be sensitive to much of the relevant parameter region and test our model. Of course, the situation is most promising at the FCC-hh/SppC with between 2,800 and 50,000 events. These predictions for the number of events are robust, since the production channels we consider are fully determined by gauge couplings. While 40-80 events at the LHC may seem small, as we discuss below, the decays of these heavy scalars can be striking and with small background. Hence, the LHC may be able to probe

masses around 1 TeV, while future colliders may be needed for masses at or above 2 TeV. A full collider study would be necessary to determine the full reach of these machines.

We will now discuss the decays of the new scalars. Due to the vev hierarchy, from Eq. (4.29) the mixing between Φ_1 and Φ_2 is $v_2/v_1 \sim 1\%$ and between Φ_1 and Φ_3 is much smaller as assumed before. The decays of the heavy scalars into quark, gauge boson, and double Higgs channels depend on the mixing and are highly suppressed. Hence, the heavy scalars predominantly decay into leptons via their Yukawa couplings. The neutral scalars h_2 and a_2 each decay mainly to a τ pair. Since we require $m_3 \gg m_{R3}$ in our baryogenesis mechanism, the neutral scalars h_3 and a_3 each decay primarily to a heavy (ν_{R3}) and a light neutrino and potentially similarly into charged leptons. For the charged scalars, since H_2 couples according to charged lepton masses, $h_2^\pm$ will decay to a τ and a light neutrino. Since H_3 couplings are not necessarily as hierarchical as the charged fermions, $h_3^\pm$ can decay into μ, e and ν_{R3}, as well as a τ and ν_{R3}.

With our sample parameters, used to derive Eq. (4.21), only ν_{R3} is potentially accessible at collider experiments, with $\nu_{R1,2}$ being too heavy (~ 10 TeV) to produce at the LHC and likely other envisioned facilities. Here, assuming that $m_{R3} \gtrsim 100$ GeV, ν_{R3} can decay to SM gauge bosons via mixing, to H_1 and a light neutrino through direct coupling leading to a "Dirac" mass of $m_{D3} \sim$ keV, or in three-body decays via an off-shell heavy scalar into leptons plus missing energy. The mixing angle $\theta \sim m_{D3}/m_{R3} \sim 10^{-8}$ for ν_{R3}-ν mixing leads to the following estimate

$$\begin{aligned} \Gamma(\nu_{R3} \sim W^\pm \ell^\mp) &\sim 4\Gamma(\nu_{R3} \to \nu_L\, Z) \\ &\sim \frac{\theta^2}{8\pi}\frac{m_{R3}^3}{v^2} \lesssim 10^{-16}\ \text{GeV}, \end{aligned} \tag{4.48}$$

with $V = W, Z$. We also find

$$\Gamma(\nu_{R3} \to \nu_L\, h_1) \sim \frac{1}{32\pi}|\lambda_1^{\nu_{R3}}|^2 m_{R3} \lesssim 10^{-16}\ \text{GeV}, \tag{4.49}$$

with $|\lambda_1^{\nu_{R3}}| \lesssim 10^{-8}$ in our preceding example. Finally, we also find, in analogy to Eq. (4.34),

$$\Gamma(\nu_{R3} \to \nu_L \, \ell \, \ell) \sim \frac{|\lambda^{\ell}_{2,3} \, \lambda^{\nu}_{2,3}|^2}{1536\pi^3} \frac{m^5_{R3}}{m^4_{2,3}} \lesssim 10^{-19} \text{ GeV}. \tag{4.50}$$

The above estimates imply that in our example the ν_{R3} decays would be quite displaced, on the order of meters. This could in principle lead to very unique signals. However, the proximity of the estimates (4.48) and (4.49) suggests that a more careful study is needed to decide the dominant decay mode, but one could end up with similar rates for the first two possibilities. Since the example parameters used to illustrate the viability of our baryogenesis mechanism were only one of many possible solutions, we do not offer a more detailed analysis here, but suffice it to say that the model can potentially yield interesting signals of ν_R decays.

The phenomenology of SM-like Higgs boson, h_1, can also be altered. Initially, in the Higgs basis of H_1, H_2, H_3, the coupling of h_1 are precisely the same as in the SM. However, there can be mixing between neutral scalars h_1 and h_2 via quartic interactions in the Higgs potential. For order one couplings, these mixings could be expected to be of the size $\sim v_1 \, v_2/m_2^2$ which, assuming TeV scale heavy Higgses, is around $\sim 0.1\%$ for h_2. Since the mixing with the heavy scalars are small, the production rate and main decay rates ($b\bar{b}$, WW, ZZ, $\gamma\gamma$) of h_1 are little changed. However, the branching ratios into rarer modes, such as $\mu^-\mu^+$, can be altered. The SM-like Yukawa coupling of h_1 to muons is $m_\mu/v_{EW} \sim 4 \times 10^{-4}$, while the h_2 coupling to muons is $m_\mu/\sqrt{2}m_\tau \sim 0.04$. Hence, after 0.1% mixing with h_2, the coupling of h_1 to muons can be shifted from the SM by $\sim 10\%$. The branching ratio of $h_1 \to \mu^+\mu^-$ is then moved away from the SM value by $\sim 20\%$. This shift is generically true of all charge leptons including τs. While $h_1 \to e^-e^+$ is unobservable at the LHC due to small electron couplings, this level of deviation in $h_1 \to \mu^+\mu^-$ and $h_1 \to \tau^+\tau^-$ will be observable at the High-Luminosity LHC with 3 ab^{-1} or the HE-LHC with 15 ab^{-1} of data [157].

Chapter 5

Neutrino Masses from Scalar Interactions with Dark Matter[11]

In some models, scalars can be a portal to cosmic dark matter (DM), mediating interactions between SM particles and DM particles. The existence of DM is strong and robust empirical evidence for the existence of BSM physics, so studying DM is extremely desireable. However, DM has, at best, very weak interactions with atoms, which makes measurement of its properties a great challenge.

Neutrinos, while being SM particles, also provide evidence of BSM physics from their measured properties. Contrary to the minimal SM predictions, neutrinos have non-zero masses $m_\nu \lesssim 0.1$ eV and mixing [158, 159]. Both neutrinos and DM, while apparently distinct in character, share the feature of having feeble interactions with atoms. While neutrinos are known to have interactions other than gravitational, the same cannot be said with certainty about DM.

This state of affairs allows one some space for speculation about possible *exotic* interactions of neutrinos and DM via a scalar portal. While we do not know the spectrum of DM states, neutrinos are characterized by the smallest non-zero masses known in Nature. Compared to the masses of other SM fermions, we approach neutrino masses from a radically different point of view: that the small but non-zero masses of neutrinos are not an inherent vacuum property, but the result of a long range scalar potential sourced by DM distributions. Long range forces have received much attention in the literature due to their

[11] This chapter is based on Ref. [29], which is ©2018 American Physical Society

various implications for dark sector dynamics. The notion of a long range force was introduced by Ref. [160] and their possible applications to dark matter interactions have been studied from the smallest scales in our galactic halo to the largest scales in cosmology [161, 162, 163, 164, 165, 166, 167, 168, 169, 170, 171, 172, 173, 174].

Adopting the formalism introduced in Ref. [165], we consider a long range force between dark matter and neutrinos, which is mediated by a light scalar ϕ. If dark matter sources neutrino masses then the neutrinos may be massless in empty space, but acquire small masses near non-trivial populations of DM. This makes the neutrino mass matrix locally established which can vary substantially depending on where it is measured and is not the same throughout space. In particular, neutrinos would have very different properties in different parts of our Galaxy.

In what follows, we will provide a simple phenomenological model of how the above neutrino mass generation mechanism can be realized. We will then address some of the potential constraints that may apply to our scenario; it is shown, generally speaking, that the most obvious concerns about the viability of our idea can be addressed. Next, we will focus on possible signals and tests of our hypothesis. Some speculations and a summary will be presented in closing. For possible effects of astrophysical backgrounds on neutrino properties, in a different framework, please see Ref. [175].

5.1 Dynamics

The basic interactions of interest for our analysis are given by

$$\mathcal{L}_i = -g_X \phi \, \bar{X} X - g_\nu \, \phi \, \bar{\nu} \, \nu \,, \tag{5.1}$$

where X is a DM fermion and ν is a neutrino in the SM. Here, we assume that both particles are *Dirac* fermions, however our mechanism can accommodate *Majorana* masses for the SM neutrinos if there is a mass term for right handed neutrinos in the Lagrangian. In what

follows, we will take the couplings of ϕ to other SM states to be negligible. The above interactions can be straightforwardly generalized to include a matrix valued g_ν that would yield the requisite mixing angles and masses. We will adopt $m_\nu \sim 0.1$ eV as a reasonable representative value for neutrino mass eigenvalues, where a mild variation can accommodate the current inferred mass squared differences. The mass terms of interest, *in vacuo*, are given by

$$\mathcal{L}_m = -m_X \bar{X} X - \frac{1}{2} m_\phi^2 \, \phi^2 \,, \tag{5.2}$$

where m_X and m_ϕ are the masses of X and ϕ, while neutrinos are *massless*, in empty space. In the presence of a constant background ϕ, neutrinos have an apparent mass of

$$m_\nu \equiv g_\nu \phi \,, \tag{5.3}$$

which can be positive or negative. This mass term can be made positive, as is typical, by performing a chiral transformation of the neutrino field. We shall use the positive mass convention.

We assume a force between the non-relativistic dark matter and neutrinos given by a Yukawa potential of the form

$$V_\phi(r) = -\frac{g_X g_\nu}{4\pi \ r} e^{-m_\phi \ r}, \tag{5.4}$$

where r is the distance between the two interacting species. The force is attractive if g_X and g_ν have the same sign, and is repulsive if g_X and g_ν have opposite sign. We shall see later that, in order to have positive masses, the force between dark matter and neutrinos will always be repulsive in our model.

We compare the strength of the long range interaction with that of gravity. In the limit where the scalar mass m_ϕ is sufficiently small, the ratio of the Yukawa coupling to the gravitational coupling is given by

$$\beta_f = \frac{M_P g_f}{\sqrt{4\pi} m_f}, \tag{5.5}$$

where $M_P \approx 1.2 \times 10^{19}$ GeV is the Planck mass [176] and fermion $f = X, \nu$. Given the above setup, the equation of motion for ϕ is given by

$$(\Box + m_\phi^2)\phi = -g_X \bar{X} X - g_\nu \bar{\nu}\nu. \tag{5.6}$$

For a fermion f of number density n_f and typical velocity v_f, Lorentz invariance yields

$$\bar{f}\, f = n_f \langle \sqrt{1 - v_f^2} \rangle. \tag{5.7}$$

Here, $\langle \ldots \rangle$ denotes an ensemble average. For the rest of our discussion, we will only consider non-relativistic DM, with $v_X \ll 1$, well after its relic density has been established. We will assume populations of X and ν that can be considered spatially uniform and static over the distance and time scales relevant to our discussion, implying $\Box\phi \approx 0$ in what follows.

The mean energy of neutrinos is given by $\langle E_\nu \rangle = m_\nu / \langle \sqrt{1 - v_\nu^2} \rangle$ and in our approximation, $\langle E_X \rangle \approx m_X + g_X \phi$, which ignores the kinetic energy of DM. Therefore, Eq. (5.6) yields

$$\phi \approx \frac{-g_X n_X}{m_\phi^2 + \omega_\nu^2}\,, \tag{5.8}$$

where $\omega_\nu^2 \equiv g_\nu^2 n_\nu / \langle E_\nu \rangle$ denotes the screening mass squared for ϕ induced by the neutrinos. Since number densities and energies are strictly positive, we note that ϕ and g_X have opposite sign. Thus, according to Eq. (5.3), m_ν is positive if g_X and g_ν have opposite sign. This confirms our statement that the Yukawa force between neutrinos and dark matter is repulsive. We will next examine how the above can allow for $m_\nu \sim 0.1$ eV from the DM distribution around the Solar System.

If the screening mass ω_ν^2 from neutrinos dominates over m_ϕ^2, then Eq. (5.8) reduces to

$$\phi \approx \frac{-g_X n_X E_\nu}{g_\nu^2 n_\nu} \tag{5.9}$$

If we replace ϕ using Eq. (5.3), we then find

$$\frac{m_\nu}{E_\nu} \approx \frac{-g_X n_X}{g_\nu n_\nu} \,. \tag{5.10}$$

which tells us that when neutrino number density is the dominant factor, neutrinos will be relativistic. Before structure formation, the number density of neutrinos dominates DM throughout the cosmos. Until DM densities become enhanced at late times, the neutrinos would then drive $\phi \to 0$ as seen in Eq. (5.9), and the neutrinos will thus remain relativistic and nearly massless. Once DM clumps sufficiently it can drive out the cosmic relic neutrinos from the DM dominated regions. To see this, note that if the local DM population generates $m_\nu \sim 0.1$ eV near the Solar System the cosmic background neutrinos, characterized today by kinetic energies of $\mathcal{O}(10^{-4}$ eV), would not have enough energy to enter this region of space and would be repelled from it (We will refer back to this discussion in the section on Observational Tests). Then the dominant population of neutrinos near the Earth is due to the Solar flux which yields $n_\nu \sim 1$ cm^{-3}. This number density falls off rapidly like the flux the further we move from the Solar System and would not affect the potential set up by the dark matter. In that case, the only relevant population for sourcing $\phi \neq 0$ is that of DM in our scenario.

In order to keep the properties of neutrinos across the Solar System uniform, one needs to assume that the size of DM distribution that contributes to m_ν is much larger than AU $\sim (10^{-18}$ eV$)^{-1}$. However, in order to avoid conflict with the inferred behavior of DM on scales of $\gtrsim 1$ kpc, where simulations and observations seem to agree, we limit the range of the scalar interaction; we will adopt $m_\phi \sim 10^{-26}$ eV $\sim (0.7$ kpc$)^{-1}$ for the following discussion. Thus one can show

$$\begin{aligned} m_\nu \;&\sim\; 0.1 \text{ eV} \left(\frac{g_\nu}{10^{-19}}\right) \left(\frac{g_X/m_X}{10^{-19} \text{ GeV}^{-1}}\right) \\ &\times\; \left(\frac{\rho_X}{0.3 \text{ GeV.cm}^{-3}}\right) \left(\frac{10^{-26}\text{eV}}{m_\phi}\right)^2 , \end{aligned} \tag{5.11}$$

where for the above set of parameters in our local Galactic neighborhood, we find that we can ignore the screening mass in Eq. (5.8). Based on the tidal stream bounds from Refs. [168, 169, 177] we require $\beta_X \lesssim 0.2$ for $m_\phi \lesssim 10^{-27}$ eV which implies $g_X/m_X \lesssim 10^{-19}$ GeV^{-1}. We are not aware of any stringent bounds on g_ν besides the requirement of neutrino free streaming in the early universe (at $T \sim 1$eV)[178]. Requiring that the neutrino scattering rate ($\sim g_\nu^4 T$) be less than the Hubble expansion rate ($\sim T^2/M_P$), leads to $g_\nu \lesssim 10^{-7}$, which is not severe bound in our case, given Eq. (5.11).

The above brief analysis shows that one could in principle account for neutrino masses and mixing in our Galactic neighborhood using the scalar potential sourced by DM. To quantify this, we consider not only the dark matter distribution in our local neighborhood, but throughout the MilkyWay Galaxy. For illustration, we assume the three DM density profiles that are popular in the literature; the Navarro-Frenk-White (NFW), Einasto and Burkert density profiles (please see Refs.[179, 180, 181] for their functional forms). From these we map the distribution of the neutrino mass as a function of the galactic radius, depicted in Fig. 5.1. For each profile, we require $\rho_X(r_\odot) = 0.3$ GeV.cm^{-3}, where $r_\odot = 8.5$ kpc is the galactic radius at the position of the solar system. For the cuspy NFW and Einasto ($\alpha = 0.17$) profiles we assume a scale radius $R = 20$ kpc, while for the cored Burkert profile we assume a core radius $r_c = 16$ kpc [181, 182].

We note here that the density of DM does not get much larger than the local value near the Solar System in other parts of the Galaxy. Even with an enhancement of $\mathcal{O}(10^3)$, the neutrino mass $m_\nu \propto n_X$ is $\mathcal{O}(100$ eV), which should not affect physical processes relevant to stellar and galactic dynamics significantly.

5.1.1 Early Time Dynamics

Let us now briefly consider earlier times, before DM has developed large scale overdensities. In particular, let us consider the cosmic microwave background (CMB) era, corresponding to $T \sim 1$ eV. At this and earlier times, we can take the DM and neutrino distributions

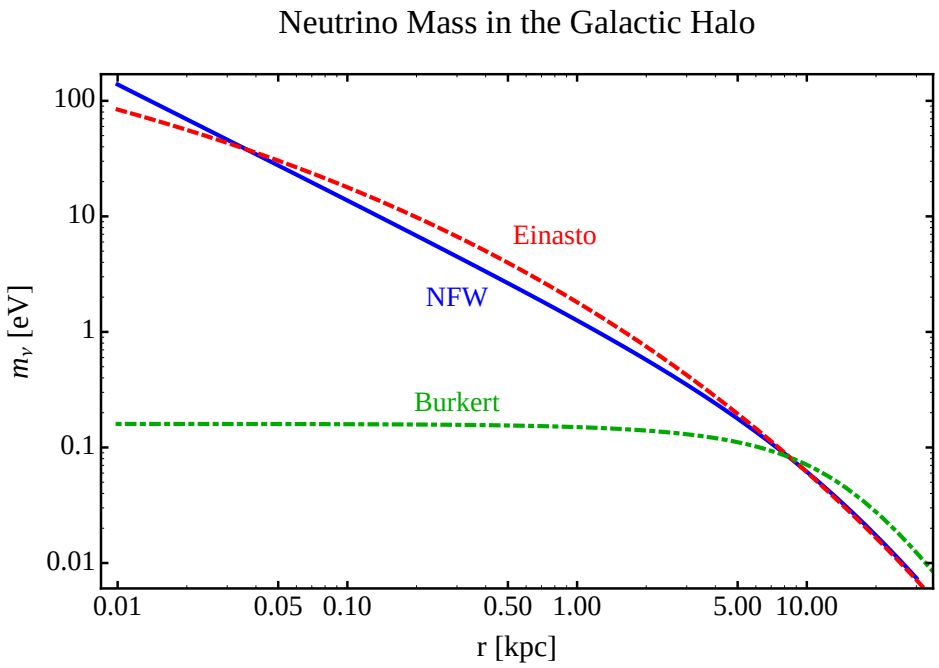

Figure 5.1: Neutrino mass as a function of the galactic radius for different dark matter density profiles. The red-dashed line represents a cuspy Einasto profile, the blue solid line represents a cuspy NFW profile and the green dot-dashed line represents a cored Burkert profile. For all the profiles we require that $\rho_X(r_\odot) = 0.3$ GeV.cm^{-3} and $m_X = 0.3$ GeV, where $r_\odot = 8.5$ kpc. With these parameters we obtain $m_\nu \sim 0.1$ eV in our local galactic neighborhood.

to be homogeneous. Also, the time scale for cosmic evolution, given by the Hubble time $H^{-1} \sim M_P/T^2$, around this era (roughly assuming radiation domination) is much larger than m_ϕ^{-1}, and hence the potential for ϕ changes slowly compared to the relevant physical scales. Therefore, we can use the approximation $\Box\phi \approx 0$ here.

The ratio of DM number density to entropy $s \sim g_s T^3$, with g_s counting the relativistic degrees of freedom [183], is roughly given by

$$\frac{n_X}{s} \sim 10^{-9} \frac{m_p}{m_X}\,, \tag{5.12}$$

where m_p is the proton mass (the above relation can be obtained from a similar one based on the baryon asymmetry). On the other hand, the neutrino number density $n_\nu \approx T^3$ in the CMB era.

Since g_X and g_ν are not taken to be very different in our discussion, we then see that the neutrino scalar charge density $g_\nu n_\nu \gg g_X n_X$ at early times. Hence, the neutrino plasma is dominant in the early universe. For our choice of parameters, we find $\omega_\nu \sim 10^{-19}$ eV $\gg m_\phi$, for $T \sim 1$ eV. Thus, in the CMB era, Eqs. (5.9) and (5.10) hold. Using Eq. (5.12), this yields

$$m_\nu \sim 10^{-9} \left| \frac{g_X}{g_\nu} \right| \left(\frac{m_p}{m_X} \right) E_\nu \,. \quad \text{(CMB era)} \tag{5.13}$$

Therefore, for the typical range of parameters considered here, neutrinos are relativistic and nearly massless around the CMB era. The above analysis is not valid at much earlier times, when the range of ϕ is limited by the horizon size instead of ω_ν. The relevant temperature is given by $H \gtrsim \omega_\nu$, which roughly yields $T \gtrsim g_\nu M_P$. For $g_\nu \sim 10^{-19}$ we find $T \gtrsim 1$ GeV. This estimate suggests that our preceding discussion is valid at least up to the era of Big Bang Nucleosynthesis ($T \sim 1$ MeV), which is the earliest cosmological time that is constrained by observations.

5.1.2 Potential Constraints

One may worry that in places where a large density of neutrinos are present considerable conflict with observations would arise. In the current cosmological epoch, the largest neutrino number densities are those characterizing the initial stages of a supernova explosion, where a *neutrino sphere* of radius $\sim$ 100 km forms, containing roughly $\mathcal{O}(10^{57})$ neutrinos. This corresponds to an enormous number density $n_\nu^{\rm sn} \sim 10^{36}$ cm^{-3}. However, these neutrinos are very relativistic, with $E_\nu \gtrsim 1$ MeV. Therefore, in the static distribution limit, we would expect $\phi \to 0$ within the neutrino sphere and hence the supernova dynamics may not change appreciably. For a related discussion on long range forces acting on neutrinos in neutron stars please see Ref. [184]. Next we show that the dark matter accumulated within the Sun would not affect the neutrino properties in the solar interior significantly. For the range of parameters we discuss here, dark matter would accumulate within a radius $R_{core} \sim 10^5$ km

[185, 186]. Then the maximum contribution of the trapped dark matter to the neutrino mass in the Sun (near the core) would be

$$\delta m_\nu \sim \frac{g_\nu g_X N_X}{R_{core}}, \tag{5.14}$$

where N_X is the number of dark matter particles within the core of the Sun. Even if one was to consider maximum dark matter accumulation due to self-interaction in the Sun, with $N_X \sim 10^{40}$ [187], one would find $\delta m_\nu \sim 10^{-15}$ eV, which is a negligible contribution to the neutrino mass and would not have an effect on the solar neutrino dynamics.

As illustrated in Fig. 5.1, as one moves away from the central parts of the Galaxy, the neutrino mass becomes smaller than $\mathcal{O}(0.1$ eV). Given that current observational bounds on the sum of the neutrino masses, from their effects on large scale structure [188, 189, 190], is at or above $\mathcal{O}(0.1$ eV), we do not expect severe constraints from these astrophysical and cosmological observations on our scenario.

At this point, we would like to address some generic model building issues. In particular, one could ask why the neutrinos would not get masses from the Higgs mechanism, like other SM fermions. This could perhaps be a consequence of underlying symmetries that forbid a neutrino-Higgs Yukawa coupling, as we will discuss next.

For example, let us assume that right-handed neutrinos are odd under a $\mathbb{Z}_2$ parity, but none of the SM states have this parity. As long as ϕ is also $\mathbb{Z}_2$ odd, then one can achieve a coupling $\phi\bar{\nu}_L\nu_R$ from the dimension-5 operator $O_1 = \phi H^* \bar{L}\nu_R/M$, where H is the Higgs doublet field and L is a lepton doublet, in the SM. For $g_\nu \sim 10^{-19}$, as in the above, $\langle H\rangle \sim$ 100 GeV implies that one then needs an effective value $M \gtrsim M_P$. This suggests that the above operator is generated by very small couplings and high mass scales. If the right-handed X, for example, is $\mathbb{Z}_2$ odd, then one can also induce $\phi\bar{X}_L X_R$. However, now, a Dirac mass term for X cannot then be written down, if $\mathbb{Z}_2$ is a good symmetry. We must then assume that m_X is generated by a "dark" sector Higgs field Φ that spontaneously breaks $\mathbb{Z}_2$. To

distinguish X from ν_R, which ensures the stability of X, we will postulate that there is a $U(1)_X$ under which only X is charged: $Q(X_L) = Q(X_R) = -1$. If $\mathbb{Z}_2(\Phi) = -1$ one can write down $\Phi\bar{X}_L X_R$ and $\phi\bar{X}_L X_R$. Note that The former interaction leads to a mass term for X with $\langle\Phi\rangle \neq 0$. For values of m_X considered in this chapter, we may expect $\langle\Phi\rangle \sim 1$ GeV.

With the above assumptions, one can write down the dimension-5 operator $O_2 = \Phi H\bar{L}\nu_R/M$ that can contribute to $m_\nu \neq 0$. The effect of O_2 is be negligible, with our assumptions. To see this, note that for $\langle\Phi\rangle \sim$ GeV, O_2 would lead to a very small neutrino mass $m_\nu \lesssim 10^{-8}$ eV and the long range mechanism we have introduced here would be the main source of $m_\nu \sim 0.1$ eV in and around the Solar System.

5.2 Observational Tests

The scenario we have introduced can pose a challenge to experimental verification. In principle, if the large scale behavior of DM shows deviations from purely gravitational dynamics, one may be led to the conclusion that there is a long range force that acts upon DM. The effect of this new force on neutrinos may be harder to establish. However, as discussed earlier, our scenario typically suggests that relic neutrinos do not enter the region around our Solar System at the current epoch, because the induced mass of $m_\nu \sim 0.1$ eV would exceed their total kinetic energy of $\mathcal{O}(10^{-4})$ eV. In the event that any of the proposed relic neutrino detection experiments, succeeds in finding a signal, one could view this prediction of our scenario to be falsified.

The detection of cosmic background neutrinos would be a major success of the field of particle physics. To date there are several proposed methods of detecting these neutrinos, including: the Stodolsky effect [191], the Cavendish-like torsion balance [192, 193, 194] and interactions with Ultra-high energy cosmic rays [193]. However it seems the most promising technique for the near future is neutrino capture (please see Refs. [195, 196] for further information) which will be exploited by the PTOLEMY experiment[197]. Hence, a near future experiment such as PTOLEMY could in principle test our model.

Chapter 6

Dark Photon and Dark Higgs in a Top Partner Model[12]

In dark sectors, new scalars can be responsible for symmetry breaking of dark gauge sectors. With the knowledge that dark matter may have some sort of self-interactions, we can motivate a new $U(1)_d$ force under which dark matter is charged. There are, however, strong constraints on additional *long range* interactions of dark matter[198] that motivate why such a $U(1)_d$ would be broken by a dark Higgs mechanism. The massive $U(1)_d$ gauge boson, the so-called dark photon, kinetically mixes with the SM hypercharge through a renormalizable interaction [199, 200, 201]. This kinetic mixing can be generated via new vector like fermions charged under both the SM and the new $U(1)_d$ [199, 202, 203], as considered here. In the limit that the dark photon is much less massive than the Z and the kinetic mixing is small, the dark photon inherits couplings to SM particles of the form $\varepsilon J^{\mu}_{\rm EM}$, where $J^{\mu}_{\rm EM}$ is the electromagnetic current and ε is the kinetic mixing parameter. Hence, the name dark photon. Most of the searches for the dark photon take place at low energy experiments such as fixed target experiments or B-factories [201]. However, it is also possible to search for dark photons through the production and decays of heavy particles at high energy colliders [204, 205, 206]. For example, Higgs decays [202, 207, 203] into dark photons is a plausible scenario for discovery.

Some of the most important searches for BSM physics at the LHC are searches for new vector like quarks (VLQs). Up-type VLQs, so-called top partners T, are ubiquitous in composite [208, 209, 210, 211, 212, 213, 214] and Little Higgs [215, 216, 217, 218, 219, 220, 221, 222] models where the top partners help solve the hierarchy problem. Traditionally,

[12]This chapter is based on Ref. [30], which is ©2020 American Physical Society

searches for VLQs rely on decays into the EW bosons from the SM: W/Z/Higgs. However, there is a class of "maverick top partners" with non-traditional decays into photons [223, 224, 225, 226, 227, 228], gluons [223, 224, 225, 226, 227, 228], new scalars [229, 230, 231, 232, 233, 234, 235, 236], etc. These new decays can easily be dominant with minor tweaks to the simplest VLQ models. We consider a VLQ that is charged under both the SM and the new $U(1)_d$, where the SM is neutral under the $U(1)_d$. As we will show, in a very large range of the parameter space, this opens new dominant decays of VLQs that have not yet been searched for.

A recent paper [237] studied the scenario where down-type VLQs and vector like leptons are charged under the SM and $U(1)_d$. Ref. [237] relied on a very large mass gap between the SM fermions and their vector-like fermion partners to suppress the traditional vector-like fermion decays into W/Z/Higgs. With this mass gap, the branching ratios of vector-like fermions into dark photons and SM fermions is enhanced. Here we point out that this mechanism does not require a mass gap in the fermion sector, although such a gap further enhances the effect. To illustrate this, we will focus on an up-type VLQ, T, that mixes with the SM top quark, t. The mass gap between t and T does not need to be as large as between the bottom quark/leptons and vector-like fermions. From the Goldstone equivalence theorem, the partial width of T into fully SM final states is

$$\Gamma(T \to b/t + W/Z/h) \sim \sin^2\theta \, \frac{M_T^3}{v_{EW}^2} \ ,$$

where θ is a mixing angle between the SM top quark and T, $v_{EW} = 246$ GeV is the Higgs vev, and M_T is the mass of the VLQ T. The partial width is inversely proportional to v_{EW}^2 due to an enhancement of decays into longitudinal Ws and Zs. If the new vector like quark is charged under the dark force (and assuming there is a dark sector Higgs mechanism), the

partial widths of T into the dark photon, γ_d, or dark Higgs, h_d, is

$$\Gamma(T \to t + \gamma_d/h_d) \sim \sin^2\theta \frac{M_T^3}{v_d^2} \ ,$$

where v_d is the vev of the dark sector Higgs boson. Note that now the partial width is inversely proportional to v_d^2. Hence, the ratio of the rates into γ_d/h_d and $W/Z/h$ is

$$\frac{\Gamma(T \to t + \gamma_d/h_d)}{\Gamma(T \to t/b + W/Z/h)} \sim \left(\frac{v_{EW}}{v_d}\right)^2 \ .$$

For dark photon masses $M_{\gamma_d} \lesssim 10$ GeV, we generically expect that the vev $v_d \lesssim 10$ GeV and

$$\frac{\Gamma(T \to t + \gamma_d/h_d)}{\Gamma(T \to t/b + W/Z/h)} \gtrsim \mathcal{O}(100) \ .$$

Hence, the VLQ preferentially decays to light dark sector bosons due to the mass gap between the dark sector bosons and the SM EW bosons. Since there is a quadratic dependence on v_{EW} and v_d, this mass gap does not have to be very large for the decays $T \to t + \gamma_d/h_d$ to be dominant.

This is a new avenue to search for light dark sectors using decays of heavy particles at the LHC, providing a connection between heavy particle searches and searches for new light sectors. The appeal of such searches is that pair production of VLQs is through the QCD interaction and is fully determined via $SU(3)$ gauge interactions. That is, the pair production rate only depends on the mass, spin, and color representation of the produced particles. Additionally, as we will show, for a very large region of parameter space VLQs will predominantly decay into dark photons and dark Higgses. Hence, the dark photon can be produced at QCD rates at the LHC independently of a small kinetic mixing parameter. The major dependence on the kinetic mixing parameter ε arises in the decay length of the dark photon, and for small ε the dark photon can be quite long lived. In fact, for small dark photon masses, its decay products will be highly collimated and may give rise to displaced

"lepton jets" [238].

In Section 6.1 we present an explicit model that realizes this mechanism for dark photon searches and review current constraints in Sec. 6.2. We calculate the decay and production rates of the new VLQ in Sec. 6.3 and the decay of the dark photon in Sec. 6.4. In Section 6.5 we present collider searches relevant for our model. This includes the current collider sensitivity as well as demonstrating the complementarity between the searches for dark photons via heavy particle decays at the LHC and low energy experiments.

6.1 Model

We consider a simple extension of the SM consisting of a new $SU(2)_L$ singlet up-type vector-like quark, t_2, and a new $U(1)_d$ gauge symmetry. For simplicity, we will only consider mixing between the new vector-like quark and 3$^{\text{rd}}$ generation SM quarks:

$$Q_L = \begin{pmatrix} t_{1L} \\ b_L \end{pmatrix} \quad , \quad t_{1R} \ , \quad \text{and} \quad b_R \ . \tag{6.1}$$

The SM particles are singlets under the new symmetry, and we give the VLQ t_2 a charge $+1$ under the new symmetry. The $U(1)_d$ is broken by a dark Higgs field H_d that is a singlet under the SM and has charge $+1$ under $U(1)_d$. The relevant field content and their charges under $SU(3) \times SU(2)_L \times U(1)_Y \times U(1)_d$ are given in Table 6.1. This particle content and charges are similar to those in Ref. [237].

This field content allows for kinetic mixing between the SM $U(1)_Y$ field, B'_μ, and the new $U(1)_d$ gauge boson, $B'_{d,\mu}$:

$$\begin{aligned} \mathcal{L}_{\text{Gauge}} &= -\frac{1}{4} G^A_{\mu\nu} G^{A,\mu\nu} - \frac{1}{4} W^a_{\mu\nu} W^{a,\mu\nu} - \frac{1}{4} B'_{\mu\nu} B'^{\mu\nu} \\ &+ \frac{\varepsilon'}{2\cos\hat{\theta}_W} B'_{d,\mu\nu} B'^{\mu\nu} - \frac{1}{4} B'_{d,\mu\nu} B'^{\,\mu\nu}_d \ , \end{aligned} \tag{6.2}$$

where $G^A_{\mu\nu}$ are the $SU(3)$ field strength tensor with $A = 1, ..., 8$ and $W^a_{\mu\nu}$ are the $SU(2)_L$ field

	$SU(3)$	$SU(2)_L$	Y	Y_d
t_{1R}	**3**	**1**	2/3	0
b_R	**3**	**1**	-1/3	0
$Q_L = \begin{pmatrix} t_{1L} \\ b_L \end{pmatrix}$	**3**	**2**	1/6	0
H	**1**	**2**	1/2	0
t_{2L}	**3**	**1**	2/3	1
t_{2R}	**3**	**1**	2/3	1
H_d	**1**	**1**	0	1

Table 6.1: Field content and their charges. t_{1R}, b_R, and Q_L are 3$^{\text{rd}}$ generation SM quarks, H is the SM Higgs doublet, t_2 is the $SU(2)_L$ singlet VLQ, and H_d is the $U(1)_d$ Higgs field. Y is the SM Hypercharge and Y_d is the $U(1)_d$ charge.

strength tensors with $a = 1, 2, 3$. The relevant fermion kinetic terms for the third generation quarks and VLQ are

$$\mathcal{L}_{F,kin} = \overline{Q}_L i\not{D} Q_L + \bar{t}_{1R} i\not{D} t_{1R} + \bar{b}_R i\not{D} b_R + \bar{t}_2 i\not{D} t_2 \ , \tag{6.3}$$

and the relevant scalar kinetic terms are

$$\mathcal{L}_{S,kin} = |D_\mu H|^2 + |D_\mu H_d|^2 \ . \tag{6.4}$$

The general covariant derivative is

$$D_\mu = \partial_\mu - ig_S t^A G^A_\mu - igT^a W^a_\mu - ig' Y B'_\mu - ig'_d Y_d B'_{d,\mu} \ , \tag{6.5}$$

where g_S is the strong coupling constant, g is the $SU(2)_L$ coupling constant, g' is the $U(1)_Y$ coupling constant, and g'_d is the $U(1)_d$ coupling constant. Values for Y, Y_d and the generators of $SU(3)$, $SU(2)_L$ are given according to the charges in Table 6.1.

6.1.1 Scalar Sector

The allowed form of the scalar potential symmetric under the gauge group $SU(3)_C \times SU(2)_L \times U(1)_Y \times U(1)_d$ is

$$V(H, H_d) = -\mu^2 |H|^2 + \lambda\, |H|^4 - \mu_{h_d}^2 |H_d|^2 + \lambda_{h_d} |H_d|^4 + \lambda_{h h_d} |H|^2 |H_d|^2 \ . \tag{6.6}$$

Since H_d does not break EW symmetry, H must have a vev of $v_{EW} = 246$ GeV. Imposing that the potential has a minimum where the SM Higgs and dark Higgs have vacuum expectation values $\langle H \rangle = (0, v_{EW}/\sqrt{2})^t$ and $\langle H_d \rangle = v_d/\sqrt{2}$, the mass parameters are found to be

$$\mu^2 = \lambda\, v_{EW}^2 + \frac{\lambda_{h h_d}}{2} v_d^2 \ , \quad \mu_{h_d}^2 = \lambda_{h_d}\, v_d^2 + \frac{\lambda_{h h_d}}{2} v_{EW}^2 \ . \tag{6.7}$$

Now we work in the unitary gauge:

$$H = \frac{1}{\sqrt{2}} \begin{pmatrix} 0 \\ v_{EW} + h \end{pmatrix} , \quad H_d = \frac{1}{\sqrt{2}} (v_d + h_d) \ . \tag{6.8}$$

The two Higgs bosons h, h_d mix and can be rotated to the mass basis:

$$\begin{pmatrix} h_1 \\ h_2 \end{pmatrix} = \begin{pmatrix} \cos\theta_S & -\sin\theta_S \\ \sin\theta_S & \cos\theta_S \end{pmatrix} \begin{pmatrix} h \\ h_d \end{pmatrix} \ , \tag{6.9}$$

where h_1 can be identified as the observed Higgs boson with a mass $M_1 = 125$ GeV, and h_2 is a new scalar boson with mass M_2. After diagonalizing the mass matrix, the free parameters of the scalar sector are

$$\theta_S, \quad M_1 = 125 \text{ GeV}, \quad M_2, \quad v_d, \quad \text{and} \quad v_{EW} = 246 \text{ GeV} \ . \tag{6.10}$$

All parameters in the Lagrangian can then be determined

$$\begin{aligned}
\lambda = \frac{M_1^2 \cos^2\theta_S + M_2^2 \sin^2\theta_S}{2\, v_{EW}^2} \ , \quad \lambda_{h_d} = \frac{M_2^2 \cos^2\theta_S + M_1^2 \sin^2\theta_S}{2\, v_d^2} \ , \\
\lambda_{hh_d} = \frac{M_2^2 - M_1^2}{2\, v_{EW}\, v_d} \sin 2\theta_S \ , \\
\mu^2 = \frac{1}{2}\left[M_1^2 \cos^2\theta_S + M_2^2 \sin^2\theta_S + \frac{\tan\beta}{2}\left(M_2^2 - M_1^2\right)\sin 2\theta_S \right] \ , \\
\mu_{h_d}^2 = \frac{1}{2}\left[M_2^2 \cos^2\theta_S + M_1^2 \sin^2\theta_S + \frac{1}{2\,\tan\beta}\left(M_2^2 - M_1^2\right)\sin 2\theta_S \right] \ ,
\end{aligned} \tag{6.11}$$

where $\tan\beta = v_d/v_{EW}$.

To check the stability of the scalar potential, we consider it when the fields H and H_d are large:

$$\begin{aligned}
V(H, H_d) &\rightarrow \lambda\,|H|^4 + \lambda_{hh_d}|H|^2|H_d|^2 + \lambda_{h_d}|H_d|^4 \\
&= \left(\lambda - \frac{1}{4}\frac{\lambda_{hh_d}^2}{\lambda_{h_d}}\right)|H|^4 + \lambda_{h_d}\left(|H_d|^2 + \frac{1}{2}\frac{\lambda_{hh_d}}{\lambda_{h_d}}|H|^2\right)^2 \ ,
\end{aligned} \tag{6.12}$$

where in the last step we completed the square. The potential is bounded when

$$4\,\lambda_{h_d}\lambda \geq \lambda_{hh_d}^2, \quad \lambda > 0, \quad \text{and} \quad \lambda_{h_d} > 0 \ . \tag{6.13}$$

From the relationships in Eq. (6.11) we have

$$4\,\lambda_{h_d}\lambda - \lambda_{hh_d}^2 = \frac{M_1^2 M_2^2}{v_d^2 v_{EW}^2} > 0 \ . \tag{6.14}$$

Hence, the boundedness condition for the potential is always satisfied as long as λ and λ_{h_d} are both positive.

For our analysis in the next sections, only two trilinear scalar couplings are relevant:

$$V(h_1, h_2) \supset \frac{1}{2}\lambda_{122}\, h_1\, h_2^2 + \frac{1}{2}\lambda_{112}\, h_1^2\, h_2 \ , \tag{6.15}$$

where

$$\begin{aligned}\lambda_{122} &= -\frac{M_1^2 + 2\,M_2^2}{2\,v_d}\sin 2\theta_S\,(\cos\theta_S - \tan\beta\,\sin\theta_S)\ , \\ \lambda_{112} &= \frac{2\,M_1^2 + M_2^2}{2\,v_d}\sin 2\theta_S\,(\tan\beta\,\cos\theta_S + \sin\theta_S)\ .\end{aligned} \tag{6.16}$$

6.1.2 Gauge Sector

From Eq.(6.2), the $U(1)_d$ gauge boson can mix with the SM electroweak gauge bosons. After diagonalizing the gauge bosons, the covariant derivative in Eq. (6.5) becomes

$$\begin{aligned}D_\mu &= \partial_\mu - ig_S t^A G_\mu^A - igT^+W^+ - igT^-W^- - ieQA_\mu \\ &\quad -i\left(\hat{g}_Z\hat{Q}_Z\cos\theta_d - g_dY_d\sin\theta_d - \varepsilon\frac{g'}{\cos\hat{\theta}_W}Y\sin\theta_d\right)Z_\mu \\ &\quad -i\left(\hat{g}_Z\hat{Q}_Z\sin\theta_d + g_dY_d\cos\theta_d + \varepsilon\frac{g'}{\cos\hat{\theta}_W}Y\cos\theta_d\right)\gamma_{d,\mu}\ ,\end{aligned} \tag{6.17}$$

where θ_d is a mixing angle between the dark photon and SM Z-boson; $e = g\sin\hat{\theta}_W = g'\cos\hat{\theta}_W$ and $Q = T^3 + Y$ are the usual electromagnetic charge and operator respectively; $\hat{g}_Z = e/\cos\hat{\theta}_W/\sin\hat{\theta}_W$ and $\hat{Q}_Z = T_3 - \hat{x}_W Q$ with $\hat{x}_W = \sin^2\hat{\theta}_W$ are the neutral current coupling and operator respectively; $T^\pm = (T^1 \pm iT^2)/\sqrt{2}$; Z is the observed EW neutral current boson with mass M_Z; and $\gamma_{d,\mu}$ is the dark photon with mass M_{γ_d}. Additionally, $\hat{\theta}_W$ is the mixing angle between B'_μ and W^3_μ. The relationship between $\hat{\theta}_W$ and other model parameters is not the same as the SM weak mixing angle. Hence, we introduce the hat notation to emphasize the difference. The relationship between the SM weak mixing angle and $\hat{\theta}_W$ is given below. For simplicity of notation, we have redefined the coupling constant and kinetic mixing parameter

$$g_d = g'_d/\sqrt{1 - \varepsilon'^2/\cos^2\hat{\theta}_W} \quad \text{and} \quad \varepsilon = \varepsilon'/\sqrt{1 - \varepsilon'^2/\cos^2\hat{\theta}_W}\ . \tag{6.18}$$

The SM EW sector has three independent parameters, which we choose to be the exper-

imentally measured Z mass, the fine-structure constant at zero momentum, and G-Fermi [134]:

$$M_Z = 91.1876 \text{ GeV}, \ \alpha_{EM}^{-1}(0) = 137.035999074, \ G_F = 1.1663787 \times 10^{-5} \text{ GeV}^{-2} \ . \quad (6.19)$$

In addition to the EW parameters, we have the new free parameters:

$$v_d, \quad M_{\gamma_d}, \quad \text{and}, \quad \varepsilon \ . \quad (6.20)$$

All other parameters in the gauge sector can be expressed in terms of these. Since $\varepsilon^2 \ll 1$, we can solve equations for $\sin\theta_d$, g_d, and $\cos\hat{\theta}_W$ iteratively as an expansion in ε:

$$\sin\theta_d \ = \ \frac{\tan\theta_W^{SM}}{1-\tau_{\gamma_d}^2}\varepsilon + \mathcal{O}(\varepsilon^3), \quad \cos\hat{\theta}_W = \cos\theta_W^{SM} + \mathcal{O}(\varepsilon^2), \quad \text{and} \quad g_d = \frac{M_{\gamma_d}}{v_d} + \mathcal{O}(\varepsilon^2) \ ,$$

where $\tau_{\gamma_d} = M_{\gamma_d}/M_Z$ and the SM value of the weak mixing angle is

$$\cos^2\theta_W^{SM} = \frac{1}{2} + \frac{1}{2}\sqrt{1 - \frac{2\sqrt{2}\,\pi\alpha_{EM}(0)}{G_F\,M_Z^2}} \ . \quad (6.21)$$

Although these are good approximations for $\varepsilon^2 \ll 1$, unless otherwise noted we will use exact expressions of parameters.

Note that in the limit of small kinetic mixing $\varepsilon \ll 1$ and dark photon mass much less than the Z-mass $M_{\gamma_d} \ll M_Z$ we find the covariant derivative

$$\begin{aligned} D_\mu \ &= \ \partial_\mu - ig_S t^A G_\mu^A - ig^{SM}T^+W^+ - ig^{SM}T^-W^- - ieQA_\mu \quad (6.22) \\ &\quad -i\left[g_Z^{SM}Q_Z^{SM} - \varepsilon g_d\,Y_d\,\tan\theta_W^{SM}\right]Z_\mu - i\left[\varepsilon eQ + g_d Y_d\right]\gamma_{d,\mu} + \mathcal{O}(\varepsilon^2, M_{\gamma_d}^2/M_Z^2) \ , \end{aligned}$$

where the superscript SM indicates the SM value of parameters. Hence we see that the dark photon couples to SM particles through the electromagnetic current with coupling strength

εeQ. Additionally, the Z-boson obtains additional couplings to particles with non-zero dark charge Y_d with strength $\varepsilon\, g_d\, Y_d\, \tan\theta_W^{SM}$.

6.1.3 Fermion Sector

To avoid flavor constraints, we only allow the VLQ t_2 to mix with the third generation SM quarks. The allowed Yukawa interactions and mass terms that are symmetric under $SU(3) \times SU(2)_L \times U(1)_Y \times U(1)_d$ are

$$\mathcal{L}_{Yuk} = -y_b \overline{Q}_L H b_R - y_t \overline{Q}_L \widetilde{H} t_{1R} - \lambda_t H_d \bar{t}_{2L} t_{1R} - M_{t_2} \bar{t}_{2L} t_{2R} + \text{h.c.}\ . \tag{6.23}$$

After symmetry breaking, the VLQ and top quark mass terms are then

$$\mathcal{L}_{T,mass} = -\overline{\chi}_L \mathcal{M} \chi_R + \text{h.c.}\ , \tag{6.24}$$

where

$$\chi_\tau = \begin{pmatrix} t_{1\tau} \\ t_{2\tau} \end{pmatrix},\ \mathcal{M} = \begin{pmatrix} \frac{y_t\, v_{EW}}{\sqrt{2}} & 0 \\ \frac{\lambda_t\, v_d}{\sqrt{2}} & M_{t_2} \end{pmatrix}\ , \tag{6.25}$$

and $\tau = L,\, R$. To diagonalize the mass matrix, we perform the bi-unitary transformation:

$$\begin{pmatrix} t_L \\ T_L \end{pmatrix} = \begin{pmatrix} \cos\theta_L^t & -\sin\theta_L^t \\ \sin\theta_L^t & \cos\theta_L^t \end{pmatrix} \begin{pmatrix} t_{1L} \\ t_{2L} \end{pmatrix}\ ,\quad \begin{pmatrix} t_R \\ T_R \end{pmatrix} = \begin{pmatrix} \cos\theta_R^t & -\sin\theta_R^t \\ \sin\theta_R^t & \cos\theta_R^t \end{pmatrix} \begin{pmatrix} t_{1R} \\ t_{2R} \end{pmatrix}\ , \tag{6.26}$$

where t and T are the mass eigenstates with masses $M_t = 173$ GeV and M_T, respectively. Since the Lagrangian only has three free parameters, the top sector only has three inputs which we choose to be

$$M_t = 173 \text{ GeV},\quad M_T,\quad \text{and}\quad \theta_L^t\ . \tag{6.27}$$

The Lagrangian parameters λ_t, y_t, M_{t_2} can be expressed by

$$\begin{aligned} y_t &= \frac{\sqrt{2}\sqrt{M_t^2\cos^2\theta_L^t + M_T^2\sin^2\theta_L^t}}{v_{EW}} \,, & (6.28)\\ \lambda_t &= \frac{(M_T^2 - M_t^2)\sin 2\theta_L^t}{\sqrt{2}v_d\sqrt{M_t^2\cos^2\theta_L^t + M_T^2\,\sin^2\theta_L^t}} \,, & (6.29)\\ M_{t_2} &= \frac{M_t\,M_T}{\sqrt{M_t^2\cos^2\theta_L^t + M_T^2\sin^2\theta_L^t}} \,. & (6.30) \end{aligned}$$

The right-handed mixing angle is redundant and can be determined via

$$\cos\theta_R^t = \frac{M_{t_2}}{M_T}\cos\theta_L^t \quad \text{and} \quad \sin\theta_R^t = \frac{M_{t_2}}{M_t}\sin\theta_L^t \,. \tag{6.31}$$

After rotating to the scalar and fermion mass eigenbases, the $h_{1,2}$ couplings to the third generation and VLQ are given by

$$\begin{aligned} \mathcal{L} \supset & -h_1\left[\lambda_{tt}^{h_1}\bar{t}t + \lambda_{TT}^{h_1}\overline{T}T + \bar{t}\left(\lambda_{tT}^{h_1}P_R + \lambda_{Tt}^{h_1}P_L\right)T + \overline{T}\left(\lambda_{Tt}^{h_1}P_R + \lambda_{tT}^{h_1}P_L\right)t\right] \quad (6.32)\\ & - h_2\left[\lambda_{tt}^{h_2}\bar{t}t + \lambda_{TT}^{h_2}\overline{T}T + \bar{t}\left(\lambda_{tT}^{h_2}P_R + \lambda_{Tt}^{h_2}P_L\right)T + \overline{T}\left(\lambda_{Tt}^{h_2}P_R + \lambda_{tT}^{h_2}P_L\right)t\right] \,, \end{aligned}$$

where the h_1 couplings are

$$\begin{aligned} \lambda_{tt}^{h_1} &= \frac{1}{\sqrt{2}}\cos\theta_R^t\left(y_t\cos\theta_L^t\cos\theta_S + \lambda_t\sin\theta_L^t\sin\theta_S\right) \,, & (6.33)\\ \lambda_{tT}^{h_1} &= \frac{1}{\sqrt{2}}\sin\theta_R^t\left(y_t\cos\theta_L^t\cos\theta_S + \lambda_t\sin\theta_L^t\sin\theta_S\right) \,,\\ \lambda_{Tt}^{h_1} &= \frac{1}{\sqrt{2}}\cos\theta_R^t\left(y_t\sin\theta_L^t\cos\theta_S - \lambda_t\cos\theta_L^t\sin\theta_S\right) \,,\\ \lambda_{TT}^{h_1} &= \frac{1}{\sqrt{2}}\sin\theta_R^t\left(y_t\sin\theta_L^t\cos\theta_S - \lambda_t\cos\theta_L^t\sin\theta_S\right) \,, \end{aligned}$$

and the h_2 couplings are

$$\begin{aligned}
\lambda_{tt}^{h_2} &= \frac{1}{\sqrt{2}} \cos\theta_R^t \left(y_t \cos\theta_L^t \sin\theta_S - \lambda_t \sin\theta_L^t \cos\theta_S \right) \ , \\
\lambda_{tT}^{h_2} &= \frac{1}{\sqrt{2}} \sin\theta_R^t \left(y_t \cos\theta_L^t \sin\theta_S - \lambda_t \sin\theta_L^t \cos\theta_S \right) \ , \\
\lambda_{Tt}^{h_2} &= \frac{1}{\sqrt{2}} \cos\theta_R^t \left(y_t \sin\theta_L^t \sin\theta_S + \lambda_t \cos\theta_L^t \cos\theta_S \right) \ , \\
\lambda_{TT}^{h_2} &= \frac{1}{\sqrt{2}} \sin\theta_R^t \left(y_t \sin\theta_L^t \sin\theta_S + \lambda_t \cos\theta_L^t \cos\theta_S \right) \ .
\end{aligned} \tag{6.34}$$

Now we consider the small angle limit $|\theta_L^t| \ll 1$. If the VLQ and top quark have similar masses $M_T \sim M_t$, then Eq. (6.30) becomes $M_{t_2} \sim M_T \sim M_t$. In this limit, from Eq. (6.31), we see that $\theta_L^t \sim \theta_R^t$ and both mixing angles are small. However, for a large fermion mass hierarchy $M_t/M_T \ll 1$, the right-handed mixing angle expressions in Eq. (6.31) become

$$\cos\theta_R^t \approx \frac{M_t/M_T}{\sqrt{\sin^2\theta_L^t + M_t^2/M_T^2}}, \quad \sin\theta_R^t \approx \frac{\sin\theta_L^t}{\sqrt{\sin^2\theta_L^t + M_t^2/M_T^2}} \ . \tag{6.35}$$

There are two cases then:

$$\sin\theta_R^t \sim \begin{cases} (M_T/M_t)\sin\theta_L^t & \text{if } |\sin\theta_L^t| < M_t/M_T \ll 1 \\ \pm 1 & \text{if } M_t/M_T \lesssim |\sin\theta_L^t| \ll 1 \ , \end{cases} \tag{6.36}$$

where the sign of ± 1 depends on the sign of θ_L^t. Hence, as discussed in Ref. [237], the right-handed mixing angle is enhanced relative to the left-handed mixing angle due to a large fermion mass hierarchy.

Since t_2 and t_1 have different quantum numbers and mix, flavor off-diagonal couplings between the VLQ T and the SM third generation quarks appear. In the small mixing angle

limit, $M_t/M_T, |\theta_L^t|, |\varepsilon| \ll 1$ the relevant couplings are

$$\begin{aligned} W-T-b &\sim i\frac{g}{\sqrt{2}}\sin\theta_L^t\,\gamma^\mu\,P_L\ , \\ Z-T-t &\sim i\frac{g_Z^{SM}}{2}\sin\theta_L^t\,\gamma^\mu\,P_L + ig_d\,\frac{(M_T/M_t)\sin\theta_L^t}{1+(M_T/M_t)^2\sin^2\theta_L^t}\sin\theta_d\,\gamma^\mu\,P_R\ , \\ \gamma_d-T-t &\sim -i\,g_d\,\sin\theta_L^t\,P_L - i\,g_d\,\frac{(M_T/M_t)\sin\theta_L^t}{1+(M_T/M_t)^2\sin^2\theta_L^t}P_R\ . \end{aligned} \tag{6.37}$$

Note that although the right-handed coupling to the Z appears of order θ^2, if $M_t/M_T \sim |\theta_L^t| \sim |\theta_d|$ the left- and right-handed couplings can be of the same order. However, with this counting the right-handed coupling of the dark photon, VLQ, and top quark is unsuppressed. This is precisely the fermionic mass hierarchy enhancement noticed in Ref. [237]. However, as we will point out, a fermionic mass hierarchy is not necessary for the VLQ decays into the dark Higgs or dark photon to be dominant.

6.2 Current Constraints

6.2.1 Electroweak Precision and Direct Searches

Electroweak precision measurements place strong constraints on the addition of new particles. In the model presented here, there are many contributions to the oblique parameters [239, 240, 241]: new loop contributions from the VLQ [242, 243, 244, 245, 246, 247] and scalar [37, 44, 248, 84, 86, 88] as well as shifts in couplings to EW gauge boson couplings from the mixing of the dark photon with hypercharge [249, 204], dark Higgs with the SM Higgs, and the VLQ with the top quark. Since there are multiple contributions to the oblique parameters in this model, there is the possibility of cancellations that could relax some of the constraints. To be conservative, we will only consider one contribution at a time.

There are also many direct searches for VLQs, new scalars, and dark photons at colliders and fixed target experiments. Here we summarize the current state of constraints:

- **VLQ:** The dashed line labeled "EW Prec" in Fig. 6.1a shows the EW precision constraints on the VLQ-top quark mixing angle. This result is taken from Ref. [247]. The current limits are $|\sin\theta_L^t| \lesssim 0.16$ (0.11) for VLQ mass $M_T = 1$ TeV (2 TeV).

  Additionally, in our model the top-bottom component of the CKM matrix is $V_{tb} = (V_{tb})_{SM}\cos\theta_L^t$, where the subscript SM denotes the SM value. The most stringent constraints on V_{tb} come from single top quark production. A combination of Tevatron and LHC single top measurements give a constraint of $|V_{tb}| = 1.019 \pm 0.025$ [134]. Another more recent analysis including differential distributions gives a bound of $|V_{tb}| = 0.986 \pm 0.008$ [250]. Both constraints give an upper bound of $|\sin\theta_L^t| \leq 0.24$ at the 95% confidence level. This limit is indicated by the orange dotted line labeled "CKM" in Fig. 6.1a, where the region above is excluded. We see that the CKM measurements are not currently as important as EW precision constraints.

  As mentioned above, in the model presented here traditional T decays into SM EW bosons Z, W, Higgs will be suppressed and not directly applicable. Nevertheless, for completeness we summarize their results here. In these traditional modes, the LHC excludes VLQ masses $M_T \lesssim 1.1 - 1.4$ TeV in pair production searches [251, 252, 253] and $M_T \lesssim 1 - 1.2$ TeV in single production searches [254, 255, 256]. Single production of an $SU(2)_L$ singlet T depends on the mixing angle θ_L^t and decouples as $\theta_L^t \to 0$ [223] weakening the above limit. Taking this into account, LHC searches for single T production have been cast into constraints on θ_L^t which are comparable to EW precision constraints for $M_T \lesssim 1$ TeV [257, 254].

- **Scalar:** The addition of a new scalar shifts Higgs boson couplings away from SM predictions, as well as contributing to new loop contributions to EW precision parameters. Additionally, many searches have been performed for new scalar production at the LHC [63, 258, 259, 260, 67, 261, 262] as well as at LEP [263, 264, 265]. However, the most stringent constraints [266] come from precision measurements of the observed

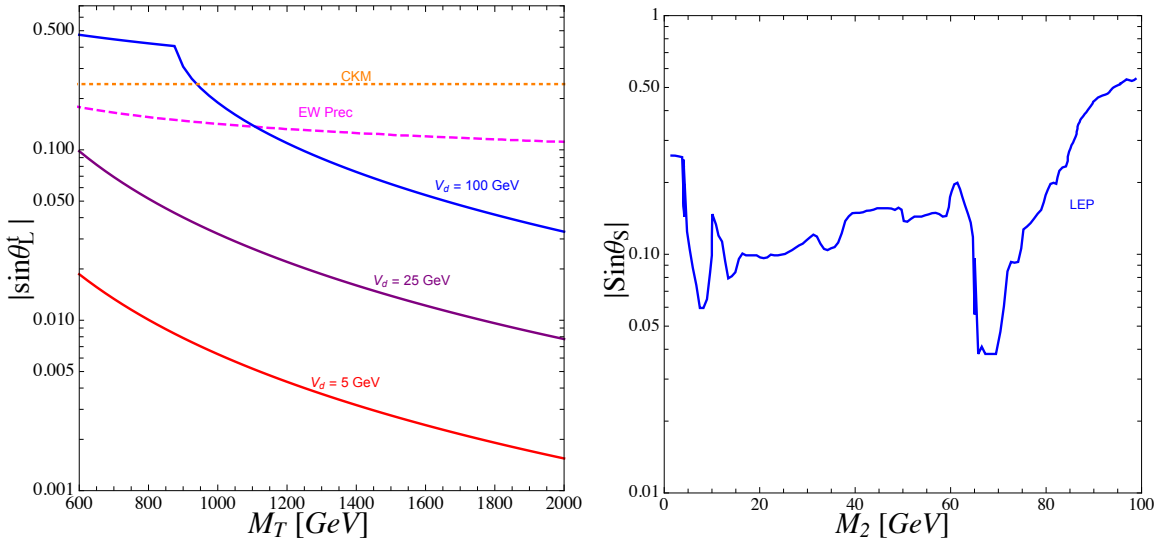

(a) (b)

Figure 6.1: (a) Upper bounds for $|\sin\theta_L^t|$ from (dashed magenta) EW precision data from Ref. [247]; (dotted orange) current CKM measurements; and (solid) requiring λ_t satisfy Eq. (6.41) for (red) $v_d = 5$ GeV, (violet) $v_d = 25$ GeV, and (blue) $v_d = 100$ GeV. (b) Upper bound on $|\sin\theta_S|$ from LEP for $M_2 < 100$ GeV as found in Ref. [88].

$M_1 = 125$ GeV Higgs boson for $M_1 \lesssim M_2 \lesssim 650$ GeV and precision W-mass constraints [86, 88, 267] for 650 GeV $\lesssim M_2 \lesssim 1$ TeV. The constraints on the scalar mixing angle is $|\sin\theta_S| \lesssim 0.21 - 0.22$ for $M_1 < M_2 < 1$ TeV [266]. For $M_2 < 100$ GeV LEP searches can be very constraining on the scalar mixing angle, as shown in Fig. 6.1b. These results are adapted from Ref. [88].

- **Kinetic Mixing:** As can be seen in covariant derivative in Eq. (6.17), the couplings between the Z and SM particles are shifted due to the kinetic mixing of the Hypercharge and $U(1)_d$ gauge boson. Hence, electroweak precision data can place bounds on the value of the kinetic mixing parameter ε [249, 204]. The most stringent constraints from EW precision are $|\varepsilon| \lesssim 3 \times 10^{-2}$ [204]. This is less constraining than direct searches for dark photons at fixed target experiments or low energy experiments [268] which require $|\varepsilon| \lesssim 10^{-3}$ for $M_{\gamma_d} = 0.1 - 10$ GeV.

6.2.2 Perturbativity Bounds

Requiring the top quark and VLQ Yukawa couplings be perturbative can place strong constraints on the top quark-VLQ mixing angle. As can be seen in Eq. (6.29), in the limit that $M_t/M_T \sim |\sin\theta_L^t| \ll 1$ the Yukawa couplings become

$$\begin{aligned} y_t &= \sqrt{2}\frac{M_t}{v_{EW}}\sqrt{1+\frac{M_T^2}{M_t^2}\sin^2\theta_L^t} + \mathcal{O}(\sin^2\theta_L^t, M_t^2/M_T^2), \\ \lambda_t &= \sqrt{2}\frac{M_T^2-M_t^2}{v_d M_t}\sin\theta_L^t + \mathcal{O}(\sin^2\theta_L^t)\ . \end{aligned} \tag{6.38}$$

While y_t is well-behaved for $M_t/M_T \sim |\sin\theta_L^t|$, λ_t is enhanced by M_T/v_d. Hence, the mixing angle must be small to compensate for this and ensure λ_t remains perturbative.

To determine when λ_t becomes non-perturbative, we calculate the perturbative unitarity limit for the $H_d t \to H_d t$ scattering process and find that

$$|\lambda_t| \leq 4\sqrt{2\pi}\ . \tag{6.39}$$

When this limit is saturated, there must be a minimum higher order correction of 41% to unitarize the S-matrix [106]. Hence, this is near or at the limit for which we can trust perturbative calculations.

To translate the limit on λ_t to a limit on the mixing angle $\sin\theta_L^t$ we solve Eq. (6.29) to find

$$|\sin\theta_L^t| = \frac{1}{2}\sqrt{\frac{2\,M_T^2 - 2\,M_t^2 - \lambda_t^2 v_d^2}{M_T^2 - M_t^2}\left(1-\sqrt{1-\frac{8\,\lambda_t^2 v_d^2 M_t^2}{(2\,M_T^2 - 2\,M_t^2 - v_d^2\lambda_t^2)^2}}\right)}\ . \tag{6.40}$$

This solution is real if $|\lambda_t| \leq \sqrt{2}(M_T - M_t)/v_d$. Combining with the perturbative unitarity limit in Eq. (6.39), we find an upper limit on λ_t:

$$|\lambda_t| \leq \sqrt{2}\min\left\{\frac{M_T - M_t}{v_d}, 4\sqrt{\pi}\right\}\ . \tag{6.41}$$

Note that for VLQ mass $M_T < 4\sqrt{\pi}\, v_d + M_t$, the perturbative unitarity limit is never saturated. Hence, for a fixed v_d there is an upper bound on M_T for which λ_t is always perturbative. Assuming M_t, $v_d \ll M_T$, the upper-bound on $\sin\theta_L^t$ becomes

$$|\sin\theta_L^t| \lesssim \begin{cases} 4\sqrt{\pi}\dfrac{v_d\, M_t}{M_T^2} & \text{for } M_T \geq 4\sqrt{\pi}\, v_d + M_t \\ \sqrt{M_t/M_T} & \text{for } M_T < 4\sqrt{\pi}\, v_d + M_t \end{cases} . \tag{6.42}$$

In Fig. 6.1a we show the limits on $|\sin\theta_L^t|$ from (solid) requiring that λ_t satisfies Eq. (6.41) for various values of v_d together with (dashed magenta) EW precision data and (dotted orange) CKM constraints. The kink in the $v_d = 100$ GeV line occurs at VLQ mass $M_T \sim 4\sqrt{\pi}\, v_d + M_t \sim 880$ GeV. For $M_T < 4\sqrt{\pi}\, v_d + M_t$ the upper bound on $\sin\theta_L^t$ is proportional to $M_T^{-1/2}$, while for $M_T \geq 4\sqrt{\pi}v_d + M_t$ it is proportional to M_T^{-2} as shown in Eq. (6.42). As can be clearly seen, over much of the parameter range the limits on λ_t in Eq. (6.41) provide the most stringent constraint on $\sin\theta_L^t$. As mentioned earlier, this is due to λ_t having an enhancement of $M_T^2/M_t/v_d$, requiring $\sin\theta_L^t$ to be quite small to ensure λ_t does not get too large. EW precision is more constraining for larger v_d and smaller M_T.

6.2.3 $h_1 \to \gamma_d\gamma_d$ Limits

There have been searches at the LHC [269] for $h_1 \to \gamma_d\gamma_d \to 4\ell$ where $\ell = e, \mu$ that place limits on combination

$$\frac{\sigma(pp \to h_1)}{\sigma_{SM}(pp \to h_1)}\mathrm{BR}(h_1 \to \gamma_d\gamma_d) \lesssim BR_{\rm lim} \ , \tag{6.43}$$

for dark photons in the mass range 1 GeV $< M_{\gamma_d} <$ 60 GeV. The subscript SM indicates a SM production rate. The h_1 production rate is dominantly via gluon fusion which in the model presented here is altered via the shift in the $h_1 - t - t$ coupling away from the SM prediction as shown in Eqs. (6.32,6.33) and new loop contributions from the new VLQ.

However, in the small mixing angle limit with the counting $\theta_L^t \sim \theta_S \sim M_t/M_T$, we have

$$\sigma(pp \to h_1) = \sigma_{SM}(pp \to h_1) + \mathcal{O}(\theta^2) \ . \tag{6.44}$$

In addition to the usual SM decay modes, h_1 can decay into $\gamma_d\gamma_d$, $\gamma_d Z$, and $h_2 h_2$ when kinematically allowed. Using the counting $\varepsilon \sim \theta_L^t \sim \theta_S \sim M_{\gamma_d}/M_Z \sim M_2/M_Z$, the partial widths into the new decay modes are

$$\begin{aligned} \Gamma(h_1 \to h_2 h_2) &\approx \Gamma(h_1 \to \gamma_d\gamma_d) = \frac{M_1^3 \sin^2\theta_S}{32\,\pi\, v_d^2} + \mathcal{O}(\theta^3) \ , \\ \Gamma(h_1 \to Z\gamma_d) &= \mathcal{O}(\theta^4) \ . \end{aligned} \tag{6.45}$$

For the decays into SM, all the couplings between h_1 and SM fermions and gauge bosons, except for the $h_1 - Z - Z$ and $h_1 - t - t$ couplings, are uniformly suppressed by $\cos\theta$. The $h_1 - Z - Z$ and $h_1 - t - t$ couplings are more complicated due to the $Z - \gamma_d$ mixing and $t - T$ mixing, respectively. Additionally, there are new contributions to the loop level decays $h_1 \to gg$, $h_1 \to \gamma\gamma$, and $h_1 \to \gamma Z$ due to the new VLQ. Since the partial widths $\Gamma(h_1 \to \gamma\gamma)$ and $\Gamma(h_1 \to Z\gamma)$ make negligible contributions to the total width, we will neglect changes in these quantities. Reweighting the SM partial widths with the new contributions, the width into fully SM final states are then

$$\begin{aligned} &\Gamma(h_1 \to X_{SM} X_{SM}^{(*)}) \\ &\quad = \cos^2\theta_S \times \Big(\Gamma_{SM}(h_1 \to X_{SM} X_{SM}^{(*)}) - \Gamma_{SM}(h_1 \to ZZ^*) - \Gamma_{SM}(h_1 \to gg)\Big) \\ &\qquad + \left(\cos\theta_S - \frac{g_d^2\, v_{EW}\, v_d}{M_Z^2} \sin^2\theta_d \left(\cos\theta_S + \sin\theta_S \frac{v_{EW}}{v_d}\right)\right)^2 \Gamma_{SM}(h_1 \to ZZ^*) \\ &\qquad + \left|\frac{v_{EW}\, \lambda_{tt}^{h_1}}{M_t} - \frac{4}{3}\frac{v_{EW}\, \lambda_{TT}^{h_1}}{M_T\, F(\tau_t)}\right|^2 \Gamma_{SM}(h_1 \to gg) \qquad (6.46) \\ &\quad = \Gamma_{SM}(h_1) + \mathcal{O}(\theta^2) \ , \qquad (6.47) \end{aligned}$$

where X_{SM} are SM fermions or gauge bosons, the subscript SM indicates SM values of

widths, $\Gamma_{SM}(h_1) = 4.088$ MeV [114], and $\lambda_{tt}^{h_1}$, $\lambda_{TT}^{h_1}$ are in Eq. (6.33). Other SM values for the partial widths of h_1 can be found in Ref. [114]. The loop function $F(\tau_i)$ can be found in Ref. [270], where $\tau_i = 4\,M_i^2/M_1^2$ and we have used $M_T \gg M_1$ such that $F(\tau_T) = F(\infty) = -4/3$.

The total width is then

$$\begin{aligned}\Gamma_{tot}(h_1) &= \Gamma(h_1 \to X_{SM} X_{SM}^{(*)}) + \Gamma(h_1 \to \gamma_d\gamma_d) + \Gamma(h_1 \to Z\gamma_d) \\ &+ \Gamma(h_1 \to h_2 h_2)\theta(M_1 - 2\,M_2) \\ &= \Gamma_{SM}(h_1) + \mathcal{O}(\theta^2)\ , \end{aligned} \tag{6.48}$$

and Eq. (6.43) becomes

$$BR_{lim} \geq \frac{\sigma(pp \to h_1)}{\sigma_{SM}(pp \to h_1)} \mathrm{BR}(h_1 \to \gamma_d\gamma_d) = \frac{\Gamma(h_1 \to \gamma_d\gamma_d)}{\Gamma_{SM}(h_1)} + \mathcal{O}(\theta^4)\ . \tag{6.49}$$

Using Eq. (6.45) we find the limit

$$|\sin\theta_S| \leq \sqrt{\frac{32\,\pi\,v_d^2 \Gamma_{SM}(h_1)}{M_1^3} BR_{lim}} = 4.6 \times 10^{-4} \left(\frac{v_d}{\mathrm{GeV}}\right) \sqrt{BR_{lim}}\ . \tag{6.50}$$

ATLAS has measured the upper limit BR_{lim} in the mass range $M_{\gamma_d} = 1 - 15$ GeV when both dark photons decay into muons [269]. However, they have assumed $\mathrm{BR}(\gamma_d \to e^- e^+) = \mathrm{BR}(\gamma_d \to \mu^-\mu^+) = 0.5$ neglecting possible hadronic decays of the dark photon. We reweight the results of Ref. [269] using the $\mathrm{BR}(\gamma_d \to \mu^+\mu^-)$ including hadronic decays[13], as shown in Fig. 6.2a. The hatched regions correspond to hadronic resonances and were not included in the search in Ref. [269]. This is the BR_{lim} to be used in Eqs. (6.43,6.50).

In Fig. 6.2b we show the upper limit on $\sin\theta_S$ from Eq. (6.50) and using BR_{lim} in Fig. 6.2a. The solid regions are ruled out by the $h_1 \to 2\gamma_d \to 4\mu$ search for (red) $v_d = 5$ GeV, (maroon) $v_d = 25$ GeV, and (blue) $v_d = 100$ GeV. These constraints are very strong with

[13] See Sec. 6.4 for details of the $\mathrm{BR}(\gamma_d \to \mu^+\mu^-)$ calculation.

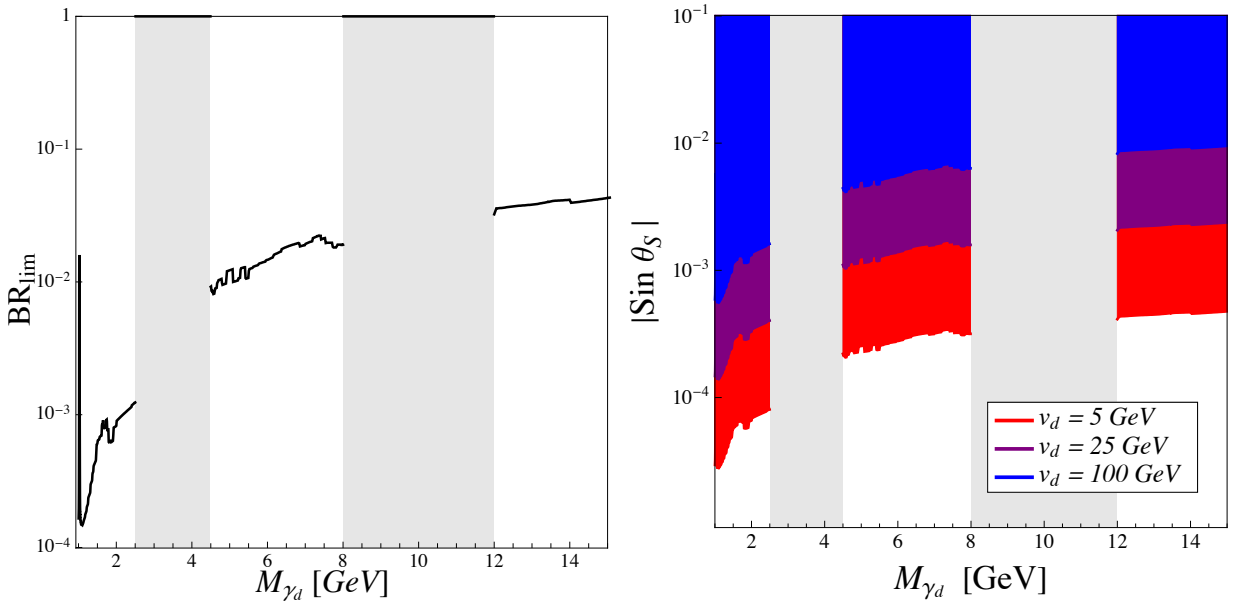

(a) (b)

Figure 6.2: (a) BR_{lim} as defined in Eq. (6.43). These are the ATLAS results for a $h_1 \to 2\gamma_d \to 4\mu$ search [269] reweighted by BR($\gamma_d \to \mu^+\mu^-$) including hadronic decays. The dashed regions are not included in the $h_1 \to 2\gamma_d \to 4\mu$ search due to resonant hadrons [269]. (b) Upper bounds on $|\sin\theta_S|$ from Eq. (6.50). The solid colored regions are ruled out for (red) $v_d = 5$ GeV, (maroon) $v_d = 25$ GeV, and (blue) $v_d = 100$ GeV.

limits in the range of $|\sin\theta_S| \lesssim 10^{-5} - 10^{-2}$. These limits are more constraining than the direct searches for h_2 as shown in Fig. 6.1b. Eq. (6.50) is linear in the dark Higgs vev v_d, so the limits on $\sin\theta_S$ become less constraining for large v_d. However, since $M_{\gamma_d} \approx g_d\, v_d$ these constraints cannot be arbitrarily relaxed without very small dark gauge coupling g_d.

If there is dark matter (DM) with mass $M_{DM} < M_{\gamma_d}/2$, it is possible that the decay of the dark photon into DM is dominant since, unlike the dark photon coupling to SM fermions, the γ_d-DM coupling would not be suppressed by the kinetic mixing parameter ε. Hence, it is possible for the Higgs to decay invisibly $h_1 \to 2\gamma_d \to$ DM. There are searches for invisible decays of h_1 with limits BR($h_1 \to$ Invisible) ≤ 0.19 [271] from CMS and BR($h_1 \to$ Invisible) ≤ 0.26 from ATLAS [272]. Assuming that BR($\gamma_d \to$ DM) $= 1$, from

Eq. (6.50) these limits correspond to

$$|\sin\theta_S| \leq \left(\frac{v_d}{\text{GeV}}\right) \times \begin{cases} 2.0 \times 10^{-4} & \text{for CMS [271]} \\ 2.3 \times 10^{-4} & \text{for ATLAS [272]} \,. \end{cases} \tag{6.51}$$

6.3 Production and Decay of Vector Like Quark

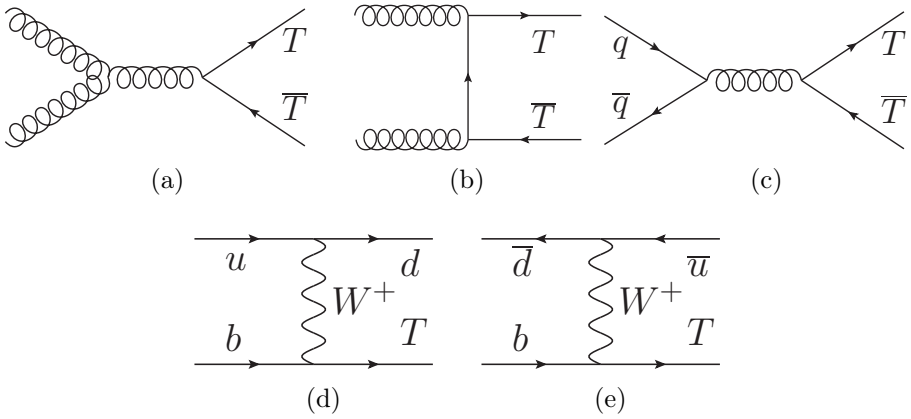

Figure 6.3: Standard production modes of VLQs at the LHC for (a-c) pair production and (d,e) VLQ plus a jet production. The conjugate processes for (d,e) are not shown here.

In this section, we focus on the production and decay of the VLQ, T, at the LHC based on the model in Sec. 6.1. Figure 6.3 displays the VLQ (a,b,c) pair production ($T\overline{T}$) and (d,e) single production in association with a jet ($T/\overline{T}$ + jet)[14]. The pair production is induced by QCD interactions so that the production cross section depends only on M_T, the spin of T, and the gauge coupling. Hence, pair production is relatively model independent[15]. The single production, on the other hand, relies on the $b - W - T$ coupling in Eq.(6.37) which is proportional to the mixing angle $\sin\theta_L^t$. Therefore the production cross section is proportional to $\sin^2\theta_L^t$ and is suppressed for small θ_L^t [223].

[14]There is also $TW^- + \overline{T}W^+$ production which is subdominant. In the model with an additional $SU(2)_L$ singlet scalar, a loop-induced $T\overline{t} + \overline{T}t$ production [223] can be as large as the pair production.

[15]In a scenario where the top partners are pair produced via a heavier resonance, the production cross section can be model dependent. See Refs. [274, 275, 276] and references therein.

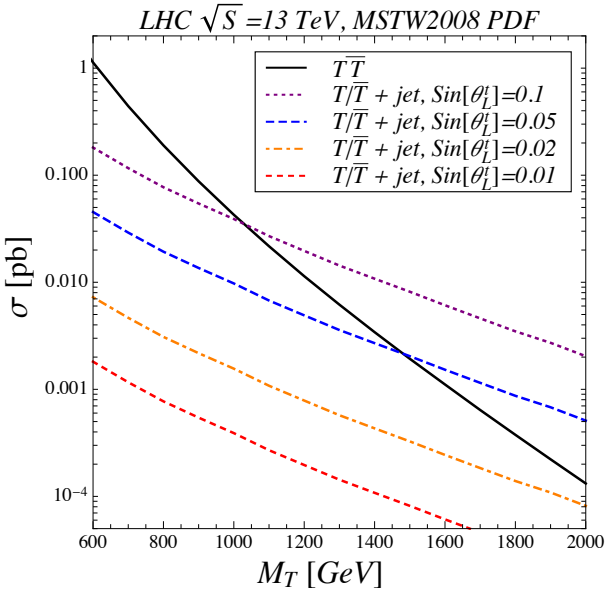

Figure 6.4: Pair $T\bar{T}$ and single T+jet production cross sections [273]. Pair production is at NNLO in QCD and single production at NLO in QCD.

In Fig. 6.4 we show cross sections for single and pair production of T from Ref. [273][16]. The pair production cross section with NNLO QCD corrections is computed using the HATHOR code [277] with the MSTW2008 parton distribution functions (PDF) [278]. The single production cross section with NLO QCD corrections is calculated using MCFM [279, 280, 281] with the same PDF. The NLO single production cross sections are rescaled by $\sin^2\theta_L^t$ to take into account the normalization of the $b-W-T$ coupling in Eq.(6.37). The single production becomes more important at high mass, where the gluon PDF sharply drops suppressing $gg \to T\overline{T}$ and the pair production phase space is squeezed relative to single production. With a sizable mixing angle $|\sin\theta_L^t| \gtrsim 0.1$, the single production outperforms the pair production in a wide range of M_T. The single production, however, vanishes as the $t-T$ mixing angle becomes very small, as required by perturbativity and EW precision [Fig. 6.1a]. This can be already seen from Figure 6.4 when $\sin\theta_L^t = 0.01$, where the T+jet cross section goes into the sub-femtobarn level which will be challenging to probe at the LHC.

[16]It should be noted that these results are for a charge 5/3 VLQ. However, a charge 2/3 partner has the same QCD and spin structure so the results are still valid since the QCD production does not depend on the electric charge of the particle.

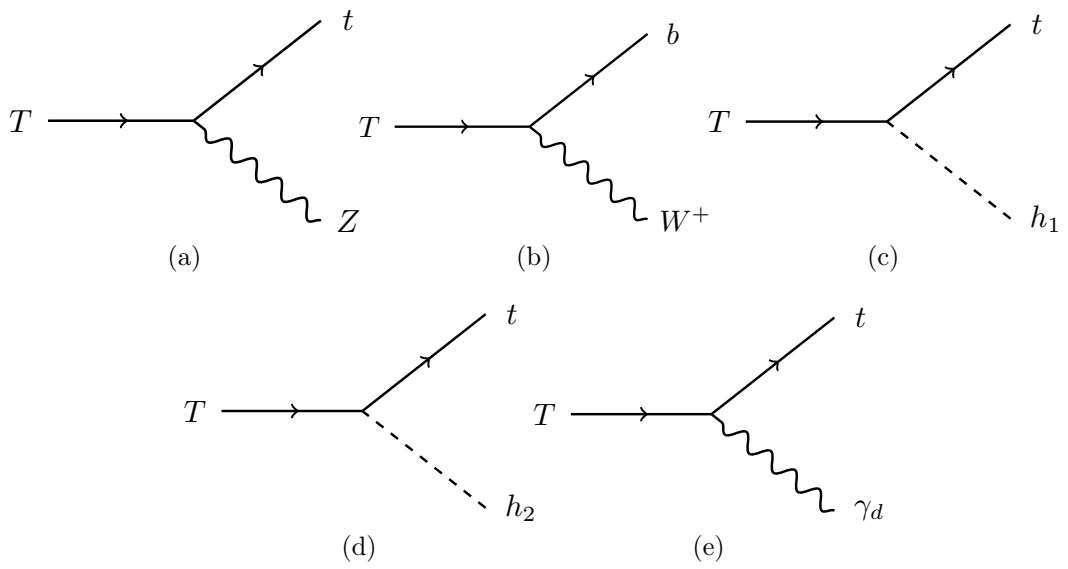

Figure 6.5: Representative Feynman diagrams for VLQ decays into (a-c) Zt, Wb, $h_1 t$. Since T is charged under both the SM and $U(1)_d$, the T is allowed to decay into (d,e) h_2 and γ_d.

Traditionally, searches for the VLQ rely on the $T \to tZ$, $T \to bW$, and $T \to th_1$ decays, as shown in Fig 6.5. However, in the scenario where T is charged under both the SM and $U(1)_d$, new decay modes into the $T \to th_2$ and $T \to t\gamma_d$ appear, which alters T phenomenology significantly. Partial widths into $Z/W/h_1$ in the limit $|\varepsilon|, |\theta_L^t|, |\theta_S| \ll 1$ and v_{EW}, $v_d \ll M_T$ are[17]

$$\Gamma(T \to t\,Z) \;\approx\; \Gamma(T \to t\,h_1) \approx \frac{1}{2}\Gamma(T \to b\,W) \approx \frac{1}{32\pi}\frac{M_T^3}{v_{EW}^2}\sin^2\theta_L^t \;. \tag{6.52}$$

For large M_T, the partial widths of T into fully SM final states are proportional to $\sim \sin^2\theta_L^t\, M_T^3/v_{EW}^2$ due to the Goldstone equivalence theorem. The partial widths into h_2 and γ_d in the limit $|\varepsilon|, |\theta_L^t|, |\theta_S| \ll 1$ and v_d, $v_{EW} \ll M_T$ are

[17]To produce numerical results and plots, however, we will use exact width expressions.

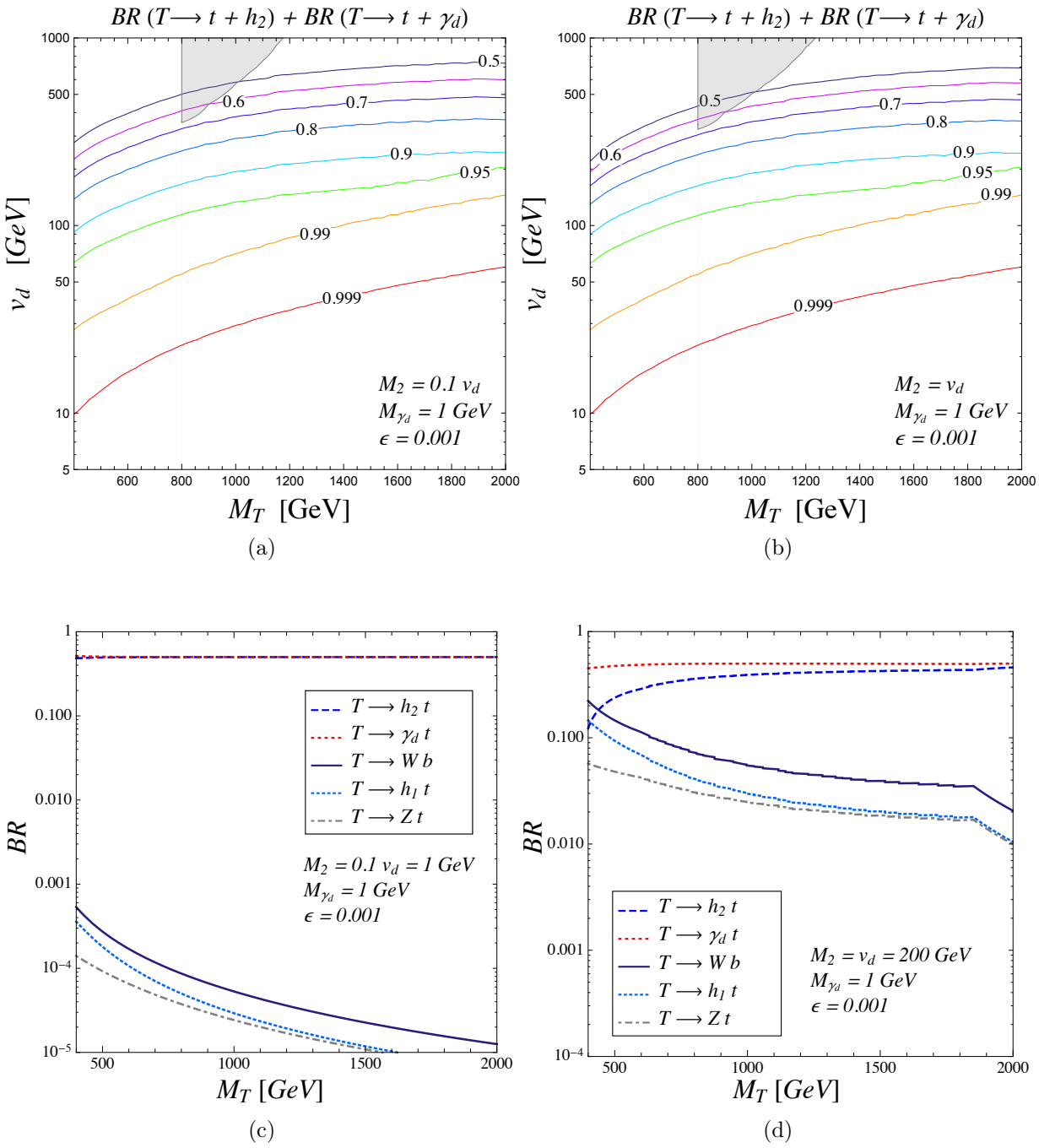

Figure 6.6: (a,b)The combined branching ratio $\mathrm{BR}(T \to t + h_2) + \mathrm{BR}(T \to t + \gamma_d)$ in $M_T - v_d$ plane for maximally allowed $\sin\theta_L^t$ and $\sin\theta_S$ in Fig. 6.1a and Eq. (6.50), respectively. In (a) $M_2 = 0.1 v_d$ and (b) $M_2 = v_d$. The full branching ratios of the T as a function of M_T for (c) $M_2 = 0.1 v_d = 1$ GeV and (d) $M_2 = v_d = 200$ GeV. For all subfigures we assume $\varepsilon = 0.001$.

$$\Gamma(T \to t\,\gamma_d) \;\approx\; \Gamma(T \to t\,h_2) \approx \frac{1}{32\pi}\frac{M_T^5}{M_t^2 v_d^2}\frac{\sin^2\theta_L^t}{1 + (M_T/M_t)^2\sin^2\theta_L^t}\,. \tag{6.53}$$

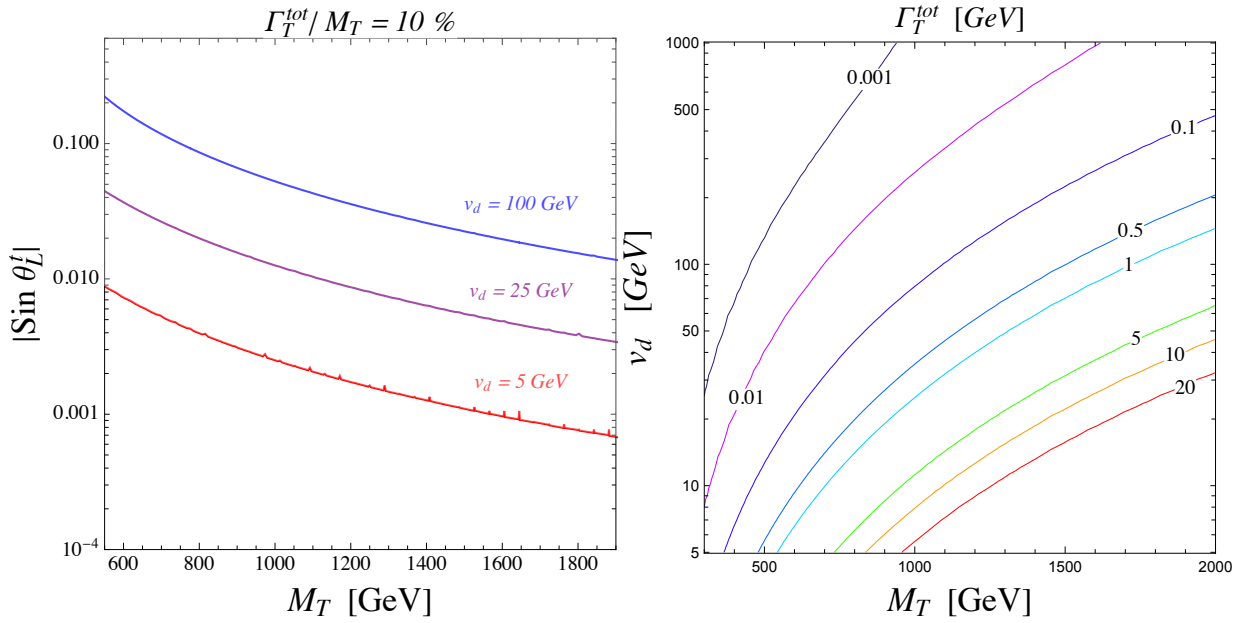

Figure 6.7: (a) Contours of $\Gamma_T^{tot}/M_T = 0.1$ in the $M_T - \sin\theta_L^t$ plane for various v_d. (b) The total width ($\Gamma_T^{\rm tot}$) of T in $M_T - v_d$ plane for $\sin\theta_L^t = 0.001$. For both sub-figures, we set $\varepsilon = 0.001$, $M_{\gamma_d} = M_2 = 2$ GeV, and $\sin\theta_S$ to its maximal value in Eq. (6.50).

Hence, the ratios of the rates of VLQ decays into the dark Higgs/photon and into fully SM final states are

$$\frac{\Gamma(T \to t + h_2/\gamma_d)}{\Gamma(T \to t/b + W/Z/h_1)} \sim \left(\frac{M_T}{M_t}\right)^2 \left(\frac{v_{EW}}{v_d}\right)^2 \frac{1}{1 + (M_T/M_t)^2 \sin^2\theta_L^t} \ . \tag{6.54}$$

There are two enhancements: (1) the $(v_{EW}/v_d)^2$ enhancement since decays into longitudinal dark photons are enhanced by v_d^{-2} compared to decays into longitudinal SM bosons which are proportional to v_{EW}^{-2}. (2) If $|\sin\theta_L^t| \lesssim M_t/M_T$ there is a $(M_T/M_t)^2$ enhancement since the right-handed top-VLQ mixing angle is larger than left-handed mixing due to a fermion mass hierarchy as seen in Eqs. (6.35-6.37). However, note that for fixed $|\sin\theta_L^t| \gg M_t/M_T$, the fermion mass hierarchy enhancement cancels and only the $(v_{EW}/v_d)^2$ enhancement survives. This is because in this limit $|\sin\theta_R^t| \to 1$ and does not grow with M_T.

Equation (6.54) shows that even in the absence of a fermionic mass hierarchy ($M_T \sim M_t$), T decays into light dark sector bosons are still strongly enhanced. This can be clearly seen

in Figure 6.6(a,b) where we show contours of the total VLQ branching ratio in h_2 and γ_d. Note that $\mathrm{BR}(T \to t + h_2) + \mathrm{BR}(T \to t + \gamma_d) \sim 0.99$ for $v_d \lesssim 30$ GeV in the entire M_T range. As M_T increases, branching ratios into the dark photon/Higgs increase due to the fermionic mass hierarchy, as discussed above. Fig. 6.6b is the same as Fig. 6.6a with a different choice of M_2. The results in both Fig. 6.6(a,b) are very similar, showing the conclusions about the branching ratio dependence on boson and fermion mass hierarchies are robust against model parameters. The reach of current searches into th, tZ, and bW [251] are shown in the gray shaded regions. We have rescaled the results of Ref. [251] according to the branching ratios in our model. There were no limits below $M_T = 800$ GeV, hence the exlusion region is truncated. As can be seen, the traditional searches are largely insensitive to our model and our approach provides a new avenue to search for T. New search strategies are necessary depending on the decays of γ_d, h_2 as we will discuss in section 6.5.

In Fig. 6.6(c,d) we show the branching ratios of T into all final states, including W, Z, h_1. The T branching ratios into the fully SM particles are less than $\sim 1\%$ for smaller $M_2 = 0.1\, v_d = 1$ GeV as shown in Fig. 6.6c. For enhanced dark sector mass scales $M_2 = v_d = 200$ GeV the rates to the SM final states can reach at most $\sim 45\%$ for $M_T \sim 300$ GeV shown in Fig. 6.6d, but then fall to the percent level for higher VLQ masses.

There is a kink in Fig. 6.6d around $M_T \sim 1.9$ TeV. For $M_T \lesssim 1.9$ TeV EW precision constraints on $\sin\theta_L^t$ are the most stringent and for $M_T \gtrsim 1.9$ TeV the perturbativity bounds on λ_t are most constraining [see Fig. 6.1a]. The EW precision and perturbativity bounds on $\sin\theta_L^t$ have different dependencies on M_T, hence the kink. The fact that the branching ratios into W/Z/Higgs become flat for M_T approaching 1.9 TeV is a reflection that the enhancement of $T \to t\, h_d/\gamma_d$ from the fermionic mass hierarchy disappears for $M_T \gg M_t$ and fixed $\sin\theta_L^t$, as discussed around Eq. (6.54). Once perturbativity constraints are dominant $\sin\theta_L^t \sim M_T/M_t$, the fermion mass hierarchy enhancement reasserts itself, and branching ratios into fully SM final states decrease precipitously.

Finally, in the limit $M_t \ll M_T$ and $v_d \ll v_{EW}$, the total width of the VLQ normalized to

M_T is

$$\frac{\Gamma_T^{tot}}{M_T} = \frac{\Gamma(T \to t\,\gamma_d) + \Gamma(T \to t\,h_2)}{M_T} \approx \frac{1}{16\pi}\frac{M_T^4}{M_t^2\,v_d^2}\frac{\sin^2\theta_L^t}{1+(M_T/M_t)^2\sin^2\theta_L^t}\ . \tag{6.55}$$

Due to the very large enhancement of $M_T^4/M_t^2/v_d^2$, the mixing angle $\sin\theta_L^t$ must be quite small for T to be narrow. In Fig. 6.7a we show contours of fixed $\Gamma_T^{tot}/M_T = 10\%$ in the $\sin\theta_L^t - M_T$ plane for various dark Higgs vevs v_d. When compared to the constraints in Fig. 6.1a, it is clear that the constraint T be narrow with $\Gamma_T^{tot} \lesssim 10\%\,M_T$ is by far the strongest constraint on $\sin\theta_L^t$. In Fig. 6.7b we show the total width Γ_T^{tot} in the $v_d - M_T$ plane. As is clear, VLQ total width grows for small v_d and larger M_T.

6.4 Decay of the dark photon

We now discuss the dark photon γ_d decays, since this specifies experimental signatures in the VLQ decay $T \to t\gamma_d$. The lowest order (LO) γ_d partial decay widths can be computed using the couplings to the light fermions from the covariant derivative in Eq. (6.22). However, this does not take into account the higher-order QCD corrections and hadronic resonances. To reflect these combined effects, we follow Ref. [204] and utilize the experimental data on electron positron collisions [134]

$$R(M_{\gamma_d}) \equiv \frac{\sigma(e^+e^- \to hadrons)}{\sigma(e^+e^- \to \mu^+\mu^-)}\ . \tag{6.56}$$

Since γ_d couplings are approximately electromagnetic, hadronic decays of γ_d can be incorporated into the total width of γ_d via

$$\begin{aligned}\Gamma_{\gamma_d}^{tot} &= R(M_{\gamma_d})\Gamma(\gamma_d \to \mu^+\mu^-) + \sum_{f=e,\mu,\tau,\nu_e,\nu_\mu,\nu_\tau}\Gamma(\gamma_d \to f\overline{f}) \\ &\approx \frac{\varepsilon^2\,e^2}{12\,\pi}M_{\gamma_d}\left[R(M_{\gamma_d}) + \sum_{\ell=e,\mu\tau}\theta(M_{\gamma_d} - 2\,M_\ell)\right]\ .\end{aligned} \tag{6.57}$$

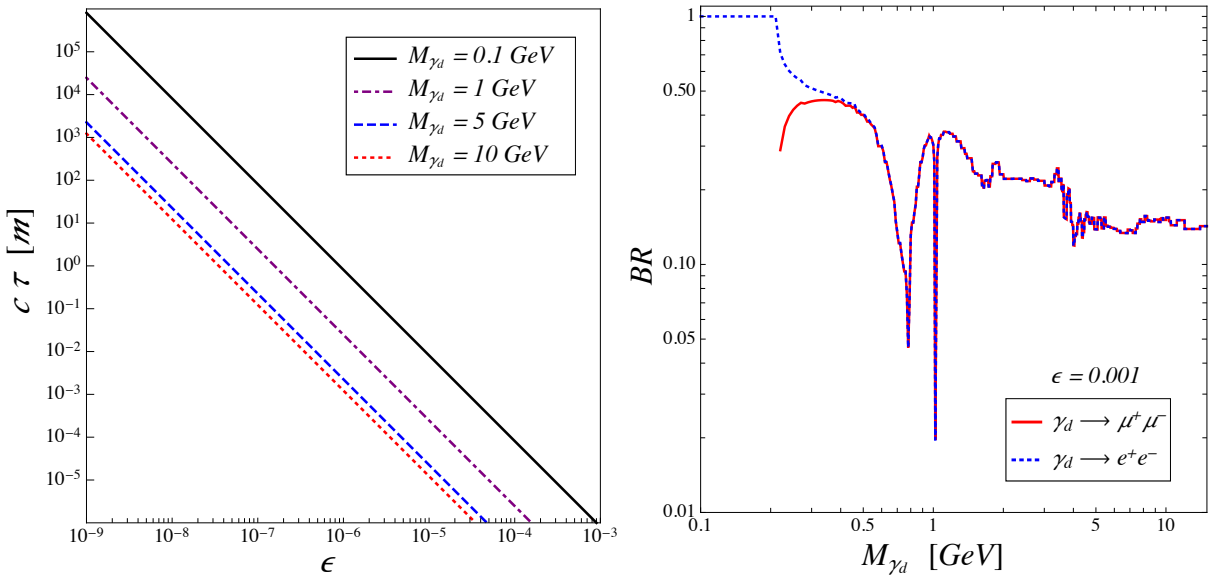

(a) (b)

Figure 6.8: (a) Decay length of γ_d as a function of the kinetic mixing parameter ε for various M_{γ_d}. (b) Branching ratios of γ_d into (solid red) $\mu^+\mu^-$ and (dotted blue) e^+e^- as a function of M_{γ_d} for $\varepsilon = 0.001$.

We have used the approximation $\varepsilon \ll 1$ and $M_{\gamma_d} \ll M_Z$ as in Eq. (6.22). We have also assumed there are no DM candidates with mass $2\,M_{DM} < M_{\gamma_d}$ and that $2\,M_2 > M_{\gamma_d}$ so that $\gamma_d \to$DM and $\gamma_d \to 2\,h_2$ decays are forbidden.

The lifetime of the dark photon can be calculated by

$$\tau = \frac{1}{\Gamma^{tot}_{\gamma_d}} \ . \tag{6.58}$$

Hence, the γ_d lifetime is inversely proportional to ε^2. For small kinetic mixing parameter the dark photon can be quite long lived and have a large decay length. In Fig. 6.8a we show the decay length $c\tau$ of the dark photon as a function of the kinetic mixing parameter ε for various dark photon masses. For ε in the range of $1 - 5 \times 10^{-6}$ the decay length can be $c\tau \sim 1$ mm. As discussed in the next section, this can lead to a spectacular collider signature of displaced vertices.

In Fig. 6.8b we show the branching ratios of the dark photon into electrons and muons.

This reproduces the results from Ref. [204], which we have recalculated and included for completeness. The branching ratios of the dark photon into electrons and muons are almost identical when $M_{\gamma_d} > 2M_\mu$. For much lower masses below $\sim$ 200 MeV, the γ_d decay to muons is kinematically closed, and hence $\gamma_d \to e^+e^-$ decays dominate. The multiple dips in the branching ratios starting around $M_{\gamma_d} \sim 770$ MeV are attributed to hadronic resonances ρ, ω, ϕ, ρ', J/ψ, $\psi(2S)$, and $\Upsilon(nS)$ for $n = 1, 2, 3, 4$ [134].

6.5 Searching for the dark photon with $T \to t\gamma_d$ decays

We now discuss the collider signatures of this model. As discussed previously, the pair production of T only depends on the spin and mass of T and $\mathrm{BR}(T \to t\,\gamma_d) \approx 50\%$ in a very large range of parameter space. Hence, the production rate of the dark photon is at QCD rates and largely independent of the model parameters. The major model dependence comes from the lifetime of γ_d. If ε is sufficiently small, the dark photon becomes long-lived.

The decay length of the dark photon from T decays is

$$d = \bar{b} c\tau \ , \tag{6.59}$$

where $c\tau$ is a proper lifetime as shown in Fig. 6.8a and $\bar{b}$ is the average boost of the dark photon. Assuming the VLQs are produced mostly at rest, the boost is

$$\begin{aligned} \bar{b} \quad &= \quad \frac{|\overrightarrow{p}_{\gamma_d}|}{M_{\gamma_d}} = \frac{1}{2M_{\gamma_d}M_T}\sqrt{(M_T^2 - M_{\gamma_d}^2 - M_t^2)^2 - 4M_{\gamma_d}^2 M_t^2} \\ &\xrightarrow[M_T \gg M_{\gamma_d}, M_t]{} \frac{M_T}{2M_{\gamma_d}} \ , \end{aligned} \tag{6.60}$$

where $|\overrightarrow{p}_{\gamma_d}|$ is the dark photon 3-momentum. Using the total γ_d width in Eq. (6.57), we can then solve for the decay length:

$$d = 580\ \mu\mathrm{m} \times \frac{7}{R(M_{\gamma_d}) + \sum_{\ell=e,\mu\tau}\theta(M_{\gamma_d} - 2\,M_\ell)} \left(\frac{M_T}{1\ \mathrm{TeV}}\right) \left(\frac{1\ \mathrm{GeV}}{M_{\gamma_d}}\right)^2 \left(\frac{10^{-4}}{\varepsilon}\right)^2 \ . \tag{6.61}$$

Hence, for reasonable parameter choices, the decay length of the dark photon can be several hundreds of microns. The precise direction of the dark photon in the detector will determine if it appears as a displaced vertex or where it will decay in the detector. Nevertheless, for $d \lesssim 500$ μm the dark photon decay can be considered prompt, for $d = 1$ mm $- 1$ m it will be a displaced vertex, for $d \sim 1$ m $- 10$ m the dark photon will decay in the detector, and $d \gtrsim 10$ m the dark photon will decay outside the detector [223]. Hence, we can solve for the values of ε for these various scenarios:

$$\varepsilon = \left(\frac{7}{R(M_{\gamma_d}) + \sum_{\ell=e,\mu\tau}\theta(M_{\gamma_d} - 2\,M_\ell)}\right)^{1/2}\left(\frac{M_T}{1\text{ TeV}}\right)^{1/2}\left(\frac{1\text{ GeV}}{M_{\gamma_d}}\right) \times \begin{cases} \gtrsim 1\times 10^{-3} & \text{for prompt decays} \\ 2.4\times 10^{-6} - 7.6\times 10^{-5} & \text{for displaced vertices} \\ 7.6\times 10^{-7} - 2.4\times 10^{-6} & \text{for decays in detector} \\ \lesssim 7.6\times 10^{-7} & \text{for decays outside the detector .} \end{cases} \tag{6.62}$$

If the dark photon decays outside the detector it is unobserved, giving rise to the final state characterized by $t\bar{t} + \not{E}_T$. This is the same signature as pair produced scalar tops, $\widetilde{t}$, in R-Parity conserving SUSY models with the decays $\widetilde{t} \to t\,\widetilde{\chi}_1^0$, where $\widetilde{\chi}_1^0$ is the lightest superpartner and stable. Hence, the currently available CMS [282, 283, 284, 285, 286, 287] and ATLAS [288, 289] searches for stop pair production can be used to obtain constraints on the model presented here. In the limit of large gluino/squark masses, the most stringent bound is at 13 TeV excludes stop masses up to 1225 GeV for a massless $\tilde{\chi}_1^0$ [287]. Since Ref. [287] assumes $\text{BR}(\widetilde{t} \to t\,\widetilde{\chi}_1^0) = 1$, the corresponding 95% CL upper limit on the NLL-NLO stop pair production cross section is given by ~ 1.3 fb [290].

Since both stop and T pair production yield similar kinematic distributions in the final states, the efficiencies of two searches are quite similar [291]. The upper bound on the stop pair production cross section can then be reinterpreted as a bound on the VLQ pair

production cross section:

$$\sigma(pp \to T\overline{T}) \times (\mathrm{BR}(T \to t\gamma_d) + \mathrm{BR}(T \to tZ \to t\nu\bar{\nu}))^2 \leq 1.3 \text{ fb} \ . \tag{6.63}$$

In Fig. 6.9a we show this limit in the $v_d - M_T$ plane for a dark photon mass of $M_{\gamma_d} = 1$ GeV (gray region is ruled out). We used the T branching ratios in Fig. 6.6 and the NNLO $T\overline{T}$ cross section in Fig. 6.4. As shown in Sec. 6.3, the production and decay rates of the VLQ are relatively independent of model parameters and this result is robust. We find that VLQ masses

$$M_T \lesssim 1.2 \text{ TeV} \ , \tag{6.64}$$

are excluded for $M_{\gamma_d} = 1$ GeV and $v_d \lesssim 500$ GeV when the dark photon is stable on collider time scales. The bound can be weakened for higher values of v_d since the branching ratio of T into SM bosons with visible decays increases, suppressing $\mathrm{BR}(T \to t\gamma_d)$ as displayed in Figure 6.6.

Searches for single T production can be important if $t - T$ mixing is not too small. It is clear from Figure 6.4 that for $\sin\theta_L^t \sim 0.1$ the single production dominates over the pair production at high VLQ masses. Refs. [313, 314] showed that the $T \to tZ(\to \nu\bar{\nu})$ channel displays a superior performance in prospects for discovering the T. The signature is then $T \to t + \not{E}_T$, which is the same as for $T \to t\gamma_d$ when γ_d is long lived. The ATLAS collaboration [292] presented results on the single production of T with the decay $T \to tZ(\to \nu\bar{\nu})$. Assuming that efficiencies of $T \to tZ \to t\nu\bar{\nu}$ and $T \to t\gamma_d$ searches are the same, we re-interpret the 95% CL upper limit on the cross section in Ref. [292] to derive constraints on $M_T - \sin\theta_L^t$ plane, as shown as dotted lines in Figure 6.9b. The regions within the curves are ruled out. As in Fig. 6.9a, we consider both $T \to t\gamma_d$ where the dark photon is assumed to escape the detector, and $T \to t\nu\bar{\nu}$. For VLQ masses around $M_T = 1 \sim 2$ TeV, the limits

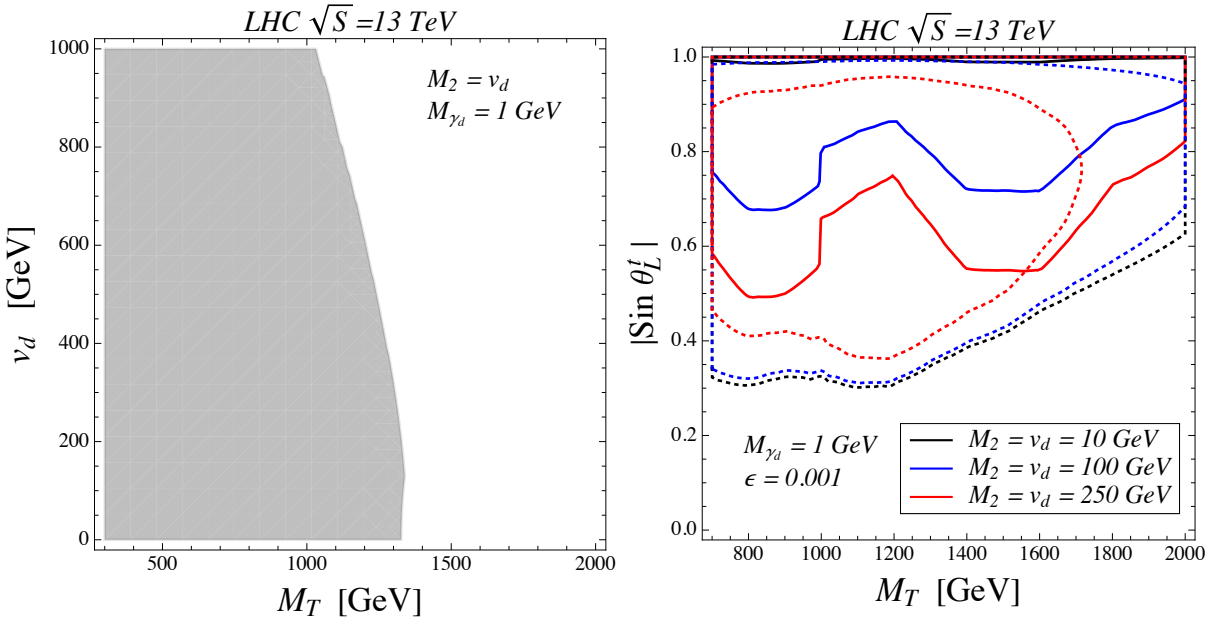

(a) (b)

Figure 6.9: (a) 95% CL exclusion regions in $M_T - v_d$ plane from the VLQ pair production with the $T \to t + \gamma_d/\nu\bar{\nu}$ decays, assuming γ_d is long lived. The constraint is obtained from re-interpreting the bounds from the CMS [287] stop searches at 13 TeV. (b) 95% CL exclusion regions in $M_T - \sin\theta_L^t$ plane based on the single production of the VLQ. The dotted constraint is obtained from a simple recast of the ATLAS [292] results on the single production of T with the decay $T \to tZ(\to \nu\bar{\nu})$. The solid lines are taken from a recasting of a CMS [293] search for single production of T with fully hadronic decays into Higgs or Z.

on $\sin\theta_L^t$ are

$$|\sin\theta_L^t| \lesssim 0.3 \sim 0.6 \ , \tag{6.65}$$

where the stronger bounds are expected for smaller values of v_d due to the enhancement of the branching ratio $\text{BR}(T \to t\gamma_d)$. For smaller $|\sin\theta_L^t|$ the single VLQ production rate is too small to be detectable yet. For larger $\sin\theta_L^t$ and larger v_d, the VLQ essentially decays like a top quark with a near 100% branching ratio into Wb. Hence, the branching ratio to $t\gamma_d$ is suppressed and a gap appears for $|\sin\theta_L^t| \gtrsim 0.9$ and $v_d = 250$ GeV. These bounds are, however, weaker as compared to the EW precision test [see Figure 6.1a].

CMS has also performed a recent search for electroweak production of T decaying through

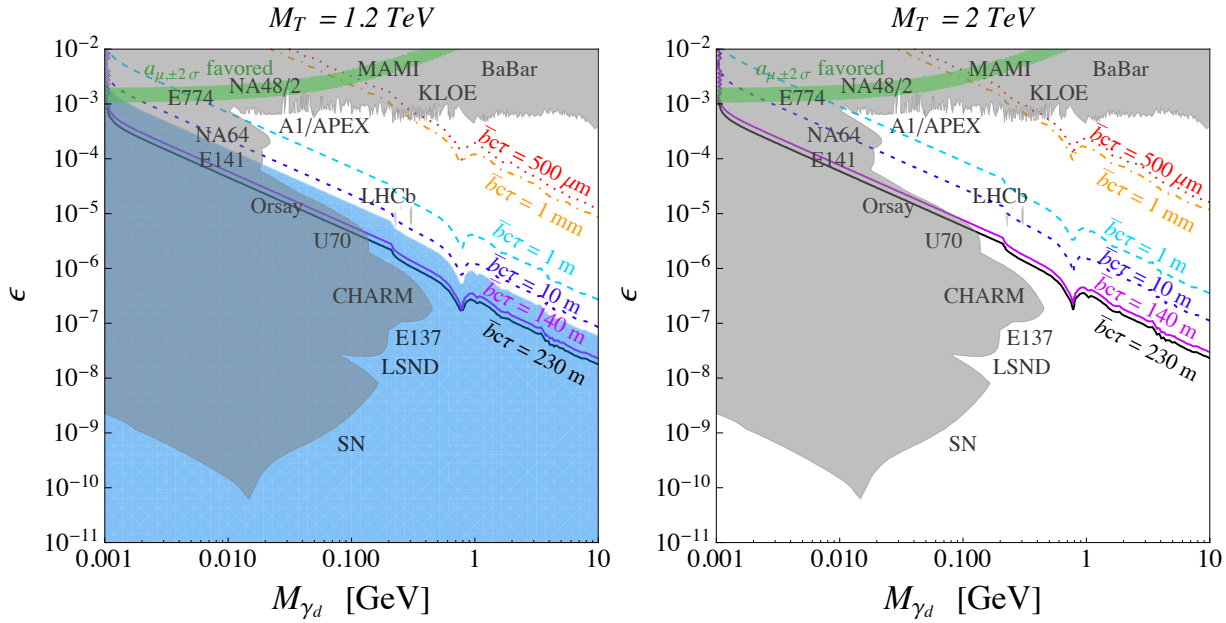

Figure 6.10: Various decay lengths of the dark photon originating from VLQs with masses (a) 1.2 TeV and (b) 2 TeV in $\varepsilon - M_{\gamma_d}$ plane. The blue shaded regions are excluded by searches for stop pair production with decay $\widetilde{t} \to t\,\widetilde{\chi}_1^0$. Gray shaded regions correspond to existing 90% confidence level limits from the SLAC and Fermilab beam dump experiments E137, E141, and E774 [200, 294, 295, 296], the U70 accelerator [297, 298], LHCb [299, 300], NA64 [301], the electron and muon anomalous magnetic moment a_μ [302, 202, 303], KLOE [304, 305], WASA-at-COSY [306], the test run results reported by APEX [307] and MAMI [308], an estimate using a BaBar result [200, 309, 310], and a constraint from supernova cooling [311, 312]. The shaded green regions are favored to explain the muon anomalous magnetic moment [302] at 95% confidence level.

Z and Higgs channels with fully hadronic decays [293]. These searches can be re-interpretted into constraints in the $M_T - \sin\theta_L^t$ plane. The 95% CL exclusions are shown as solid lines in Figure 6.9b with the regions inside the curves ruled out. In the small v_d limit ($v_d = 10$ GeV) the branching ratios into SM final states are neglible so there are not strong constraints. As v_d increases the branching ratios become viable and some constraints emerge. In the high v_d the generic search constraints start to become more stringent than $T \to tZ(\to \nu\bar{\nu})$ constraints. Hence, there is a complementarity between the fully hadronic and missing energy searches.

Figure 6.10 shows the decay lengths of dark photons originating from the VLQ with masses (a) $M_T = 1.2$ TeV and (b) $M_T = 2$ TeV in $M_{\gamma_d} - \varepsilon$ plane. We show several lines

of the dark photon decay length $d = \overline{b}c\tau$ that are indicative of prompt decays (d=500 μm), displaced vertices (d=1 mm), decays in the detector (d=1 m), and decays outside the detector (d=10 m). Additionally, there is a proposed MATHUSLA detector [315] to search for long lived particles. MATHUSLA will be on the surface $140 - 230$ m away from the interaction point. Hence, we also show lines for dark photons that could decay inside the MATHUSLA detector. The blue shaded regions are excluded by searches for stop pair production with decay $\widetilde{t} \to t\,\widetilde{\chi}_1^0$, as discussed above. This blue exclusion region exists for $M_T \lesssim 1.3$ TeV. Hence, it appears in Fig. 6.10a but not Fig. 6.10b. The grey shaded regions are excluded by various low energy experiments [268] and supernova measurements [311, 312]. As can be clearly seen, searches for $T \to t\,\gamma_d$ with a wide range of possible signals can cover a substantial portion of the parameter space. This is because in the model presented here the production of γ_d from VLQ production is largely independent of the small kinetic mixing parameter. Hence, the production rate of γ_d is unsuppressed at low ε and the LHC can be quite sensitive to this region.

The dark photon branching ratios into e^-e^+ and $\mu^-\mu^+$ is non-negligible as shown in Fig. 6.8b. Hence, the most promising signature of the $T \to t\,\gamma_d$ would be the leptonic decays of the dark photon, which would help avoid large QCD backgrounds. Since the dark photon is highly boosted, its decay products are highly collimated. The angular distance between the leptons from γ_d decays can be estimated as

$$\Delta R_{\ell\ell} \sim \frac{2\,M_{\gamma_d}}{E_{\gamma_d}} = \frac{4\,M_{\gamma_d}}{M_T} = 4 \times 10^{-3} \left(\frac{M_{\gamma_d}}{1\text{ GeV}}\right)\left(\frac{1\text{ TeV}}{M_T}\right)\,, \tag{6.66}$$

where $\Delta R_{\ell\ell} = \sqrt{(\phi_{\ell^-} - \phi_{\ell^+})^2 + (\eta_{\ell^-} - \eta_{\ell^+})^2}$, ϕ are the azimuthal angles of the leptons, and η are their rapidities. At such small angular separation, the leptons are very difficult to isolate and the dark photon can give rise to so-called "lepton jets" [238, 237] which are highly collimated clusters of electrons and muons. In fact, for not too small kinetic mixing ε, there could be displaced lepton jets or even lepton jets originating in the detector.

Chapter 7

Conclusions

Adding additional scalars to the SM can produce a rich phenomenology, as we have seen. The natural avenue that leads to searching for new scalars is the drive to further understand the Higgs sector. However, the signs of new scalars can show up in other interesting ways as well.

In Chapter 2, we investigated one of the simplest SM extensions. Although simple, adding a real gauge singlet scalar is theoretically well-motivated and has interesting phenomenology. In particular, if the new scalar h_2 is sufficiently heavy $m_2 \geq 2\,m_1$, this model can give rise to resonant double Higgs production at the LHC. We investigated this signature and determined benchmark parameter points that maximize the double Higgs production rate in this model at the $\sqrt{S_H} = 13$ TeV LHC. These benchmark points are important for gauging when the ongoing experimental searches for resonant double Higgs production are probing interesting regions of parameter space of well-motivated models. We have found that $\mathrm{BR}(h_2 \to h_1 h_1)$ can be as high as 0.83. Double Higgs production can be the dominant decay mode for new scalars, and $h_1 h_1$ production rate can be significantly higher than the SM rate. In Chapter 3, we studied a similar extension with a complex scalar singlet. We considered the most general renormalizable scalar potential and imposed no additional symmetries. In this scenario, there are 3 scalar bosons, one of which, h_3, can have very small couplings to SM particles and will be primarily observed through double Higgs decays, $h_2 \to h_1 h_3$. Subject to the constraints of electroweak precision measurements, single Higgs production rates, and perturbative unitarity, there are regions of parameter space where the rate for $h_1 h_3$ production is significantly enhanced relative to the SM $h_1 h_1$ rate. Therefore, the search for

pair production of Higgs bosons with different masses is a distinctive signature of this class of model. The LHC will continue to have sensitivity to these models, and future upgrades like the High-Luminosity LHC or High-Energy LHC will be useful as well for probing smaller mixing angles and larger scalar masses in these types of models.

In Chapter 4, we discussed a more complicated scalar sector that provided a mechanism for the generation of the baryon asymmetry via heavy Higgs doublet decays into lepton doublets and right-handed neutrino singlets. These decays produce an asymmetry in the lepton doublets that then gets processed into a baryon asymmetry via the electroweak sphalerons. This scenario is a nearly minimal extension of the SM, in which we only need right-handed neutrinos which can help explain neutrino masses, and additional Higgs doublets. Since the Yukawa couplings between the SM Higgs boson and neutrinos is constrained to be small, at minimum two additional Higgs doublets are required to guarantee that the asymmetry parameter in Eq. (4.12) is sufficiently large. In addition to generating the baryon asymmetry, this scenario could have many signatures at current and future experiments. To generate the baryon asymmetry, there needs to be a misalignment between the Yukawas of the different Higgs doublets. Once all Higgs doublets obtain a vev, this necessarily leads to flavor changing currents in the lepton sector as well as EDMs. As shown above, the baryon asymmetry can be generated and current constraints on charged lepton flavor violation accommodated within a realistic Yukawa structure. Furthermore, future $\mu \to e\gamma$ and electron EDM experiments may be expected to show signatures of this baryon asymmetry mechanism. Finally, we studied the collider signatures of the heavy Higgs doublets. Via double scalar production, the scenario presented here can provide striking signatures of many leptons, missing energy, b-jets, and possibly displaced vertices. While the double scalar production rates can be favorable at the LHC, future colliders may be needed to observe much of the interesting parameter space. Additionally, we may expect the observed Higgs boson decays into muons and taus, $h_1 \to \mu^+\mu^-/\tau^+\tau^-$, to differ from SM predictions by upwards of 20%. This is an observable amount of deviation at the High-Luminosity LHC with 3 ab^{-1} or the High-Energy

LHC with 15 ab^{-1} of data [157].

In Chapter 5, we introduced a model with a dark sector containing a scalar portal to dark matter. This leads to a new long ranged scalar-mediated interaction and allows for a new mechanism for neutrino masses. Neutrinos are much lighter than any other fermion, which perhaps points to a different mechanism for the generation of their tiny masses. We raised an interesting possibility that neutrinos may be massless in empty space. We introduced a model in which there exists a long range scalar mediated force between neutrinos and dark matter, and the background scalar potential sourced by the Galactic population of dark matter provides non-zero masses for the neutrinos. With the local dark matter densities in our galaxy, our model can give $m_\nu \lesssim 0.1$ eV neutrino masses around our solar system and different masses in other areas of the Galaxy. In addition, because this scalar potential is the source of the neutrino mass and thus determines the sign of the neutrino mass term, the force between dark matter and neutrinos will always be repulsive. As a consequence, relic neutrinos have been forced out of our local Galactic neighborhood by the dark matter due to this repulsive force and no longer have enough energy in the present day to enter the Solar System. Thus the two main features of this proposed neutrino mass mechanism are neutrino masses which depend on local dark matter concentrations and the absence of relic neutrinos in our Galactic vicinity. A future experiment like PTOLEMY that will search for the cosmic relic neutrinos is the natural testing ground for this model.

In Chapter 6, we moved on to a more complicated dark sector, with a new scalar responsible for symmetry breaking of a dark sector gauge group. This model has an up-type VLQ charged under a new $U(1)_d$, which is spontaneously broken by a dark Higgs mechanism. The $U(1)_d$ gauge boson kinetically mixes with the SM hypercharge, and the remaining dark Higgs boson mixes with the SM Higgs boson. One of the most significant aspects of this model is that the decay patterns of the VLQ can be substantially altered from the usual scenario when this dark sector is included. That is, the VLQ is a "maverick top partner." The appeal of this scenario is that the production rate of the dark photon γ_d is largely independent of

model parameters. The VLQs can be pair produced via the strong interaction. This pair production rate is governed by gauge interactions and only depends on the VLQ mass and spin. The branching ratio BR($T \to t\,\gamma_d$) = 50% in a very wide range of parameter space. Hence, the dark photon production rate is almost completely governed the strong interaction and is independent of the small kinetic mixing parameter ε. While the production rate of the dark photon is independent of the kinetic mixing parameter, the collider searches are not. As we showed, for reasonable ε, the dark photon can give rise to displaced vertices, decay inside the detector, or even escape the detector and appear as missing energy as shown in Fig. 6.10. Besides the missing energy, the most promising signatures of the dark photon would be its decays into electrons and muons. For dark photon masses much below the VLQ masses, the electrons and muons would be highly collimated giving rise to lepton jets [238] or even displaced lepton jets. The model presented here is a mild perturbation from the typical simplified models of dark photons and VLQs. However, as we demonstrated, the collider phenomenology is significantly changed from the usual scenarios. Hence, this provides a robust framework in which searches for heavy particles at the LHC can illuminate a light dark sector force. Though the dark photon is one of the interesting parts of this model, the existence of a dark Higgs mechanism and a corresponding dark Higgs boson is a necessary feature.

The LHC is scheduled to begin Run 3 in 2021, and the High-Luminosity LHC upgrade is scheduled to begin running by 2027. The LHC will continue to push the SM to its limits and studying electroweak scale physics. But to truly probe the TeV scale, higher energy colliders are important. The proposed High-Energy LHC, at a center of mass energy of 27 TeV, could probe larger mass regions of parameter space in many of these sorts of models. In the longer term, one of the main future goals of the experimental community is the development of a 100 TeV collider. This would provide the ultimate testing grounds for many models in which new physics would "naturally" be not much larger than the TeV scale, which includes most scalar models. Outside of hadron colliders, there are also proposals for electron-positron

colliders, such as the International Linear Collider (ILC), which are generally much cleaner than hadron colliders. The ILC has a proposed energy range of 250 GeV to 1 TeV, which would make it a fantastic experiment for precisely measuring the properties of the 125 GeV Higgs boson. Beyond colliders, there are numerous dark matter detector experiments, present and future, which can probe portions of the parameter space of many dark matter models, including portal models. All of these experimental avenues, and more, are important for the future of high energy physics.

In this dissertation, we have seen many models for new physics that include new scalars. This serves as a comprehensive analysis of the new physics possible with additional scalars. The Higgs boson has an interesting place in the SM, being present as a necessary consequence of the Higgs mechanism. The SM scalar sector, with just a single Higgs boson, is extremely simple compared to the fermion sector, with three generations of quarks and leptons. With the understanding that the SM is a low energy effective theory, we realize that the scalar sector of a new model might have many more new particles to discover. Understanding extended scalar sectors not only leads to furthering our knowledge of possible new particles, but also can further our knowledge of the discovered Higgs-like scalar and the mechanism of EWSB. Models with new scalars also have the potential to explain some of the open problems in physics, as we have seen. Studying extended scalar sectors is an important endeavor.

Bibliography

[1] S. Glashow, *Partial Symmetries of Weak Interactions*, *Nucl. Phys.* **22** (1961) 579–588.

[2] S. Weinberg, *A Model of Leptons*, *Phys. Rev. Lett.* **19** (1967) 1264–1266.

[3] A. Salam, *Weak and Electromagnetic Interactions*, *Conf. Proc. C* **680519** (1968) 367–377.

[4] P. W. Higgs, *Broken symmetries, massless particles and gauge fields*, *Phys. Lett.* **12** (1964) 132–133.

[5] P. W. Higgs, *Broken Symmetries and the Masses of Gauge Bosons*, *Phys. Rev. Lett.* **13** (1964) 508–509.

[6] P. W. Higgs, *Spontaneous Symmetry Breakdown without Massless Bosons*, *Phys. Rev.* **145** (1966) 1156–1163.

[7] S. Glashow, J. Iliopoulos, and L. Maiani, *Weak Interactions with Lepton-Hadron Symmetry*, *Phys. Rev. D* **2** (1970) 1285–1292.

[8] J. Augustin *et al.*, , **SLAC-SP-017** Collaboration, *Discovery of a Narrow Resonance in e^+e^- Annihilation*, *Phys. Rev. Lett.* **33** (1974) 1406–1408.

[9] J. Aubert *et al.*, *Experimental observation of a heavy Particle J*, *Adv. Exp. Phys.* **5** (1976) 128.

[10] J. Christenson, J. Cronin, V. Fitch, and R. Turlay, *Evidence for the 2π Decay of the K_2^0 Meson*, *Phys. Rev. Lett.* **13** (1964) 138–140.

[11] M. Kobayashi and T. Maskawa, *CP Violation in the Renormalizable Theory of Weak Interaction*, *Prog. Theor. Phys.* **49** (1973) 652–657.

[12] S. Herb *et al.*, *Observation of a Dimuon Resonance at 9.5-GeV in 400-GeV Proton-Nucleus Collisions*, *Phys. Rev. Lett.* **39** (1977) 252–255.

[13] F. Abe *et al.*, , **CDF** Collaboration, *Observation of top quark production in $\bar{p}p$ collisions*, *Phys. Rev. Lett.* **74** (1995) 2626–2631, arXiv:hep-ex/9503002.

[14] S. Abachi *et al.*, , **D0** Collaboration, *Observation of the top quark*, *Phys. Rev. Lett.* **74** (1995) 2632–2637, arXiv:hep-ex/9503003.

[15] M. Banner *et al.*, , **UA2** Collaboration, *Observation of Single Isolated Electrons of High Transverse Momentum in Events with Missing Transverse Energy at the CERN anti-p p Collider*, *Phys. Lett. B* **122** (1983) 476–485.

[16] G. Arnison *et al.*, , **UA1** Collaboration, *Experimental Observation of Isolated Large Transverse Energy Electrons with Associated Missing Energy at s**(1/2) = 540-GeV*, *Phys. Lett. B* **122** (1983) 103–116.

[17] G. Arnison *et al.*, , **UA1** Collaboration, *Experimental Observation of Lepton Pairs of Invariant Mass Around 95-GeV/c**2 at the CERN SPS Collider*, *Phys. Lett. B* **126** (1983) 398–410.

[18] P. Bagnaia *et al.*, , **UA2** Collaboration, *Evidence for $Z^0 \to e^+e^-$ at the CERN $\bar{p}p$ Collider*, *Phys. Lett. B* **129** (1983) 130–140.

[19] S. Dawson, *Introduction to electroweak symmetry breaking*, in *ICTP Summer School in High-Energy Physics and Cosmology*, pp. 1–83. 6, 1998. arXiv:hep-ph/9901280.

[20] A. Djouadi, *The Anatomy of electro-weak symmetry breaking. I: The Higgs boson in the standard model*, *Phys. Rept.* **457** (2008) 1–216, arXiv:hep-ph/0503172.

[21] F. Englert and R. Brout, *Broken Symmetry and the Mass of Gauge Vector Mesons*, *Phys. Rev. Lett.* **13** (1964) 321–323.

[22] G. Guralnik, C. Hagen, and T. Kibble, *Global Conservation Laws and Massless Particles*, *Phys. Rev. Lett.* **13** (1964) 585–587.

[23] T. Kibble, *Symmetry breaking in nonAbelian gauge theories*, *Phys. Rev.* **155** (1967) 1554–1561.

[24] Y. Nambu, *Quasiparticles and Gauge Invariance in the Theory of Superconductivity*, *Phys. Rev.* **117** (1960) 648–663.

[25] J. Goldstone, *Field Theories with Superconductor Solutions*, *Nuovo Cim.* **19** (1961) 154–164.

[26] I. M. Lewis and M. Sullivan, *Benchmarks for Double Higgs Production in the Singlet Extended Standard Model at the LHC*, *Phys. Rev.* **D96** no. 3, (2017) 035037, arXiv:1701.08774 [hep-ph].

[27] S. Dawson and M. Sullivan, *Enhanced di-Higgs boson production in the complex Higgs singlet model*, *Phys. Rev. D* **97** no. 1, (2018) 015022, arXiv:1711.06683 [hep-ph].

[28] H. Davoudiasl, I. M. Lewis, and M. Sullivan, *Higgs Troika for Baryon Asymmetry*, *Phys. Rev. D* **101** no. 5, (2020) 055010, arXiv:1909.02044 [hep-ph].

[29] H. Davoudiasl, G. Mohlabeng, and M. Sullivan, *Galactic Dark Matter Population as the Source of Neutrino Masses*, *Phys. Rev. D* **98** no. 2, (2018) 021301, arXiv:1803.00012 [hep-ph].

[30] J. H. Kim, S. D. Lane, H.-S. Lee, I. M. Lewis, and M. Sullivan, *Searching for Dark Photons with Maverick Top Partners*, *Phys. Rev. D* **101** no. 3, (2020) 035041, arXiv:1904.05893 [hep-ph].

[31] S. Chatrchyan *et al.*, , **CMS** Collaboration, *Observation of a new boson at a mass of 125 GeV with the CMS experiment at the LHC*, *Phys. Lett.* **B716** (2012) 30–61, arXiv:1207.7235 [hep-ex].

[32] G. Aad *et al.*, , **ATLAS** Collaboration, *Observation of a new particle in the search for the Standard Model Higgs boson with the ATLAS detector at the LHC*, *Phys. Lett.* **B716** (2012) 1–29, arXiv:1207.7214 [hep-ex].

[33] T. Binoth and J. J. van der Bij, *Influence of strongly coupled, hidden scalars on Higgs signals*, *Z. Phys.* **C75** (1997) 17–25, arXiv:hep-ph/9608245 [hep-ph].

[34] H. Davoudiasl, R. Kitano, T. Li, and H. Murayama, *The New minimal standard model*, *Phys. Lett.* **B609** (2005) 117–123, arXiv:hep-ph/0405097 [hep-ph].

[35] R. M. Schabinger and J. D. Wells, *A Minimal spontaneously broken hidden sector and its impact on Higgs boson physics at the large hadron collider*, *Phys. Rev.* **D72** (2005) 093007, arXiv:hep-ph/0509209 [hep-ph].

[36] B. Patt and F. Wilczek, *Higgs-field portal into hidden sectors*, arXiv:hep-ph/0605188 [hep-ph].

[37] M. Bowen, Y. Cui, and J. D. Wells, *Narrow trans-TeV Higgs bosons and $H \to hh$ decays: Two LHC search paths for a hidden sector Higgs boson*, *JHEP* **03** (2007) 036, arXiv:hep-ph/0701035 [hep-ph].

[38] S. Bock, R. Lafaye, T. Plehn, M. Rauch, D. Zerwas, and P. M. Zerwas, *Measuring Hidden Higgs and Strongly-Interacting Higgs Scenarios*, *Phys. Lett.* **B694** (2010) 44–53, arXiv:1007.2645 [hep-ph].

[39] A. Djouadi, O. Lebedev, Y. Mambrini, and J. Quevillon, *Implications of LHC searches for Higgs–portal dark matter*, *Phys. Lett.* **B709** (2012) 65–69, arXiv:1112.3299 [hep-ph].

[40] C. Englert, T. Plehn, M. Rauch, D. Zerwas, and P. M. Zerwas, *LHC: Standard Higgs and Hidden Higgs*, *Phys. Lett.* **B707** (2012) 512–516, arXiv:1112.3007 [hep-ph].

[41] C. Englert, T. Plehn, D. Zerwas, and P. M. Zerwas, *Exploring the Higgs portal*, *Phys. Lett.* **B703** (2011) 298–305, arXiv:1106.3097 [hep-ph].

[42] T. Alanne, K. Tuominen, and V. Vaskonen, *Strong phase transition, dark matter and vacuum stability from simple hidden sectors*, *Nucl. Phys.* **B889** (2014) 692–711, arXiv:1407.0688 [hep-ph].

[43] S. W. Ham, Y. S. Jeong, and S. K. Oh, *Electroweak phase transition in an extension of the standard model with a real Higgs singlet*, *J. Phys.* **G31** no. 8, (2005) 857–871, arXiv:hep-ph/0411352 [hep-ph].

[44] S. Profumo, M. J. Ramsey-Musolf, and G. Shaughnessy, *Singlet Higgs phenomenology and the electroweak phase transition*, *JHEP* **08** (2007) 010, arXiv:0705.2425 [hep-ph].

[45] A. Ashoorioon and T. Konstandin, *Strong electroweak phase transitions without collider traces*, *JHEP* **07** (2009) 086, arXiv:0904.0353 [hep-ph].

[46] D. Bodeker and G. D. Moore, *Can electroweak bubble walls run away?*, *JCAP* **0905** (2009) 009, arXiv:0903.4099 [hep-ph].

[47] J. R. Espinosa, T. Konstandin, and F. Riva, *Strong Electroweak Phase Transitions in the Standard Model with a Singlet*, *Nucl. Phys.* **B854** (2012) 592–630, arXiv:1107.5441 [hep-ph].

[48] J. M. No and M. Ramsey-Musolf, *Probing the Higgs Portal at the LHC Through Resonant di-Higgs Production*, *Phys. Rev.* **D89** no. 9, (2014) 095031, arXiv:1310.6035 [hep-ph].

[49] D. Curtin, P. Meade, and C.-T. Yu, *Testing Electroweak Baryogenesis with Future Colliders*, *JHEP* **11** (2014) 127, arXiv:1409.0005 [hep-ph].

[50] S. Profumo, M. J. Ramsey-Musolf, C. L. Wainwright, and P. Winslow, *Singlet-catalyzed electroweak phase transitions and precision Higgs boson studies*, *Phys. Rev.* **D91** no. 3, (2015) 035018, arXiv:1407.5342 [hep-ph].

[51] F. P. Huang and C. S. Li, *Electroweak baryogenesis in the framework of the effective field theory*, *Phys. Rev.* **D92** no. 7, (2015) 075014, arXiv:1507.08168 [hep-ph].

[52] P. H. Damgaard, A. Haarr, D. O'Connell, and A. Tranberg, *Effective Field Theory and Electroweak Baryogenesis in the Singlet-Extended Standard Model*, *JHEP* **02** (2016) 107, arXiv:1512.01963 [hep-ph].

[53] J. Kozaczuk, *Bubble Expansion and the Viability of Singlet-Driven Electroweak Baryogenesis*, *JHEP* **10** (2015) 135, arXiv:1506.04741 [hep-ph].

[54] P. Huang, A. Joglekar, B. Li, and C. E. M. Wagner, *Probing the Electroweak Phase Transition at the LHC*, *Phys. Rev.* **D93** no. 5, (2016) 055049, arXiv:1512.00068 [hep-ph].

[55] M.-L. Xiao and J.-H. Yu, *Electroweak baryogenesis in a scalar-assisted vectorlike fermion model*, *Phys. Rev.* **D94** no. 1, (2016) 015011, arXiv:1509.02931 [hep-ph].

[56] P. Huang, A. J. Long, and L.-T. Wang, *Probing the Electroweak Phase Transition with Higgs Factories and Gravitational Waves*, *Phys. Rev.* **D94** no. 7, (2016) 075008, arXiv:1608.06619 [hep-ph].

[57] A. V. Kotwal, M. J. Ramsey-Musolf, J. M. No, and P. Winslow, *Singlet-catalyzed electroweak phase transitions in the 100 TeV frontier*, *Phys. Rev.* **D94** no. 3, (2016) 035022, arXiv:1605.06123 [hep-ph].

[58] D. Curtin, P. Meade, and H. Ramani, *Thermal Resummation and Phase Transitions*, *Eur. Phys. J. C* **78** no. 9, (2018) 787, arXiv:1612.00466 [hep-ph].

[59] V. Vaskonen, *Electroweak baryogenesis and gravitational waves from a real scalar singlet*, *Phys. Rev.* **D95** (2017) , arXiv:1611.02073 [hep-ph].

[60] G. Aad *et al.*, , **ATLAS** Collaboration, *Constraints on new phenomena via Higgs boson couplings and invisible decays with the ATLAS detector*, *JHEP* **11** (2015) 206, arXiv:1509.00672 [hep-ex].

[61] G. Aad *et al.*, , **ATLAS, CMS** Collaboration, *Measurements of the Higgs boson production and decay rates and constraints on its couplings from a combined ATLAS and CMS analysis of the LHC pp collision data at* $\sqrt{s} = 7$ *and 8 TeV*, *JHEP* **08** (2016) 045, arXiv:1606.02266 [hep-ex].

[62] G. Aad *et al.*, , **ATLAS** Collaboration, *Search for a high-mass Higgs boson decaying to a* W *boson pair in pp collisions at* $\sqrt{s} = 8$ *TeV with the ATLAS detector*, *JHEP* **01** (2016) 032, arXiv:1509.00389 [hep-ex].

[63] V. Khachatryan *et al.*, , **CMS** Collaboration, *Search for a Higgs boson in the mass range from 145 to 1000 GeV decaying to a pair of W or Z bosons*, *JHEP* **10** (2015) 144, arXiv:1504.00936 [hep-ex].

[64] G. Aad *et al.*, , **ATLAS** Collaboration, *Search for an additional, heavy Higgs boson in the* $H \to ZZ$ *decay channel at* $\sqrt{s} = 8$ *TeV in pp collision data with the ATLAS detector*, *Eur. Phys. J.* **C76** no. 1, (2016) 45, arXiv:1507.05930 [hep-ex].

[65] G. Aad *et al.*, , **ATLAS** Collaboration, *Searches for Higgs boson pair production in the* $hh \to bb\tau\tau, \gamma\gamma WW^*, \gamma\gamma bb, bbbb$ *channels with the ATLAS detector*, *Phys. Rev.* **D92** (2015) 092004, arXiv:1509.04670 [hep-ex].

[66] V. Khachatryan *et al.*, , **CMS** Collaboration, *Search for resonant pair production of Higgs bosons decaying to two bottom quark–antiquark pairs in proton–proton collisions at 8 TeV*, *Phys. Lett.* **B749** (2015) 560–582, arXiv:1503.04114 [hep-ex].

[67] V. Khachatryan *et al.*, , **CMS** Collaboration, *Search for two Higgs bosons in final states containing two photons and two bottom quarks in proton-proton collisions at 8 TeV*, *Phys. Rev.* **D94** no. 5, (2016) 052012, arXiv:1603.06896 [hep-ex].

[68] **CMS** Collaboration, *Search for resonant Higgs boson pair production in the* $\mathrm{b\bar{b}}\tau^{+}\tau^{-}$ *final state using 2016 data*, Tech. Rep. CMS-PAS-HIG-16-029, 2016.

[69] **CMS** Collaboration, *Search for resonant pair production of Higgs bosons decaying to two bottom quark-antiquark pairs in proton-proton collisions at 13 TeV*, Tech. Rep. CMS-PAS-HIG-16-002, 2016.

[70] **ATLAS** Collaboration, *Search for pair production of Higgs bosons in the* $b\bar{b}b\bar{b}$ *final state using proton−proton collisions at* $\sqrt{s} = 13$ *TeV with the ATLAS detector*, Tech. Rep. ATLAS-CONF-2016-049, 2016.

[71] **ATLAS** Collaboration, *Search for Higgs boson pair production in the* $b\bar{b}\gamma\gamma$ *final state using pp collision data at* $\sqrt{s} = 13$ *TeV with the ATLAS detector*, Tech. Rep. ATLAS-CONF-2016-004, 2016.

[72] **CMS** Collaboration, *Measurements of properties of the Higgs boson and search for an additional resonance in the four-lepton final state at sqrt(s) = 13 TeV*, Tech. Rep. CMS-PAS-HIG-16-033, 2016.

[73] **CMS** Collaboration, *Search for high mass Higgs to WW with fully leptonic decays using 2015 data*, Tech. Rep. CMS-PAS-HIG-16-023, 2016.

[74] **ATLAS** Collaboration, *Study of the Higgs boson properties and search for high-mass scalar resonances in the $H \to ZZ^* \to 4\ell$ decay channel at $\sqrt{s}$ = 13 TeV with the ATLAS detector*, Tech. Rep. ATLAS-CONF-2016-079, 2016.

[75] **ATLAS** Collaboration, *Search for a high-mass Higgs boson decaying to a pair of W bosons in pp collisions at $\sqrt{s}$=13 TeV with the ATLAS detector*, Tech. Rep. ATLAS-CONF-2016-074, 2016.

[76] M. Aaboud *et al.*, , **ATLAS** Collaboration, *Searches for heavy diboson resonances in pp collisions at $\sqrt{s} = 13$ TeV with the ATLAS detector*, *JHEP* **09** (2016) 173, arXiv:1606.04833 [hep-ex].

[77] **CMS** Collaboration, *Search for $\mathrm{t\bar{t}}$ resonances in boosted semileptonic final states in pp collisions at $\sqrt{s} = 13$ TeV*, Tech. Rep. CMS-PAS-B2G-15-002, 2016.

[78] V. Khachatryan *et al.*, , **CMS** Collaboration, *Search for resonant $t\bar{t}$ production in proton-proton collisions at $\sqrt{s}$ = 8 TeV*, *Phys. Rev.* **D93** no. 1, (2016) 012001, arXiv:1506.03062 [hep-ex].

[79] G. Aad *et al.*, , **ATLAS** Collaboration, *A search for $t\bar{t}$ resonances using lepton-plus-jets events in proton-proton collisions at $\sqrt{s} = 8$ TeV with the ATLAS detector*, *JHEP* **08** (2015) 148, arXiv:1505.07018 [hep-ex].

[80] D. O'Connell, M. J. Ramsey-Musolf, and M. B. Wise, *Minimal Extension of the Standard Model Scalar Sector*, *Phys. Rev.* **D75** (2007) 037701, arXiv:hep-ph/0611014 [hep-ph].

[81] V. Barger, P. Langacker, M. McCaskey, M. Ramsey-Musolf, and G. Shaughnessy, *Complex Singlet Extension of the Standard Model*, *Phys. Rev.* **D79** (2009) 015018, arXiv:0811.0393 [hep-ph].

[82] S. Dawson and W. Yan, *Hiding the Higgs Boson with Multiple Scalars*, *Phys. Rev.* **D79** (2009) 095002, arXiv:0904.2005 [hep-ph].

[83] D. Bertolini and M. McCullough, *The Social Higgs*, *JHEP* **12** (2012) 118, arXiv:1207.4209 [hep-ph].

[84] G. M. Pruna and T. Robens, *Higgs singlet extension parameter space in the light of the LHC discovery*, *Phys. Rev.* **D88** no. 11, (2013) 115012, arXiv:1303.1150 [hep-ph].

[85] C. Caillol, B. Clerbaux, J.-M. Frère, and S. Mollet, *Precision versus discovery: A simple benchmark*, *Eur. Phys. J. Plus* **129** (2014) 93, arXiv:1304.0386 [hep-ph].

[86] D. López-Val and T. Robens, Δr *and the W-boson mass in the singlet extension of the standard model*, *Phys. Rev.* **D90** (2014) 114018, arXiv:1406.1043 [hep-ph].

[87] D. Buttazzo, F. Sala, and A. Tesi, *Singlet-like Higgs bosons at present and future colliders*, *JHEP* **11** (2015) 158, arXiv:1505.05488 [hep-ph].

[88] T. Robens and T. Stefaniak, *Status of the Higgs Singlet Extension of the Standard Model after LHC Run 1*, *Eur. Phys. J.* **C75** (2015) 104, arXiv:1501.02234 [hep-ph].

[89] A. Falkowski, C. Gross, and O. Lebedev, *A second Higgs from the Higgs portal*, *JHEP* **05** (2015) 057, arXiv:1502.01361 [hep-ph].

[90] F. Bojarski, G. Chalons, D. Lopez-Val, and T. Robens, *Heavy to light Higgs boson decays at NLO in the Singlet Extension of the Standard Model*, *JHEP* **02** (2016) 147, arXiv:1511.08120 [hep-ph].

[91] R. Costa, M. Mühlleitner, M. O. P. Sampaio, and R. Santos, *Singlet Extensions of the Standard Model at LHC Run 2: Benchmarks and Comparison with the NMSSM*, *JHEP* **06** (2016) 034, arXiv:1512.05355 [hep-ph].

[92] O. Fischer, *Clues on the Majorana scale from scalar resonances at the LHC*, *Mod. Phys. Lett.* **A32** no. 06, (2017) 1750035, arXiv:1607.00282 [hep-ph].

[93] S. Fichet, G. von Gersdorff, E. Pontón, and R. Rosenfeld, *The Global Higgs as a Signal for Compositeness at the LHC*, *JHEP* **01** (2017) 012, arXiv:1608.01995 [hep-ph].

[94] M. J. Dolan, C. Englert, and M. Spannowsky, *New Physics in LHC Higgs boson pair production*, *Phys. Rev.* **D87** no. 5, (2013) 055002, arXiv:1210.8166 [hep-ph].

[95] B. Cooper, N. Konstantinidis, L. Lambourne, and D. Wardrope, *Boosted $hh \to b\bar{b}b\bar{b}$: A new topology in searches for TeV-scale resonances at the LHC*, *Phys. Rev.* **D88** no. 11, (2013) 114005, arXiv:1307.0407 [hep-ex].

[96] C.-Y. Chen, S. Dawson, and I. M. Lewis, *Exploring resonant di-Higgs boson production in the Higgs singlet model*, *Phys. Rev.* **D91** no. 3, (2015) 035015, arXiv:1410.5488 [hep-ph].

[97] V. Martín Lozano, J. M. Moreno, and C. B. Park, *Resonant Higgs boson pair production in the $hh \to b\bar{b}\,WW \to b\bar{b}\ell^+\nu\ell^-\overline{\nu}$ decay channel*, *JHEP* **08** (2015) 004, arXiv:1501.03799 [hep-ph].

[98] S. Dawson and I. M. Lewis, *NLO corrections to double Higgs boson production in the Higgs singlet model*, *Phys. Rev.* **D92** no. 9, (2015) 094023, arXiv:1508.05397 [hep-ph].

[99] S. I. Godunov, A. N. Rozanov, M. I. Vysotsky, and E. V. Zhemchugov, *Extending the Higgs sector: an extra singlet*, *Eur. Phys. J.* **C76** (2016) 1, arXiv:1503.01618 [hep-ph].

[100] T. Robens and T. Stefaniak, *LHC Benchmark Scenarios for the Real Higgs Singlet Extension of the Standard Model*, *Eur. Phys. J.* **C76** no. 5, (2016) 268, arXiv:1601.07880 [hep-ph].

[101] K. Nakamura, K. Nishiwaki, K.-y. Oda, S. C. Park, and Y. Yamamoto, *Di-higgs enhancement by neutral scalar as probe of new colored sector*, *Eur. Phys. J.* **C77** no. 5, (2017) 273, arXiv:1701.06137 [hep-ph].

[102] T. Huang, J. No, L. Pernié, M. Ramsey-Musolf, A. Safonov, M. Spannowsky, and P. Winslow, *Resonant di-Higgs boson production in the $b\bar{b}WW$ channel: Probing the electroweak phase transition at the LHC*, *Phys. Rev. D* **96** no. 3, (2017) 035007, arXiv:1701.04442 [hep-ph].

[103] J. Chang, C.-R. Chen, and C.-W. Chiang, *Higgs boson pair productions in the Georgi-Machacek model at the LHC*, *JHEP* **03** (2017) 137, arXiv:1701.06291 [hep-ph].

[104] L.-C. Lü, C. Du, Y. Fang, H.-J. He, and H. Zhang, *Searching for Heavier Higgs Boson via Di-Higgs Production at LHC Run-2*, *Phys. Lett.* **B755** (2016) 509–522, arXiv:1507.02644 [hep-ph].

[105] J. Ren, R.-Q. Xiao, M. Zhou, Y. Fang, H.-J. He, and W. Yao, *LHC Search of New Higgs Boson via Resonant Di-Higgs Production with Decays into 4W*, *JHEP* **06** (2018) 090, arXiv:1706.05980 [hep-ph].

[106] A. Schuessler and D. Zeppenfeld, *Unitarity constraints on MSSM trilinear couplings*, in *SUSY 2007 Proceedings, 15th International Conference on Supersymmetry and Unification of Fundamental Interactions, July 26 - August 1, 2007, Karlsruhe, Germany*, pp. 236–239. 2007. arXiv:0710.5175 [hep-ph].

[107] **CMS** Collaboration, *Combined Higgs boson production and decay measurements with up to 137 fb-1 of proton-proton collision data at sqrts = 13 TeV*, Tech. Rep. CMS-PAS-HIG-19-005, 2020.

[108] G. Aad *et al.*, , **ATLAS** Collaboration, *Combined measurements of Higgs boson production and decay using up to 80 fb^{-1} of proton-proton collision data at $\sqrt{s} = 13$ TeV collected with the ATLAS experiment*, *Phys. Rev. D* **101** no. 1, (2020) 012002, arXiv:1909.02845 [hep-ex].

[109] P. Bechtle, O. Brein, S. Heinemeyer, G. Weiglein, and K. E. Williams, *HiggsBounds: Confronting Arbitrary Higgs Sectors with Exclusion Bounds from LEP and the Tevatron*, *Comput. Phys. Commun.* **181** (2010) 138–167, arXiv:0811.4169 [hep-ph].

[110] P. Bechtle, O. Brein, S. Heinemeyer, G. Weiglein, and K. E. Williams, *HiggsBounds 2.0.0: Confronting Neutral and Charged Higgs Sector Predictions with Exclusion Bounds from LEP and the Tevatron*, *Comput. Phys. Commun.* **182** (2011) 2605–2631, arXiv:1102.1898 [hep-ph].

[111] P. Bechtle *et al.*, *Recent Developments in HiggsBounds and a Preview of HiggsSignals*, *PoS* **CHARGED2012** (2012) 024, arXiv:1301.2345 [hep-ph].

[112] P. Bechtle *et al.*, *HiggsBounds-4: Improved Tests of Extended Higgs Sectors against Exclusion Bounds from LEP, the Tevatron and the LHC*, *Eur. Phys. J.* **C74** (2014) 2693, arXiv:1311.0055 [hep-ph].

[113] P. Bechtle, S. Heinemeyer, O. Stal, T. Stefaniak, and G. Weiglein, *Applying Exclusion Likelihoods from LHC Searches to Extended Higgs Sectors*, *Eur. Phys. J.* **C75** no. 9, (2015) 421, arXiv:1507.06706 [hep-ph].

[114] D. de Florian *et al.*, , **LHC Higgs Cross Section Working Group** Collaboration, *Handbook of LHC Higgs Cross Sections: 4. Deciphering the Nature of the Higgs Sector*, arXiv:1610.07922 [hep-ph].

[115] S. Borowka, N. Greiner, G. Heinrich, S. P. Jones, M. Kerner, J. Schlenk, and T. Zirke, *Full top quark mass dependence in Higgs boson pair production at NLO*, *JHEP* **10** (2016) 107, arXiv:1608.04798 [hep-ph].

[116] S. Dawson *et al.*, *Working Group Report: Higgs Boson*, in *Proceedings, 2013 Community Summer Study on the Future of U.S. Particle Physics: Snowmass on the Mississippi (CSS2013): Minneapolis, MN, USA, July 29-August 6, 2013*. 2013. arXiv:1310.8361 [hep-ex].

[117] R. Coimbra, M. O. P. Sampaio, and R. Santos, *ScannerS: Constraining the phase diagram of a complex scalar singlet at the LHC*, *Eur. Phys. J.* **C73** (2013) 2428, arXiv:1301.2599 [hep-ph].

[118] M. Gonderinger, H. Lim, and M. J. Ramsey-Musolf, *Complex Scalar Singlet Dark Matter: Vacuum Stability and Phenomenology*, *Phys. Rev.* **D86** (2012) 043511, arXiv:1202.1316 [hep-ph].

[119] M. Muhlleitner, M. O. P. Sampaio, R. Santos, and J. Wittbrodt, *Phenomenological Comparison of Models with Extended Higgs Sectors*, *JHEP* **08** (2017) 132, arXiv:1703.07750 [hep-ph].

[120] J. Alison *et al.*, *Higgs Boson Pair Production at Colliders: Status and Perspectives*, in *Double Higgs Production at Colliders*, B. Di Micco, M. Gouzevitch, J. Mazzitelli, and C. Vernieri, eds. 9, 2019. arXiv:1910.00012 [hep-ph].

[121] J. de Blas, M. Ciuchini, E. Franco, S. Mishima, M. Pierini, L. Reina, and L. Silvestrini, *Electroweak precision observables and Higgs-boson signal strengths in*

the Standard Model and beyond: present and future, *JHEP* **12** (2016) 135, arXiv:1608.01509 [hep-ph].

[122] M. Aaboud *et al.*, , **ATLAS** Collaboration, *Search for heavy resonances decaying into WW in the $e\nu\mu\nu$ final state in pp collisions at $\sqrt{s} = 13$ TeV with the ATLAS detector*, *Eur. Phys. J. C* **78** no. 1, (2018) 24, arXiv:1710.01123 [hep-ex].

[123] G. Chalons, D. Lopez-Val, T. Robens, and T. Stefaniak, *The Higgs singlet extension at LHC Run 2*, *PoS* **DIS2016** (2016) 113, arXiv:1606.07793 [hep-ph].

[124] B. W. Lee, C. Quigg, and H. B. Thacker, *Weak Interactions at Very High-Energies: The Role of the Higgs Boson Mass*, *Phys. Rev.* **D16** (1977) 1519.

[125] T. Plehn, M. Spira, and P. M. Zerwas, *Pair production of neutral Higgs particles in gluon-gluon collisions*, *Nucl. Phys.* **B479** (1996) 46–64, arXiv:hep-ph/9603205 [hep-ph]. [Erratum: Nucl. Phys.B531,655(1998)].

[126] J. Butterworth *et al.*, *PDF4LHC recommendations for LHC Run II*, *J. Phys.* **G43** (2016) 023001, arXiv:1510.03865 [hep-ph].

[127] A. Buckley, J. Ferrando, S. Lloyd, K. Nordström, B. Page, M. Rüfenacht, M. Schönherr, and G. Watt, *LHAPDF6: parton density access in the LHC precision era*, *Eur. Phys. J. C* **75** (2015) 132, arXiv:1412.7420 [hep-ph].

[128] S. Dittmaier *et al.*, , **LHC Higgs Cross Section Working Group** Collaboration, *Handbook of LHC Higgs Cross Sections: 1. Inclusive Observables*, arXiv:1101.0593 [hep-ph].

[129] M. Fukugita and T. Yanagida, *Baryogenesis Without Grand Unification*, *Phys. Lett.* **B174** (1986) 45–47.

[130] K. Dick, M. Lindner, M. Ratz, and D. Wright, *Leptogenesis with Dirac neutrinos*, *Phys. Rev. Lett.* **84** (2000) 4039–4042, arXiv:hep-ph/9907562 [hep-ph].

[131] H. Murayama and A. Pierce, *Realistic Dirac leptogenesis*, *Phys. Rev. Lett.* **89** (2002) 271601, arXiv:hep-ph/0206177 [hep-ph].

[132] H. Davoudiasl and I. Lewis, *Technicolor Assisted Leptogenesis with an Ultra-Heavy Higgs Doublet*, *Phys. Rev.* **D86** (2012) 015024, arXiv:1112.1939 [hep-ph].

[133] P.-H. Gu and H.-J. He, *Neutrino Mass and Baryon Asymmetry from Dirac Seesaw*, *JCAP* **0612** (2006) 010, arXiv:hep-ph/0610275 [hep-ph].

[134] M. Tanabashi *et al.*, , **Particle Data Group** Collaboration, *Review of Particle Physics*, *Phys. Rev.* **D98** no. 3, (2018) 030001.

[135] T. Hambye and D. Teresi, *Higgs doublet decay as the origin of the baryon asymmetry*, *Phys. Rev. Lett.* **117** no. 9, (2016) 091801, arXiv:1606.00017 [hep-ph].

[136] T. Hambye and D. Teresi, *Baryogenesis from L-violating Higgs-doublet decay in the density-matrix formalism*, *Phys. Rev.* **D96** no. 1, (2017) 015031, arXiv:1705.00016 [hep-ph].

[137] H. Davoudiasl, D. E. Morrissey, K. Sigurdson, and S. Tulin, *Hylogenesis: A Unified Origin for Baryonic Visible Matter and Antibaryonic Dark Matter*, *Phys. Rev. Lett.* **105** (2010) 211304, arXiv:1008.2399 [hep-ph].

[138] M. Flanz, E. A. Paschos, and U. Sarkar, *Baryogenesis from a lepton asymmetric universe*, *Phys. Lett.* **B345** (1995) 248–252, arXiv:hep-ph/9411366 [hep-ph]. [Erratum: Phys. Lett.B382,447(1996)].

[139] A. Pilaftsis, *CP violation and baryogenesis due to heavy Majorana neutrinos*, *Phys. Rev.* **D56** (1997) 5431–5451, arXiv:hep-ph/9707235 [hep-ph].

[140] A. Pilaftsis, *Heavy Majorana neutrinos and baryogenesis*, *Int. J. Mod. Phys.* **A14** (1999) 1811–1858, arXiv:hep-ph/9812256 [hep-ph].

[141] J. A. Harvey and M. S. Turner, *Cosmological baryon and lepton number in the presence of electroweak fermion number violation*, *Phys. Rev.* **D42** (1990) 3344–3349.

[142] A. Alloul, N. D. Christensen, C. Degrande, C. Duhr, and B. Fuks, *FeynRules 2.0 - A complete toolbox for tree-level phenomenology*, *Comput. Phys. Commun.* **185** (2014) 2250–2300, arXiv:1310.1921 [hep-ph].

[143] J. Alwall, R. Frederix, S. Frixione, V. Hirschi, F. Maltoni, O. Mattelaer, H. S. Shao, T. Stelzer, P. Torrielli, and M. Zaro, *The automated computation of tree-level and next-to-leading order differential cross sections, and their matching to parton shower simulations*, *JHEP* **07** (2014) 079, arXiv:1405.0301 [hep-ph].

[144] E. Bertuzzo, Y. F. Perez G., O. Sumensari, and R. Zukanovich Funchal, *Limits on Neutrinophilic Two-Higgs-Doublet Models from Flavor Physics*, *JHEP* **01** (2016) 018, arXiv:1510.04284 [hep-ph].

[145] J. D. Bjorken and S. Weinberg, *A Mechanism for Nonconservation of Muon Number*, *Phys. Rev. Lett.* **38** (1977) 622.

[146] S. M. Barr and A. Zee, *Electric Dipole Moment of the Electron and of the Neutron*, *Phys. Rev. Lett.* **65** (1990) 21–24. [Erratum: Phys. Rev. Lett.65,2920(1990)].

[147] V. Andreev *et al.*, , **ACME** Collaboration, *Improved limit on the electric dipole moment of the electron*, *Nature* **562** no. 7727, (2018) 355–360.

[148] A. M. Baldini *et al.*, , **MEG** Collaboration, *Search for the lepton flavour violating decay $\mu^+ \to e^+\gamma$ with the full dataset of the MEG experiment*, *Eur. Phys. J.* **C76** no. 8, (2016) 434, arXiv:1605.05081 [hep-ex].

[149] K. S. Babu and S. Jana, *Enhanced Di-Higgs Production in the Two Higgs Doublet Model*, *JHEP* **02** (2019) 193, arXiv:1812.11943 [hep-ph].

[150] T. P. Cheng and M. Sher, *Mass Matrix Ansatz and Flavor Nonconservation in Models with Multiple Higgs Doublets*, *Phys. Rev.* **D35** (1987) 3484.

[151] A. M. Baldini *et al.*, , **MEG II** Collaboration, *The design of the MEG II experiment*, *Eur. Phys. J.* **C78** no. 5, (2018) 380, arXiv:1801.04688 [physics.ins-det].

[152] R. Barbieri, L. J. Hall, and V. S. Rychkov, *Improved naturalness with a heavy Higgs: An Alternative road to LHC physics*, *Phys. Rev.* **D74** (2006) 015007, arXiv:hep-ph/0603188 [hep-ph].

[153] L. Medina Medrano, A. Apollonio, G. Arduini, O. Brüning, M. Giovannozzi, S. Papadopoulou, Y. Papaphilippou, S. Redaelli, and R. Tomás, *New High Luminosity LHC Baseline and Performance at Ultimate Energy*, Tech. Rep. CERN-ACC-2018-069, 2018.

[154] A. Abada *et al.*, , **FCC** Collaboration, *HE-LHC: The High-Energy Large Hadron Collider*, *Eur. Phys. J. ST* **228** no. 5, (2019) 1109–1382.

[155] M. Ahmad *et al.*, *CEPC-SPPC Preliminary Conceptual Design Report. 1. Physics and Detector*, Tech. Rep. IHEP-CEPC-DR-2015-01, IHEP-TH-2015-01, IHEP-EP-2015-01, 2015.

[156] A. Abada *et al.*, , **FCC** Collaboration, *FCC-hh: The Hadron Collider*, *Eur. Phys. J. ST* **228** no. 4, (2019) 755–1107.

[157] M. Cepeda *et al.*, , **HL/HE WG2 group** Collaboration, *Higgs Physics at the HL-LHC and HE-LHC*, arXiv:1902.00134 [hep-ph].

[158] Y. Fukuda *et al.*, , **Super-Kamiokande** Collaboration, *Evidence for oscillation of atmospheric neutrinos*, *Phys. Rev. Lett.* **81** (1998) 1562–1567, arXiv:hep-ex/9807003 [hep-ex].

[159] S. N. Ahmed *et al.*, , **SNO** Collaboration, *Measurement of the total active B-8 solar neutrino flux at the Sudbury Neutrino Observatory with enhanced neutral current sensitivity*, *Phys. Rev. Lett.* **92** (2004) 181301, arXiv:nucl-ex/0309004 [nucl-ex].

[160] T. D. Lee and C.-N. Yang, *Conservation of Heavy Particles and Generalized Gauge Transformations*, *Phys. Rev.* **98** (1955) 1501.

[161] J. A. Frieman and B.-A. Gradwohl, *Dark matter and the equivalence principle*, *Phys. Rev. Lett.* **67** (1991) 2926–2929.

[162] B.-A. Gradwohl and J. A. Frieman, *Dark matter, long range forces, and large scale structure*, *Astrophys. J.* **398** (1992) 407–424.

[163] A. D. Dolgov, *Long range forces in the universe*, *Phys. Rept.* **320** (1999) 1–15.

[164] G. R. Farrar and P. J. E. Peebles, *Interacting dark matter and dark energy*, *Astrophys. J.* **604** (2004) 1–11, arXiv:astro-ph/0307316 [astro-ph].

[165] S. S. Gubser and P. J. E. Peebles, *Cosmology with a dynamically screened scalar interaction in the dark sector*, *Phys. Rev.* **D70** (2004) 123511, arXiv:hep-th/0407097 [hep-th].

[166] S. S. Gubser and P. J. E. Peebles, *Structure formation in a string inspired modification of the cold dark matter model*, *Phys. Rev.* **D70** (2004) 123510, arXiv:hep-th/0402225 [hep-th].

[167] A. Nusser, S. S. Gubser, and P. J. E. Peebles, *Structure formation with a long-range scalar dark matter interaction*, *Phys. Rev.* **D71** (2005) 083505, arXiv:astro-ph/0412586 [astro-ph].

[168] M. Kesden and M. Kamionkowski, *Tidal Tails Test the Equivalence Principle in the Dark Sector*, *Phys. Rev.* **D74** (2006) 083007, arXiv:astro-ph/0608095 [astro-ph].

[169] M. Kesden and M. Kamionkowski, *Galilean Equivalence for Galactic Dark Matter*, *Phys. Rev. Lett.* **97** (2006) 131303, arXiv:astro-ph/0606566 [astro-ph].

[170] G. R. Farrar and R. A. Rosen, *A New Force in the Dark Sector?*, *Phys. Rev. Lett.* **98** (2007) 171302, arXiv:astro-ph/0610298 [astro-ph].

[171] H. Davoudiasl, *Dark matter repulsion could thwart direct detection*, *Phys. Rev.* **D96** no. 9, (2017) 095019, arXiv:1705.00028 [hep-ph].

[172] A. Berlin, *Neutrino Oscillations as a Probe of Light Scalar Dark Matter*, *Phys. Rev. Lett.* **117** no. 23, (2016) 231801, arXiv:1608.01307 [hep-ph].

[173] G. Krnjaic, P. A. N. Machado, and L. Necib, *Distorted Neutrino Oscillations From Ultralight Scalar Dark Matter*, arXiv:1705.06740 [hep-ph].

[174] H. Davoudiasl and P. P. Giardino, *Variation of α from a Dark Matter Force*, *Phys. Lett. B* **788** (2019) 270–273, arXiv:1804.01098 [hep-ph].

[175] R. Fardon, A. E. Nelson, and N. Weiner, *Dark energy from mass varying neutrinos*, *JCAP* **0410** (2004) 005, arXiv:astro-ph/0309800 [astro-ph].

[176] C. Patrignani *et al.*, , **Particle Data Group** Collaboration, *Review of Particle Physics*, *Chin. Phys.* **C40** no. 10, (2016) 100001.

[177] S. M. Carroll, S. Mantry, M. J. Ramsey-Musolf, and C. W. Stubbs, *Dark-Matter-Induced Weak Equivalence Principle Violation*, *Phys. Rev. Lett.* **103** (2009) 011301, arXiv:0807.4363 [hep-ph].

[178] A. Basboll, O. E. Bjaelde, S. Hannestad, and G. G. Raffelt, *Are cosmological neutrinos free-streaming?*, *Phys. Rev.* **D79** (2009) 043512, arXiv:0806.1735 [astro-ph].

[179] J. F. Navarro, C. S. Frenk, and S. D. M. White, *The Structure of cold dark matter halos*, *Astrophys. J.* **462** (1996) 563–575, arXiv:astro-ph/9508025 [astro-ph].

[180] J. Bramante, N. Desai, P. Fox, A. Martin, B. Ostdiek, and T. Plehn, *Towards the Final Word on Neutralino Dark Matter*, *Phys. Rev.* **D93** no. 6, (2016) 063525, arXiv:1510.03460 [hep-ph].

[181] F. Nesti and P. Salucci, *The Dark Matter halo of the Milky Way, AD 2013*, *JCAP* **1307** (2013) 016, arXiv:1304.5127 [astro-ph.GA].

[182] E. V. Karukes and P. Salucci, *Modeling the Mass Distribution in the Spiral Galaxy NGC 3198*, in *Journal of Physics Conference Series*, vol. 566 of *Journal of Physics Conference Series*, p. 012008. Dec., 2014.

[183] E. W. Kolb and M. S. Turner, *The Early Universe*, *Front. Phys.* **69** (1990) 1–547.

[184] A. D. Dolgov and G. G. Raffelt, *Screening of long range leptonic forces by cosmic background neutrinos*, *Phys. Rev.* **D52** (1995) 2581–2582, arXiv:hep-ph/9503438 [hep-ph].

[185] A. Gould, *Resonant Enhancements in WIMP Capture by the Earth*, *Astrophys. J.* **321** (1987) 571.

[186] H. Davoudiasl, D. E. Morrissey, K. Sigurdson, and S. Tulin, *Baryon Destruction by Asymmetric Dark Matter*, *Phys. Rev.* **D84** (2011) 096008, arXiv:1106.4320 [hep-ph].

[187] K. Kong, G. Mohlabeng, and J.-C. Park, *Boosted dark matter signals uplifted with self-interaction*, *Phys. Lett.* **B743** (2015) 256–266, arXiv:1411.6632 [hep-ph].

[188] R. Allison, P. Caucal, E. Calabrese, J. Dunkley, and T. Louis, *Towards a cosmological neutrino mass detection*, *Phys. Rev.* **D92** no. 12, (2015) 123535, arXiv:1509.07471 [astro-ph.CO].

[189] M. LoVerde, *Spherical collapse in $\nu\Lambda CDM$*, *Phys. Rev.* **D90** no. 8, (2014) 083518, arXiv:1405.4858 [astro-ph.CO].

[190] A. C. Hall and A. Challinor, *Probing the neutrino mass hierarchy with CMB weak lensing*, *Mon. Not. Roy. Astron. Soc.* **425** (2012) 1170–1184, arXiv:1205.6172 [astro-ph.CO].

[191] L. Stodolsky, *Speculations on Detection of the Neutrino Sea*, *Phys. Rev. Lett.* **34** (1975) 110. [Erratum: Phys. Rev. Lett.34,508(1975)].

[192] G. Duda, G. Gelmini, and S. Nussinov, *Expected signals in relic neutrino detectors*, *Phys. Rev.* **D64** (2001) 122001, arXiv:hep-ph/0107027 [hep-ph].

[193] A. Strumia and F. Vissani, *Neutrino masses and mixings and...*, arXiv:hep-ph/0606054 [hep-ph].

[194] V. Domcke and M. Spinrath, *Detection prospects for the Cosmic Neutrino Background using laser interferometers*, *JCAP* **1706** no. 06, (2017) 055, arXiv:1703.08629 [astro-ph.CO].

[195] S. Weinberg, *Universal Neutrino Degeneracy*, *Phys. Rev.* **128** (1962) 1457–1473.

[196] Y. F. Perez-Gonzalez, , *Massive Neutrinos: Phenomenological and Cosmological Consequences*. PhD thesis, 2017. arXiv:1712.06675 [hep-ph].

[197] S. Betts *et al.*, *Development of a Relic Neutrino Detection Experiment at PTOLEMY: Princeton Tritium Observatory for Light, Early-Universe, Massive-Neutrino Yield*, in *Proceedings, 2013 Community Summer Study on the Future of U.S. Particle Physics: Snowmass on the Mississippi (CSS2013): Minneapolis, MN, USA, July 29-August 6, 2013*. 2013. arXiv:1307.4738 [astro-ph.IM].

[198] Y. Bai, J. Salvado, and B. A. Stefanek, *Cosmological Constraints on the Gravitational Interactions of Matter and Dark Matter*, *JCAP* **10** (2015) 029, arXiv:1505.04789 [hep-ph].

[199] B. Holdom, *Two U(1)'s and Epsilon Charge Shifts*, *Phys. Lett.* **166B** (1986) 196–198.

[200] J. D. Bjorken, R. Essig, P. Schuster, and N. Toro, *New Fixed-Target Experiments to Search for Dark Gauge Forces*, *Phys. Rev.* **D80** (2009) 075018, arXiv:0906.0580 [hep-ph].

[201] R. Essig *et al.*, *Working Group Report: New Light Weakly Coupled Particles*, in *Proceedings, 2013 Community Summer Study on the Future of U.S. Particle Physics: Snowmass on the Mississippi (CSS2013): Minneapolis, MN, USA, July 29-August 6, 2013*. 2013. arXiv:1311.0029 [hep-ph].

[202] H. Davoudiasl, H.-S. Lee, and W. J. Marciano, *Dark Side of Higgs Diphoton Decays and Muon g-2*, *Phys. Rev.* **D86** (2012) 095009, arXiv:1208.2973 [hep-ph].

[203] Q. Lu, D. E. Morrissey, and A. M. Wijangco, *Higgs Boson Decays to Dark Photons through the Vectorized Lepton Portal*, *JHEP* **06** (2017) 138, arXiv:1705.08896 [hep-ph].

[204] D. Curtin, R. Essig, S. Gori, and J. Shelton, *Illuminating Dark Photons with High-Energy Colliders*, *JHEP* **02** (2015) 157, arXiv:1412.0018 [hep-ph].

[205] K. Kong, H.-S. Lee, and M. Park, *Dark decay of the top quark*, *Phys. Rev.* **D89** no. 7, (2014) 074007, arXiv:1401.5020 [hep-ph].

[206] J. Alimena *et al.*, *Searching for long-lived particles beyond the Standard Model at the Large Hadron Collider*, arXiv:1903.04497 [hep-ex].

[207] H. Davoudiasl, H.-S. Lee, I. Lewis, and W. J. Marciano, *Higgs Decays as a Window into the Dark Sector*, *Phys. Rev.* **D88** no. 1, (2013) 015022, arXiv:1304.4935 [hep-ph].

[208] K. Agashe, R. Contino, and A. Pomarol, *The Minimal composite Higgs model*, *Nucl. Phys.* **B719** (2005) 165–187, arXiv:hep-ph/0412089 [hep-ph].

[209] K. Agashe and R. Contino, *The Minimal composite Higgs model and electroweak precision tests*, *Nucl. Phys.* **B742** (2006) 59–85, arXiv:hep-ph/0510164 [hep-ph].

[210] K. Agashe, R. Contino, L. Da Rold, and A. Pomarol, *A Custodial symmetry for $Zb\bar{b}$*, *Phys. Lett.* **B641** (2006) 62–66, arXiv:hep-ph/0605341 [hep-ph].

[211] R. Contino, L. Da Rold, and A. Pomarol, *Light custodians in natural composite Higgs models*, *Phys. Rev.* **D75** (2007) 055014, arXiv:hep-ph/0612048 [hep-ph].

[212] G. F. Giudice, C. Grojean, A. Pomarol, and R. Rattazzi, *The Strongly-Interacting Light Higgs*, *JHEP* **06** (2007) 045, arXiv:hep-ph/0703164 [hep-ph].

[213] A. Azatov and J. Galloway, *Light Custodians and Higgs Physics in Composite Models*, *Phys. Rev.* **D85** (2012) 055013, arXiv:1110.5646 [hep-ph].

[214] J. Serra, *Beyond the Minimal Top Partner Decay*, *JHEP* **09** (2015) 176, arXiv:1506.05110 [hep-ph].

[215] N. Arkani-Hamed, A. G. Cohen, E. Katz, and A. E. Nelson, *The Littlest Higgs*, *JHEP* **07** (2002) 034, arXiv:hep-ph/0206021 [hep-ph].

[216] N. Arkani-Hamed, A. G. Cohen, T. Gregoire, and J. G. Wacker, *Phenomenology of electroweak symmetry breaking from theory space*, *JHEP* **08** (2002) 020, arXiv:hep-ph/0202089 [hep-ph].

[217] I. Low, W. Skiba, and D. Tucker-Smith, *Little Higgses from an antisymmetric condensate*, *Phys. Rev.* **D66** (2002) 072001, arXiv:hep-ph/0207243 [hep-ph].

[218] S. Chang and J. G. Wacker, *Little Higgs and custodial SU(2)*, *Phys. Rev.* **D69** (2004) 035002, arXiv:hep-ph/0303001 [hep-ph].

[219] C. Csaki, J. Hubisz, G. D. Kribs, P. Meade, and J. Terning, *Variations of little Higgs models and their electroweak constraints*, *Phys. Rev.* **D68** (2003) 035009, arXiv:hep-ph/0303236 [hep-ph].

[220] M. Perelstein, M. E. Peskin, and A. Pierce, *Top quarks and electroweak symmetry breaking in little Higgs models*, *Phys. Rev.* **D69** (2004) 075002, arXiv:hep-ph/0310039 [hep-ph].

[221] M.-C. Chen and S. Dawson, *One loop radiative corrections to the rho parameter in the littlest Higgs model*, *Phys. Rev.* **D70** (2004) 015003, arXiv:hep-ph/0311032 [hep-ph].

[222] J. Berger, J. Hubisz, and M. Perelstein, *A Fermionic Top Partner: Naturalness and the LHC*, *JHEP* **07** (2012) 016, arXiv:1205.0013 [hep-ph].

[223] J. H. Kim and I. M. Lewis, *Loop Induced Single Top Partner Production and Decay at the LHC*, *JHEP* **05** (2018) 095, arXiv:1803.06351 [hep-ph].

[224] H. Alhazmi, J. H. Kim, K. Kong, and I. M. Lewis, *Shedding Light on Top Partner at the LHC*, *JHEP* **01** (2019) 139, arXiv:1808.03649 [hep-ph].

[225] A. De Rujula, L. Maiani, and R. Petronzio, *Search for Excited Quarks*, *Phys. Lett.* **140B** (1984) 253–258.

[226] J. H. Kuhn and P. M. Zerwas, *Excited Quarks and Leptons*, *Phys. Lett.* **147B** (1984) 189–196.

[227] U. Baur, I. Hinchliffe, and D. Zeppenfeld, *Excited Quark Production at Hadron Colliders*, *Int. J. Mod. Phys.* **A2** (1987) 1285.

[228] U. Baur, M. Spira, and P. M. Zerwas, *Excited Quark and Lepton Production at Hadron Colliders*, *Phys. Rev.* **D42** (1990) 815–824.

[229] A. Anandakrishnan, J. H. Collins, M. Farina, E. Kuflik, and M. Perelstein, *Odd Top Partners at the LHC*, *Phys. Rev.* **D93** no. 7, (2016) 075009, arXiv:1506.05130 [hep-ph].

[230] M. J. Dolan, J. L. Hewett, M. Krämer, and T. G. Rizzo, *Simplified Models for Higgs Physics: Singlet Scalar and Vector-like Quark Phenomenology*, *JHEP* **07** (2016) 039, arXiv:1601.07208 [hep-ph].

[231] N. Bizot, G. Cacciapaglia, and T. Flacke, *Common exotic decays of top partners*, *JHEP* **06** (2018) 065, arXiv:1803.00021 [hep-ph].

[232] M. Chala, R. Gröber, and M. Spannowsky, *Searches for vector-like quarks at future colliders and implications for composite Higgs models with dark matter*, *JHEP* **03** (2018) 040, arXiv:1801.06537 [hep-ph].

[233] J. A. Aguilar-Saavedra, D. E. López-Fogliani, and C. Muñoz, *Novel signatures for vector-like quarks*, *JHEP* **06** (2017) 095, arXiv:1705.02526 [hep-ph].

[234] M. Chala, *Direct bounds on heavy toplike quarks with standard and exotic decays*, *Phys. Rev.* **D96** no. 1, (2017) 015028, arXiv:1705.03013 [hep-ph].

[235] R. Balkin, M. Ruhdorfer, E. Salvioni, and A. Weiler, *Charged Composite Scalar Dark Matter*, *JHEP* **11** (2017) 094, arXiv:1707.07685 [hep-ph].

[236] K. Das, T. Mondal, and S. K. Rai, *Nonstandard signatures of vectorlike quarks in a leptophobic 221 model*, *Phys. Rev.* **D99** no. 11, (2019) 115002, arXiv:1807.08160 [hep-ph].

[237] T. G. Rizzo, *Kinetic Mixing and Portal Matter Phenomenology*, *Phys. Rev.* **D99** no. 11, (2019) 115024, arXiv:1810.07531 [hep-ph].

[238] N. Arkani-Hamed and N. Weiner, *LHC Signals for a SuperUnified Theory of Dark Matter*, *JHEP* **12** (2008) 104, arXiv:0810.0714 [hep-ph].

[239] M. E. Peskin and T. Takeuchi, *Estimation of oblique electroweak corrections*, *Phys. Rev.* **D46** (1992) 381–409.

[240] G. Degrassi and A. Sirlin, *Gauge invariant selfenergies and vertex parts of the Standard Model in the pinch technique framework*, *Phys. Rev.* **D46** (1992) 3104–3116.

[241] G. Degrassi, B. A. Kniehl, and A. Sirlin, *Gauge invariant formulation of the S, T, and U parameters*, *Phys. Rev.* **D48** (1993) R3963–R3966.

[242] L. Lavoura and J. P. Silva, *The Oblique corrections from vector - like singlet and doublet quarks*, *Phys. Rev.* **D47** (1993) 2046–2057.

[243] H.-J. He, N. Polonsky, and S.-f. Su, *Extra families, Higgs spectrum and oblique corrections*, *Phys. Rev.* **D64** (2001) 053004, arXiv:hep-ph/0102144 [hep-ph].

[244] J. A. Aguilar-Saavedra, R. Benbrik, S. Heinemeyer, and M. Pérez-Victoria, *Handbook of vectorlike quarks: Mixing and single production*, *Phys. Rev.* **D88** no. 9, (2013) 094010, arXiv:1306.0572 [hep-ph].

[245] S. Dawson and E. Furlan, *A Higgs Conundrum with Vector Fermions*, *Phys. Rev.* **D86** (2012) 015021, arXiv:1205.4733 [hep-ph].

[246] S. A. R. Ellis, R. M. Godbole, S. Gopalakrishna, and J. D. Wells, *Survey of vector-like fermion extensions of the Standard Model and their phenomenological implications*, *JHEP* **09** (2014) 130, arXiv:1404.4398 [hep-ph].

[247] C.-Y. Chen, S. Dawson, and E. Furlan, *Vectorlike fermions and Higgs effective field theory revisited*, *Phys. Rev.* **D96** no. 1, (2017) 015006, arXiv:1703.06134 [hep-ph].

[248] V. Barger, P. Langacker, M. McCaskey, M. J. Ramsey-Musolf, and G. Shaughnessy, *LHC Phenomenology of an Extended Standard Model with a Real Scalar Singlet*, *Phys.Rev.* **D77** (2008) 035005, arXiv:0706.4311 [hep-ph].

[249] A. Hook, E. Izaguirre, and J. G. Wacker, *Model Independent Bounds on Kinetic Mixing*, *Adv. High Energy Phys.* **2011** (2011) 859762, arXiv:1006.0973 [hep-ph].

[250] B. Clerbaux, W. Fang, A. Giammanco, and R. Goldouzian, *Model-independent constraints on the CKM matrix elements $|V_{tb}|$, $|V_{ts}|$ and $|V_{td}|$*, *JHEP* **03** (2019) 022, arXiv:1807.07319 [hep-ph]. [Physics2019,22(2019)].

[251] M. Aaboud *et al.*, , **ATLAS** Collaboration, *Combination of the searches for pair-produced vector-like partners of the third-generation quarks at $\sqrt{s} = 13$ TeV with the ATLAS detector*, *Phys. Rev. Lett.* **121** no. 21, (2018) 211801, arXiv:1808.02343 [hep-ex].

[252] **CMS Collaboration** Collaboration, *Search for Pair Production of Vector-Like Quarks in the Fully Hadronic Channel*, Tech. Rep. CMS-PAS-B2G-18-005, CERN, Geneva, 2019.

[253] A. M. Sirunyan *et al.*, , **CMS** Collaboration, *Search for vector-like T and B quark pairs in final states with leptons at $\sqrt{s} = 13$ TeV*, *JHEP* **08** (2018) 177, arXiv:1805.04758 [hep-ex].

[254] M. Aaboud *et al.*, , **ATLAS** Collaboration, *Search for pair- and single-production of vector-like quarks in final states with at least one Z boson decaying into a pair of electrons or muons in pp collision data collected with the ATLAS detector at $\sqrt{s} = 13$ TeV*, *Phys. Rev.* **D98** no. 11, (2018) 112010, arXiv:1806.10555 [hep-ex].

[255] A. M. Sirunyan *et al.*, , **CMS** Collaboration, *Search for single production of a vector-like T quark decaying to a Z boson and a top quark in proton-proton collisions at $\sqrt{s} = 13$ TeV*, *Phys. Lett.* **B781** (2018) 574–600, arXiv:1708.01062 [hep-ex].

[256] A. M. Sirunyan *et al.*, , **CMS** Collaboration, *Search for single production of vector-like quarks decaying into a b quark and a W boson in proton-proton collisions at $\sqrt{s} = 13$ TeV*, *Phys. Lett.* **B772** (2017) 634–656, arXiv:1701.08328 [hep-ex].

[257] M. Aaboud *et al.*, , **ATLAS** Collaboration, *Search for single production of vector-like quarks decaying into Wb in pp collisions at $\sqrt{s} = 13$ TeV with the ATLAS detector*, *JHEP* **05** (2019) 164, arXiv:1812.07343 [hep-ex].

[258] A. M. Sirunyan *et al.*, , **CMS** Collaboration, *Search for a new scalar resonance decaying to a pair of Z bosons in proton-proton collisions at $\sqrt{s} = 13$ TeV*, *JHEP* **06** (2018) 127, arXiv:1804.01939 [hep-ex].

[259] M. Aaboud *et al.*, , **ATLAS** Collaboration, *Search for heavy ZZ resonances in the $\ell^+\ell^-\ell^+\ell^-$ and $\ell^+\ell^-\nu\bar{\nu}$ final states using proton-proton collisions at $\sqrt{s} = 13$ TeV with the ATLAS detector*, *Eur. Phys. J.* **C78** no. 4, (2018) 293, arXiv:1712.06386 [hep-ex].

[260] G. Aad *et al.*, , **ATLAS** Collaboration, *Search For Higgs Boson Pair Production in the $\gamma\gamma b\bar{b}$ Final State using pp Collision Data at $\sqrt{s} = 8$ TeV from the ATLAS Detector*, *Phys. Rev. Lett.* **114** no. 8, (2015) 081802, arXiv:1406.5053 [hep-ex].

[261] P. Bechtle, S. Heinemeyer, O. Stål, T. Stefaniak, and G. Weiglein, *Applying Exclusion Likelihoods from LHC Searches to Extended Higgs Sectors*, *Eur. Phys. J.* **C75** no. 9, (2015) 421, arXiv:1507.06706 [hep-ph].

[262] U. Haisch, J. F. Kamenik, A. Malinauskas, and M. Spira, *Collider constraints on light pseudoscalars*, *JHEP* **03** (2018) 178, arXiv:1802.02156 [hep-ph].

[263] P. Bechtle, O. Brein, S. Heinemeyer, G. Weiglein, and K. E. Williams, *HiggsBounds: Confronting Arbitrary Higgs Sectors with Exclusion Bounds from LEP and the Tevatron*, *Comput. Phys. Commun.* **181** (2010) 138–167, arXiv:0811.4169 [hep-ph].

[264] P. Bechtle, O. Brein, S. Heinemeyer, G. Weiglein, and K. E. Williams, *HiggsBounds 2.0.0: Confronting Neutral and Charged Higgs Sector Predictions with Exclusion*

Bounds from LEP and the Tevatron, *Comput. Phys. Commun.* **182** (2011) 2605–2631, arXiv:1102.1898 [hep-ph].

[265] P. Bechtle, O. Brein, S. Heinemeyer, O. Stål, T. Stefaniak, G. Weiglein, and K. E. Williams, HiggsBounds – 4*: Improved Tests of Extended Higgs Sectors against Exclusion Bounds from LEP, the Tevatron and the LHC*, *Eur. Phys. J.* **C74** no. 3, (2014) 2693, arXiv:1311.0055 [hep-ph].

[266] T. Robens, . Personal communication.

[267] A. Ilnicka, T. Robens, and T. Stefaniak, *Constraining Extended Scalar Sectors at the LHC and beyond*, *Mod. Phys. Lett.* **A33** no. 10n11, (2018) 1830007, arXiv:1803.03594 [hep-ph].

[268] M. Battaglieri *et al.*, *US Cosmic Visions: New Ideas in Dark Matter 2017: Community Report*, in *U.S. Cosmic Visions: New Ideas in Dark Matter College Park, MD, USA, March 23-25, 2017*. 2017. arXiv:1707.04591 [hep-ph].

[269] M. Aaboud *et al.*, , **ATLAS** Collaboration, *Search for Higgs boson decays to beyond-the-Standard-Model light bosons in four-lepton events with the ATLAS detector at* $\sqrt{s} = 13$ *TeV*, *JHEP* **06** (2018) 166, arXiv:1802.03388 [hep-ex].

[270] J. F. Gunion, H. E. Haber, G. L. Kane, and S. Dawson, *The Higgs Hunter's Guide*, *Front.Phys.* **80** (2000) 1–448.

[271] A. M. Sirunyan *et al.*, , **CMS** Collaboration, *Search for invisible decays of a Higgs boson produced through vector boson fusion in proton-proton collisions at* $\sqrt{s} = 13$ *TeV*, arXiv:1809.05937 [hep-ex].

[272] **ATLAS Collaboration** Collaboration, *Combination of searches for invisible Higgs boson decays with the ATLAS experiment*, Tech. Rep. ATLAS-CONF-2018-054, CERN, Geneva, Nov, 2018.

[273] O. Matsedonskyi, G. Panico, and A. Wulzer, *On the Interpretation of Top Partners Searches*, *JHEP* **12** (2014) 097, arXiv:1409.0100 [hep-ph].

[274] M. Chala, J. Juknevich, G. Perez, and J. Santiago, *The Elusive Gluon*, *JHEP* **01** (2015) 092, arXiv:1411.1771 [hep-ph].

[275] A. Azatov, D. Chowdhury, D. Ghosh, and T. S. Ray, *Same sign di-lepton candles of the composite gluons*, *JHEP* **08** (2015) 140, arXiv:1505.01506 [hep-ph].

[276] J. P. Araque, N. F. Castro, and J. Santiago, *Interpretation of Vector-like Quark Searches: Heavy Gluons in Composite Higgs Models*, *JHEP* **11** (2015) 120, arXiv:1507.05628 [hep-ph].

[277] M. Aliev, H. Lacker, U. Langenfeld, S. Moch, P. Uwer, and M. Wiedermann, *HATHOR: HAdronic Top and Heavy quarks crOss section calculatoR*, *Comput. Phys. Commun.* **182** (2011) 1034–1046, arXiv:1007.1327 [hep-ph].

[278] A. D. Martin, W. J. Stirling, R. S. Thorne, and G. Watt, *Parton distributions for the LHC*, *Eur. Phys. J.* **C63** (2009) 189–285, arXiv:0901.0002 [hep-ph].

[279] J. M. Campbell, R. Frederix, F. Maltoni, and F. Tramontano, *NLO predictions for t-channel production of single top and fourth generation quarks at hadron colliders*, *JHEP* **10** (2009) 042, arXiv:0907.3933 [hep-ph].

[280] J. M. Campbell, R. Frederix, F. Maltoni, and F. Tramontano, *Next-to-Leading-Order Predictions for t-Channel Single-Top Production at Hadron Colliders*, *Phys. Rev. Lett.* **102** (2009) 182003, arXiv:0903.0005 [hep-ph].

[281] J. M. Campbell, R. K. Ellis, and F. Tramontano, *Single top production and decay at next-to-leading order*, *Phys. Rev.* **D70** (2004) 094012, arXiv:hep-ph/0408158 [hep-ph].

[282] A. M. Sirunyan *et al.*, , **CMS** Collaboration, *Search for top squark pair production in pp collisions at* $\sqrt{s} = 13$ *TeV using single lepton events*, *JHEP* **10** (2017) 019, arXiv:1706.04402 [hep-ex].

[283] A. M. Sirunyan *et al.*, , **CMS** Collaboration, *Search for top squarks and dark matter particles in opposite-charge dilepton final states at* $\sqrt{s} = 13$ *TeV*, *Phys. Rev.* **D97** no. 3, (2018) 032009, arXiv:1711.00752 [hep-ex].

[284] A. M. Sirunyan *et al.*, , **CMS** Collaboration, *Search for supersymmetry in multijet events with missing transverse momentum in proton-proton collisions at 13 TeV*, *Phys. Rev.* **D96** no. 3, (2017) 032003, arXiv:1704.07781 [hep-ex].

[285] A. M. Sirunyan *et al.*, , **CMS** Collaboration, *Search for new phenomena with the* M_{T2} *variable in the all-hadronic final state produced in proton–proton collisions at* $\sqrt{s} = 13$ *TeV*, *Eur. Phys. J.* **C77** no. 10, (2017) 710, arXiv:1705.04650 [hep-ex].

[286] A. M. Sirunyan *et al.*, , **CMS** Collaboration, *Search for supersymmetry in proton-proton collisions at 13 TeV using identified top quarks*, *Phys. Rev.* **D97** no. 1, (2018) 012007, arXiv:1710.11188 [hep-ex].

[287] **CMS Collaboration** Collaboration, *Searches for new phenomena in events with jets and high values of the* M_{T2} *variable, including signatures with disappearing tracks, in proton-proton collisions at* $\sqrt{s} = 13$ TeV, Tech. Rep. CMS-PAS-SUS-19-005, CERN, Geneva, 2019.

[288] M. Aaboud *et al.*, , **ATLAS** Collaboration, *Search for a scalar partner of the top quark in the jets plus missing transverse momentum final state at* $\sqrt{s}$*=13 TeV with the ATLAS detector*, *JHEP* **12** (2017) 085, arXiv:1709.04183 [hep-ex].

[289] M. Aaboud *et al.*, , **ATLAS** Collaboration, *Search for direct top squark pair production in final states with two leptons in* $\sqrt{s} = 13$ *TeV pp collisions with the*

ATLAS detector, *Eur. Phys. J.* **C77** no. 12, (2017) 898, arXiv:1708.03247 [hep-ex].

[290] C. Borschensky, M. Krämer, A. Kulesza, M. Mangano, S. Padhi, T. Plehn, and X. Portell, *Squark and gluino production cross sections in pp collisions at $\sqrt{s}$ = 13, 14, 33 and 100 TeV*, *Eur. Phys. J.* **C74** no. 12, (2014) 3174, arXiv:1407.5066 [hep-ph].

[291] S. Kraml, U. Laa, L. Panizzi, and H. Prager, *Scalar versus fermionic top partner interpretations of $t\bar{t} + E_T^{\text{miss}}$ searches at the LHC*, *JHEP* **11** (2016) 107, arXiv:1607.02050 [hep-ph].

[292] M. Aaboud *et al.*, , **ATLAS** Collaboration, *Search for large missing transverse momentum in association with one top-quark in proton-proton collisions at $\sqrt{s}$ = 13 TeV with the ATLAS detector*, *JHEP* **05** (2019) 041, arXiv:1812.09743 [hep-ex].

[293] A. M. Sirunyan *et al.*, , **CMS** Collaboration, *Search for electroweak production of a vector-like T quark using fully hadronic final states*, *JHEP* **01** (2020) 036, arXiv:1909.04721 [hep-ex].

[294] J. D. Bjorken, S. Ecklund, W. R. Nelson, A. Abashian, C. Church, B. Lu, L. W. Mo, T. A. Nunamaker, and P. Rassmann, *Search for Neutral Metastable Penetrating Particles Produced in the SLAC Beam Dump*, *Phys. Rev.* **D38** (1988) 3375.

[295] E. M. Riordan *et al.*, *A Search for Short Lived Axions in an Electron Beam Dump Experiment*, *Phys. Rev. Lett.* **59** (1987) 755.

[296] A. Bross, M. Crisler, S. H. Pordes, J. Volk, S. Errede, and J. Wrbanek, *A Search for Shortlived Particles Produced in an Electron Beam Dump*, *Phys. Rev. Lett.* **67** (1991) 2942–2945.

[297] J. Blümlein and J. Brunner, *New Exclusion Limits on Dark Gauge Forces from Proton Bremsstrahlung in Beam-Dump Data*, *Phys. Lett.* **B731** (2014) 320–326, arXiv:1311.3870 [hep-ph].

[298] J. Blumlein and J. Brunner, *New Exclusion Limits for Dark Gauge Forces from Beam-Dump Data*, *Phys. Lett.* **B701** (2011) 155–159, arXiv:1104.2747 [hep-ex].

[299] R. Aaij *et al.*, , **LHCb** Collaboration, *Search for Dark Photons Produced in 13 TeV pp Collisions*, *Phys. Rev. Lett.* **120** no. 6, (2018) 061801, arXiv:1710.02867 [hep-ex].

[300] P. Ilten, Y. Soreq, M. Williams, and W. Xue, *Serendipity in dark photon searches*, *JHEP* **06** (2018) 004, arXiv:1801.04847 [hep-ph].

[301] D. Banerjee *et al.*, , **NA64** Collaboration, *Search for a Hypothetical 16.7 MeV Gauge Boson and Dark Photons in the NA64 Experiment at CERN*, *Phys. Rev. Lett.* **120** no. 23, (2018) 231802, arXiv:1803.07748 [hep-ex].

[302] M. Pospelov, *Secluded U(1) below the weak scale*, *Phys. Rev.* **D80** (2009) 095002, arXiv:0811.1030 [hep-ph].

[303] M. Endo, K. Hamaguchi, and G. Mishima, *Constraints on Hidden Photon Models from Electron g-2 and Hydrogen Spectroscopy*, *Phys. Rev.* **D86** (2012) 095029, arXiv:1209.2558 [hep-ph].

[304] D. Babusci *et al.*, , **KLOE-2** Collaboration, *Limit on the production of a light vector gauge boson in phi meson decays with the KLOE detector*, *Phys. Lett.* **B720** (2013) 111–115, arXiv:1210.3927 [hep-ex].

[305] F. Archilli *et al.*, , **KLOE-2** Collaboration, *Search for a vector gauge boson in ϕ meson decays with the KLOE detector*, *Phys. Lett.* **B706** (2012) 251–255, arXiv:1110.0411 [hep-ex].

[306] P. Adlarson *et al.*, , **WASA-at-COSY** Collaboration, *Search for a dark photon in the $\pi^0 \to e^+e^-\gamma$ decay*, *Phys. Lett.* **B726** (2013) 187–193, arXiv:1304.0671 [hep-ex].

[307] S. Abrahamyan *et al.*, , **APEX** Collaboration, *Search for a New Gauge Boson in Electron-Nucleus Fixed-Target Scattering by the APEX Experiment*, *Phys. Rev. Lett.* **107** (2011) 191804, arXiv:1108.2750 [hep-ex].

[308] H. Merkel *et al.*, , **A1** Collaboration, *Search for Light Gauge Bosons of the Dark Sector at the Mainz Microtron*, *Phys. Rev. Lett.* **106** (2011) 251802, arXiv:1101.4091 [nucl-ex].

[309] M. Reece and L.-T. Wang, *Searching for the light dark gauge boson in GeV-scale experiments*, *JHEP* **07** (2009) 051, arXiv:0904.1743 [hep-ph].

[310] B. Aubert *et al.*, , **BaBar** Collaboration, *Search for Dimuon Decays of a Light Scalar Boson in Radiative Transitions Upsilon $\to$ gamma A0*, *Phys. Rev. Lett.* **103** (2009) 081803, arXiv:0905.4539 [hep-ex].

[311] J. H. Chang, R. Essig, and S. D. McDermott, *Revisiting Supernova 1987A Constraints on Dark Photons*, *JHEP* **01** (2017) 107, arXiv:1611.03864 [hep-ph].

[312] J. H. Chang, R. Essig, and S. D. McDermott, *Supernova 1987A Constraints on Sub-GeV Dark Sectors, Millicharged Particles, the QCD Axion, and an Axion-like Particle*, *JHEP* **09** (2018) 051, arXiv:1803.00993 [hep-ph].

[313] M. Backović, T. Flacke, J. H. Kim, and S. J. Lee, *Discovering heavy new physics in boosted Z channels: $Z \to l^+l^-$ vs $Z \to \nu\bar{\nu}$*, *Phys. Rev.* **D92** no. 1, (2015) 011701, arXiv:1501.07456 [hep-ph].

[314] M. Backovic, T. Flacke, J. H. Kim, and S. J. Lee, *Search Strategies for TeV Scale Fermionic Top Partners with Charge 2/3*, *JHEP* **04** (2016) 014, arXiv:1507.06568 [hep-ph].

[315] D. Curtin and M. E. Peskin, *Analysis of Long Lived Particle Decays with the MATHUSLA Detector*, *Phys. Rev.* **D97** no. 1, (2018) 015006, arXiv:1705.06327 [hep-ph].